Title

Flash Sintering of Multiphase Composites

Author

Kok, David

Publication Date

2019

UNIVERSITY OF CALIFORNIA,
IRVINE

Flash Sintering of Multi-Phase Ceramic Composites

DISSERTATION

submitted in partial satisfaction of the requirements
for the degree of

DOCTOR OF PHILOSOPHY

in Material Science and Engineering

by

David Kok

Dissertation Committee:
Professor Martha L. Mecartney Irvine, Chair
Professor Rishi Raj
Professor James C. Earthman

2019

DEDICATION

To

my brothers of 2nd Battalion 3rd Marines

Fortune Favors the Brave

In the end, we were willing to die not for a flag, apple pie, or the American dream. We were willing to die for the those fighting to the left and right of us.

In memoriam of the fallen during my deployments in Afghanistan and Iraq

Lt. Col. Joseph T. McCloud
2nd Lt. Joshua L. Booth
GySgt. Terry J. Elliott
Cpl. Derek W. Jones
Cpl. Jeremy S. Sanvickmonroe
Cpl. Joshua C. Sticklen
HN Matthew G. Conte
LCpl. Joshua C. Alonzo
LCpl. Donald S. Brown
LCpl. Timothy W. Brown
LCpl. Daniel B. Chaires
LCpl. James Chamroeun
LCpl. Matthew W. Clark
LCpl. James R. Davenport
LCpl. Phillip C. George
LCpl. Mario D. Gonzalez
LCpl. Kevin B. Joyce
LCpl. Stephen L. Morris
LCpl. Ryan J. Nass
LCpl. Michael D. Scholl
LCpl. Steven A. Valdez
LCpl. Jeromy D. West
PFC. Daniel T. Morris
PFC. Christopher T. Riviere
PVT. Edwardo J. Lopez
PVT. Heath D. Warner

TABLE OF CONTENTS

LIST OF FIGURES

LIST OF TABLES

ACKNOWLEDGMENTS

I would like to first and foremost thank my committee chair, Professor Martha L. Mecartney. It is my distinct honor to call her my mentor, adviser, and a personal hero. In 2011 she took a chance and allowed me to join her research lab as a community college student. From then on, she has served as a pinnacle of knowledge, guidance and inspiration.

I would also like to thank Professor's Rishi Raj and James C. Earthman for serving on my dissertation committee and for their mentorship. My research would not have been possible if not for the amazing collaboration work with Professor Rishi Raj. He has been nothing by welcoming and encouraging since the first day we met. The knowledge that I gained from Professor James C. Earthman classroom instruction and advising was critical to my research.

To my mother and family for all their sacrifices in allowing me to succeed in life and graduate school. Thank you for all you have done and continue to do to support me.

Thank you to Professor Winny Dong and the McNair Scholars Program from Cal Poly Pomona, for showing me that graduate school was a real possibility. Even for a poor kid from an immigrant family.

A special acknowledgment goes out to all my past and present graduate student peers in the Mecartney research group. Your collective advice, and energy for research was invaluable. Also, the support and efforts of the Materials Science and Engineering department faculty and staff is greatly appreciated.

Finally, thank you to the National Defense Science and Engineering Graduate Fellowship (NDSEG) program for funding my graduate research.

CURRICULUM VITAE

EDUCATION

Transfer, Mt. San Antonio Community College, CA (2011)
B.S. Chemistry, Cal Poly Pomona, Pomona, CA (2014)
M.S. Materials Science and Engineering, University of California, Irvine, Irvine, CA (2015)
Ph.D. Materials Science and Engineering, University of California, Irvine (2019)

PROFESSIONAL EXPERIENCE

UNIVERSITY OF CALIFORNIA, IRVINE, Irvine, CA **2014 -2019**
Ph.D. Candidate

- Electric field assisted sintering of ceramic composites
- Ceramic processing and characterization of multiphase ceramics

CAL POLY POMONA, Pomona, CA **2011 - 2014**
Undergraduate Student Researcher

- Produced MgO aerogels for CO_2 capture and storage
- Worked in collaboration with a local community college to teach research skills

NASA GLENN RESEARCH CENTER, Cleveland, OH **Summer 2013**
Summer Undergraduate Student Intern

- Synthesized aerogel/ceramic composite heat shields

UNIVERSITY OF CALIFORNIA, IRVINE, Irvine, CA **Summer 2011**
Summer Community College Student Researcher

- Processing of multiphase ceramics for optical transparency

UNITED STATES MARINE CORPS **2004 -2011**
Infantryman

- Sergeant of Marines
- Deployed to combat operations in Iraq and Afghanistan

ACADEMIC FELLOWSHIPS

National Defense Science and Engineering Graduate (NDSEG) Fellowship, US Department of Defense (2016-2019)
Graduate Assistantships in Areas of National Need (GAANN) Fellowship, US Department of Education (2015-2016)
Graduate Opportunity Fellowship (GOF), University of California, Irvine (2014-2015)

ACADEMIC ACHIEVEMENTS

Ludo Frevel Crystallography Scholarship, International Centre for Diffraction Data (Winter 2017)
Graduate Excellence in Materials Science (GEMS) Diamond Award, American Ceramics Society (Fall 2016)
Competitive Edge Program, University of California, Irvine (Summer 2014)
Dean's List, Cal Poly Pomona (Winter, Spring 2014)
Ronald E. McNair Scholarship, Cal Poly Pomona (2012-2014)

PUBLICATIONS

Kok, D., Jha, S., Raj, R., Mecartney, M.L., "Flash Sintering of a three-phase alumina, spinel, and yttria-stabilized zirconia composite," *J. Am. Ceram. Soc.,* **100** [7] 3262-3268 (2017).

Kok, D., Yadav, D., Sortino E., McCormack S. J., Tseng K., Kriven W. M., Raj R., Mecartney M. L., "α-Alumina and spinel react into single phase high-alumina spinel in < 3 seconds during flash sintering," *J. Am. Ceram. Soc.,* **102** [2] 644-653 (2019)

SELECTED PRESENTATIONS

Kok, D., Mecartney, M.L., "Investigation of Mechanical properties for Flash Sintered Ceramics," Electric Field Assisted Sintering and Related Phenomena Far from Equilibrium II, Tomar, Portugal (2019)

Kok, D., Emanuele, S., Yadav, D., McCormack, S.J., Kuo-Pin T., Kriven, W.M., Raj, R., Mecartney, M.L., "Ultra-Rapid Formation of Single Phase High-Alumina Spinel During Flash Sintering," Gordon Research Seminar– Ceramics, Solid State Studies in, Mount Holyoke, MA (2018).

Kok, D., Jha, S., Emanuele, S., Yadav, D., McCormack, S.J., Kuo-Pin T., Kriven, W.M., Raj, R., Mecartney, M.L., "Flash Sintering of a Two- and Three- Phase Composites Constituted of Alumina, Spinel, and Yttria-Stabilized Zirconia," EAM 2018, Orlando, Florida (2018).

Kok, D., Jha, S., Emanuele, S., Yadav, D., McCormack, S.J., Kuo-Pin T., Kriven, W.M., Raj, R., Mecartney, M.L., "Flash Sintering of a Three-Phase Alumina, Spinel, and Yttria-Stabilized Zirconia Composite," ECerS 2017, Budapest, Hungary (2017).

Kok, D., Jha, S., Raj, R., Mecartney, M.L., "Flash Sintering of α-Al_2O_3, $MgAl_2O_4$ and 8 mol% Y_2O_3 Stabilized ZrO_2 Composites," MS&T 2016, Salt Lake City, UT (2016).

MATERIALS CHARACTERIZATION PROFICIENCY

Expert/Unsupervised 24-Hours Access

- Tescan GAIA3 SEM-FIB
    - Duel beam flagship SEM
    - High-current ion column FIB
    - EBSD and EDS with Oxford AZtec software
- FEI Magellan 400 XHR SEM
    - High resolution SEM
    - EDS with Oxford AZtec software
- Rigaku SmartLab XRD
    - Powder, and solid material characterization
- Various Standard Laboratory Materials Testing and Sample Preparation
    - Indentation (Vickers and Knoop) hardness and fracture toughness
    - Three-point bend and Instron tensile testing
    - SEM, AFM, and XRD sample preparation (Polishing, etching, sputtering)

Intermediate/Supervised Working Hours Access

- JEOL JEM-2100F TEM
    - High resolution nano- and convergent beam TEM
- Veeco Caliber AFM
    - High resolution surface topography measurement

PROFESSIONAL ASSOCIATIONS

American Ceramic Society (ACerS)

- Student Member
- Delegate, President's Council of Student Advisors (PCSA)
- Executive Committee**,** Global Graduate Researcher Network (GGRN)

American Chemical Society (ACS), Student Member
Materials Research Society (MRS), Student Member

STEM OUTREACH

Competitive Edge Program Mentor, University of California, Irvine (Summer 2018)
ASM International Student Assistant, Orange Coast Chapter (Summer 2018)
ACS Science Coach (Fall 2015- Spring 2016)
Communications Committee, ACerS PCSA (Fall 2015- Spring 2016)

ABSTRACT OF THE DISSERTATION

Flash Sintering of Multiphase Ceramic Composites

By

David Kok

Doctor of Philosophy in Materials Science and Engineering

University of California, Irvine, 2019

Professor Martha L. Mecartney, Chair

The method of using an applied electric field during the sintering process (flash sintering) has the potential to be a cost and energy saving method for the manufacturing of many ceramic products. Since flash sintering is still an emerging field of research, most of the work has been centered on single phase systems. This study will evaluate the viability of applying flash sintering to a multiphase composite system; more specifically ceramic composites consisting of Al_2O_3 (alumina), 8 mol % yttria-stabilized zirconia (8YSZ), and $MgAl_2O_4$ (Spinel). Various flash sintering conditions were studied, as well as in-situ characterization methods. By tailoring the flash sintering parameters, fully dense, fine grained, three-phase composites were formed with improved mechanical properties. Reaction sintering was also found to be possible with flash sintering of multiphase composites, with the formation of high alumina spinel specifically. In addition, 8YSZ was discovered to have a catalytic effect with flash sintering. The results of this study show that flash sintering has promise as a quick and energy efficient method to sinter complex systems as well as form unique phases when applied to ceramic composites.

CHAPTER 1: INTRODUCTION AND BACKGROUND

1.1 Introduction

Field assisted sintering techniques (FAST) involves the application of an electric field during the sintering process (Figure 1.1). Two aspects of FAST are flash and fast sintering. Both sintering methods involve the application of an electrical field during sintering without any applied pressure and has been shown to be a novel method to quickly densify ceramics.[1–6] In *flash sintering,* densification under an electric field occurs in seconds, at a threshold temperature and field, which is accompanied by a non-linear increase in conductivity.[1] *Fast sintering* can be considered a separate but related phenomenon, when the rate of densification is enhanced by the application of an electric field but there is no abrupt densification. Fast sintering occurs at lower applied voltages compared to flash sintering.[3, 6] This study will limit its scope to only flash sintering, although it is noted that fast sintering itself merits further investigation.

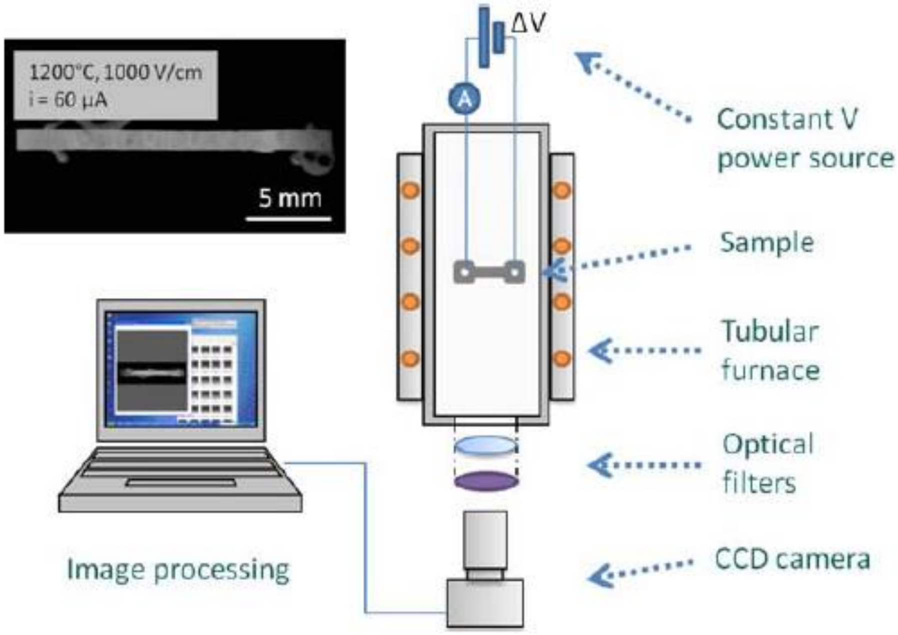

Figure 1.1: Flash and fast sintering apparatus (Cologna et al.[3])

The ability to rapidly densify ceramics at lower temperatures than normal sintering temperature allows flash sintering to be potentially a large energy and cost saving method to produce fully dense ceramics. Conventional sintering of 8 mol % yttria stabilized zirconia (8YSZ) requires a furnace temperature hold of 1500°C for 12 hours for a theoretical density of 97%.[7] This equals to a power consumption of ~ 20 kW if done in a medium sized laboratory furnace. In results shown later in this manuscript, approximately the same density can be achieved with flash sintering of 8YSZ at a furnace temperature hold of 1550°C for 6 minutes. Even accounting for the additional power being applied to the sample, the power consumption is only ~ 2.5 W or 13% of the power required compared to conventional sintering. Lowering sintering temperatures can also allow for the reduction of grain sizes in fully dense materials, which can lead to improved mechanical properties as well as increased super plasticity.[8, 9] This would allow for the development of a fine-grained size multiphase inert matrix nuclear fuel for higher efficiency, increased stability, and improved radiation damage tolerance.[9–14] In-situ X-ray diffraction (XRD) experiments have shown that flash sintering can also increase the kinetics of phase reaction between different phases and promote new phase formation.[15] This has shown that flash sintering has the potential to allow for the development of a novel processing route for the formation of complex or new phases though the use of multiphase ceramics and flash sintering.

The scope of this study will include 1) the effects of flash sintering on two- and three- phase ceramic composites 2) how flash sintering can be used to reaction sinter ceramics or form non-stoichiometric composites 3) the mechanical properties of flash sintered single phase and multi-phase composites. This will allow for a better understand of flash sintering and its effect on composite materials. Furthermore, this study aims to progress the transition of flash sintering from the research laboratory setting to industrial application by highlighting the beneficial applications of flash sintering.

1.2 Review of Flash Sintering

1.2.1 Overview of Flash Sintering

Initial studies on flash sintering were conducted by the Raj research group in with Cologna et al. publishing the first data of flash sintering of 3 mol % yttria-stabilized zirconia (3YSZ) in 2010[1]. In this paper, the first sintering curves with flash sintering show the rapid densification that can be possible (Figure 1.2). Ever since, flash sintering has been a quickly emerging field of study.[16, 17] A review paper published in 2017 by Yu et al. list 71 different unique papers published on the flash sintering of various materials from oxides to non-oxide ceramics and composites (Figure 1.3).[17]

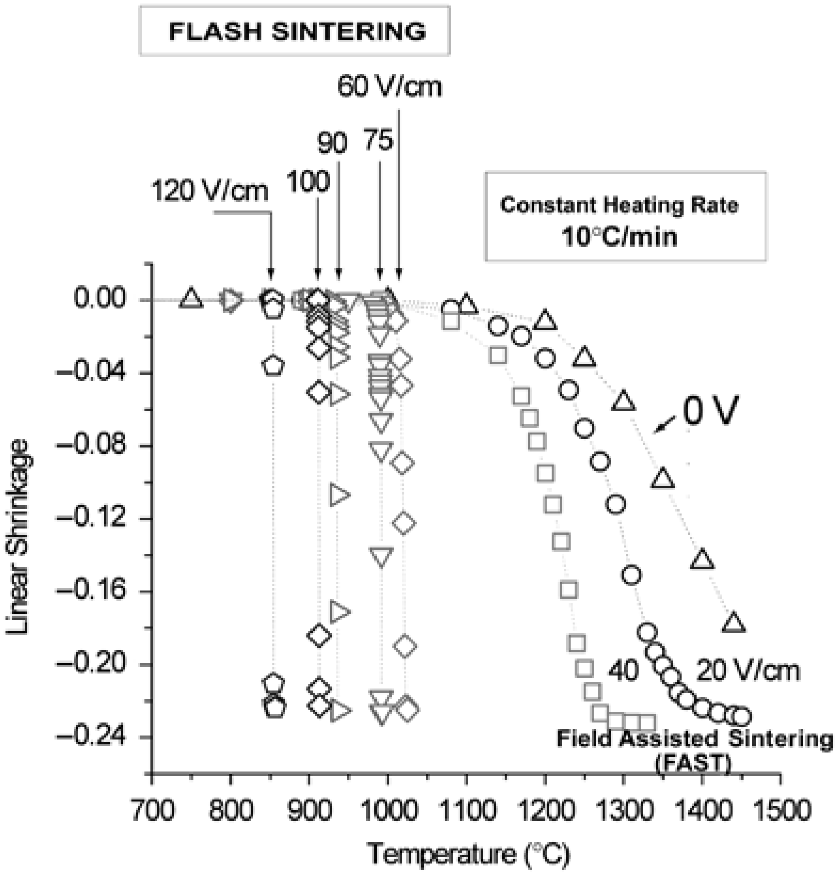

Figure 1.2: Sintering curve of flash sintered 3YSZ (Cologna et al.[1])

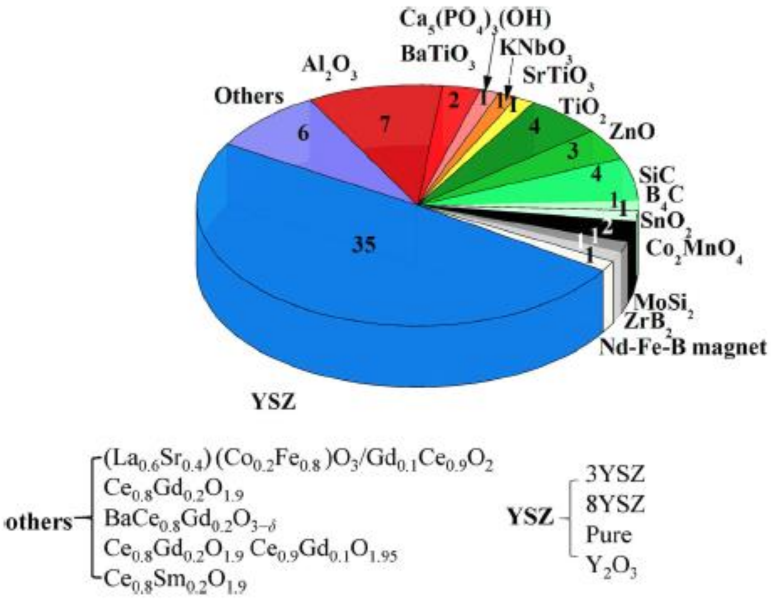

Figure 1.3: Pie chart representation of the published papers on flash sintering clustered by the different material system (Yu et al.[17])

Regardless of material, all flash sintering experiments follow the same general procedures and trends. An electric field applied is directly to the sample during the sintering process. This is typically done with platinum electrodes, but some experiments has been carried out with other types of high conductive metals.[18] Experiments also have been done with contactless plasma electrodes with successful results.[19] The flash sintering process is described by three distinct stages.[20] A pre-flash incubation period (Stage 1) is followed by rapid densification and increased conductivity (Stage II), and finally, a quasi-steady-state, current-controlled state called Stage III. Examples of each of the stages can be seen in Figure 1.4A. The plotting of power density as a function of temperature or time can also be used to show the process of flash sintering (Figure 1.4B). The power density spike in this plot correlates with the onset of flash sintering or Stage II in the flash sintering process.

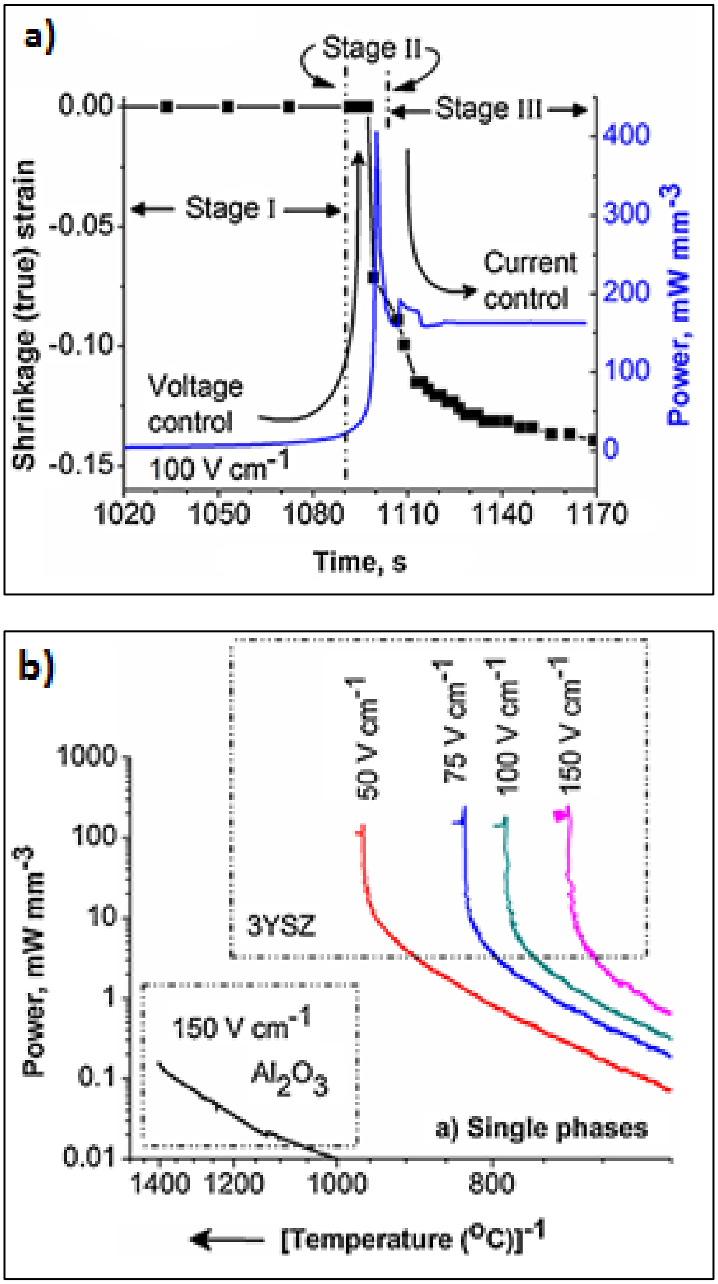

Figure 1.4: Power density and shrinkage strain curve (A) and Arrhenius plot for the power dissipated in flash sintering (B) (Modified from Naik et al.[20])

At the onset of flash sintering, the power supply is switched to current control in Stage III. This is done to limit Joule heating to prevent thermal runaway.[21] While the temperature for the onset of flash sintering depends on the applied field, the final density depends on the current flowing through the specimen.[4, 22]

The mechanisms for flash and fast sintering are still controversial but three main proposals have been mainly highlighted. Strictly Joule heating has been early debated as the mechanism of flash sintering since very beginning of flash sintering research, with Cologna proposing a rapid rise in grain boundary temperatures may be an important factor in flash sintering[1]. More recently evidence for Joule heating during thermal runaway, and localized melting of particles causing enhanced densification have strengthen the theory of flash sintering being solely related to Joule heating.[23–26]

Another proposed mechanism of flash sintering is Frenkel pairs nucleation caused by the electric field.[3, 27, 28] In this hypothesis, the electric field causes both cation and anion form interstitials and vacancies. The electric field also forces electron hole pairs from the Frenkel pairs to recombine, resulting in the Frenkel pair becoming charge neutral relative to the lattice. This charge neutrality results in higher mobility of the Frenkel pairs. Sintering pressure than drive the interstitials to the pores and the vacancy to the grain boundaries, resulting in densification.

More recently, electrochemical reduction has also been offered as a proposed mechanism for flash sintering, particularly in ionic conductors.[17, 29–31] Early on in flash sintering experiments of zirconia blackening of the material was observed, particular in the cathode region.[1] As flash experiments progress, this blackening continued to be observed in zirconia as well as alumina[29, 30] A explanation for this is that the applied electric field causes a electrochemical reduction starting at the cathode region (Figure 1.5). This reduction can eventually progress to the anode as more oxygen ions migrate from the anode as electrons move away from the cathode. As the reduction is taking place, the conductivity of the sample increases until the flash event occurs.

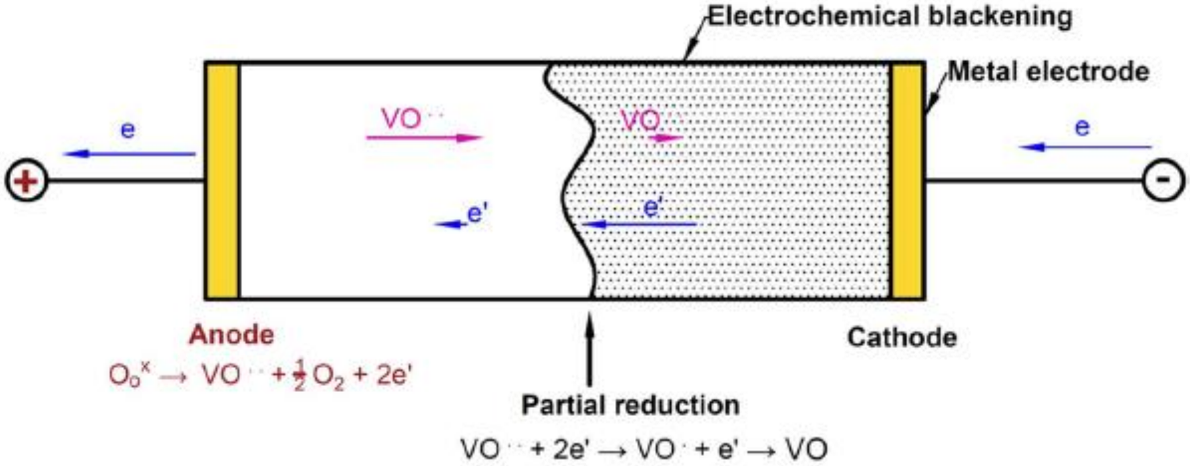

Figure 1.5: Electrochemical reduction mechanism for flash sintering (Biesuz et al.[30])

1.2.2 Comparing Flash Sintering to Spark Plasma Sintering

Flash sintering is often compared to spark plasma sintering (SPS) due to both methods utilizing an applied electric field while sintering. Although both methods of sintering do share this common trait, SPS is vastly different sintering process. In SPS sintering is done with mechanical pressure with the powder contained in a electrically conductive die, usually made of graphite (Figure 1.6).[32] No external heating elements are used in SPS, with high temperatures generated with a pulsed DC current is passed though the die. This allows for very high heating rates, as much as 1000°C/min[33] The field involved with SPS is typically low voltage and high current, whereas is flash sintering usually involves a high voltage and low current electric field.[16, 32] The role of the electric field also differs between flash sintering and SPS. In flash sintering, the field is applied directly to the sample to the sample. With SPS Joule heating of the die is the main reason the current is applied during SPS, although modeling of the current flow has shown that the current can pass though the sample itself.[34, 35] It should be noted that the process of SPS can be referred to as various names, but SPS is the most widely accepted name for this process.[34]

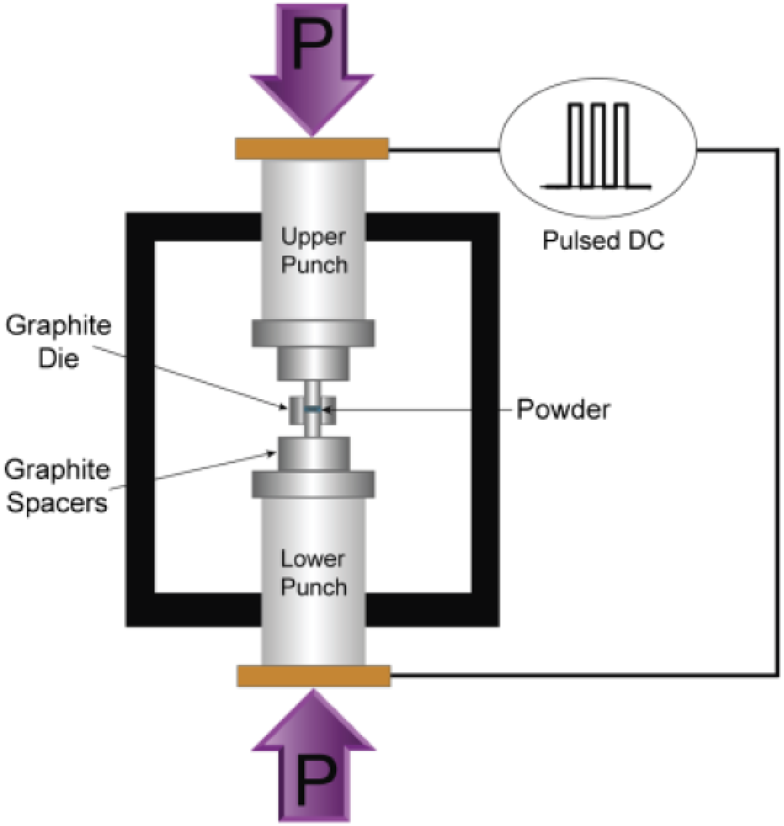

Figure 1.6: Diagram of Spark Plasma Sintering (Munir, et al.[32])

1.2.3 Newest Development of Flash Sintering

One of the most promising aspect of flash sintering is how rapid the sintering process occurs, but this is a disadvantage in terms of conducting research due to the sintering occurring within seconds. To increase the sintering time with flash sintering, a current ramping profile was developed.[36] This procedure involves ramping up of the current at a set rate after the onset of flash, instead of a large current jump usually done in conventional flash sintering experiments (Figure 1.7). This allowed for the sintering process to be extended from seconds to minutes.[36] Using this current ramping profile also was found to be an effective method to control the flash sintering process by preventing a large current injection into the system. [37, 38] This prevent inhomogeneity of the microstructures in the sintered sample by limiting the form of localized hotspots.[37]

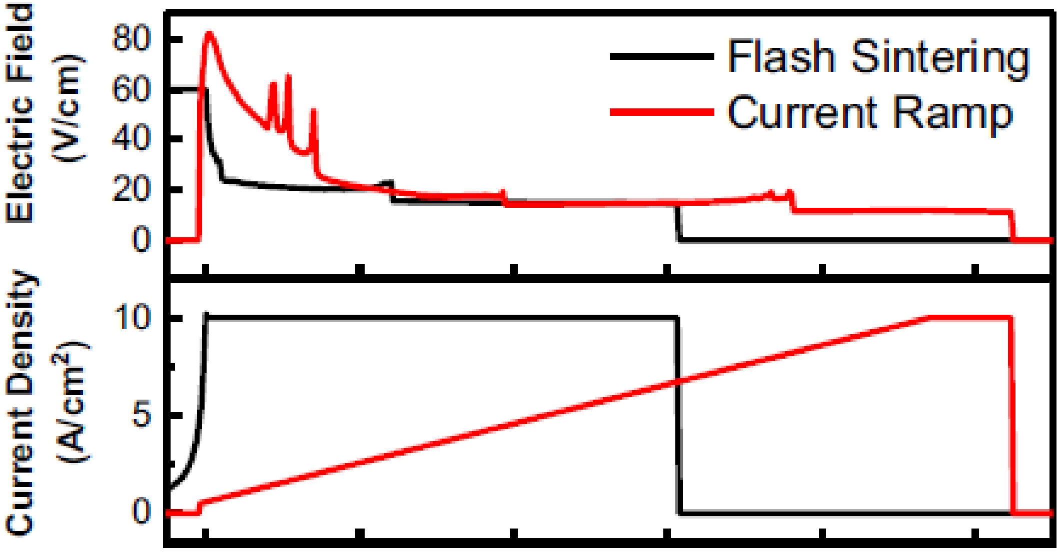

Figure 1.7: Current ramping profile compared to conventional flash sintering (modified from Phuah et al.[38])

The use of flash sintering as a method to reaction sinter ceramics has also recently gained traction. The formation of $BiFeO_3$ from reaction flash sintering of Bi_2O_3 and Fe_2O_3 was shown to be achievable in a single step[39]. Highly dense, single phase $MgAl_2O_4$ has also been formed by reaction flash sintering of MgO and Al_2O_3[40, 41]. High quality eutectic compositions have also been shown to be possible to produce by reaction flash sintering.[42]

In all of the above cases, an enhanced solid state reaction is observed during the reaction flash sintering processes.[39–42]

Other developments with flash sintering include utilizing flash sintering for other purposes than sintering. Ma et al. has using flash sintering as a method to pyrolyzed SiOC at 500°C lower than conventional pyrolysis methods for SiOC.[43] The almost instantaneously joining of two ZrO_2 of ceramics at 600°C has also been demonstrated with flash sintering.[44] As flash sintering is becoming more researched, organizations such as the US Army Research Laboratory and Oak Ridge National Laboratory have shown interest in flash sintering for national defense and nuclear energy needs.[45–47]

CHAPTER 2: EXPERIMENTAL SET-UP AND PROCEDURES

2.1 Starting Materials and Composite Synthesis

Commercial starting powders of cubic 8 mol % yttria stabilized zirconia (8YSZ) (Tosoh TZ-8YS), spinel (Baikowski S30CR) and alumina (Taimei TM-DAR) were used for this study. Two- and three- phase composites were made by mixing the individual components in a Union Process attritor mill. Milling was done with 1 kg of alumina or zirconia milling media to 35 g of powder. Isopropyl alcohol was then added to the media and powder to a level line just above the media. Attrition milling was done for 8 hours to ensure a homogenous mixture. After attrition milling was completed, the slurry was dried with a rotary evaporator and sieved to 106 μm.

For mechanical testing, cylindrical samples were made by cold isostatic pressing (CIP) with an Avure CIP. This began with the powders being packed in silicone molds. Filling of the molds was done in small intervals with intermediate tapping to ensure no void spaces were present. The filled molds were than taped shut and vacuumed sealed in a balloon and tied off. This was then placed inside of the CIP and pressed at 55 KPSI (~380 MPa). The formed ceramic green bodies by CIP typically had a green body density of 50-55 % theoretical density.

Dog-bone samples (Figure 2.1) were required for all the flash sintering experiments in this study. To make these samples, polyvinyl alcohol binder (Sigma-Aldrich) was mixed in with the powders for better structural integrity during the green body forming process. This was done by dissolving 2.5 weight % of the binder into 100 mL of water before adding in the milled and sieved powder. The resulting slurry was than dried at 100°C overnight and sieved again to 106 μm. Custom machined dog-bone molds were than filled with the powder and green bodies were pressed with a uniaxial Carver press at 300 MPa. Finally, a binder burn-out was done at 600°C for 1 hour. The dog-bone green bodies formed in this matter had a 50-54 % theoretical density. The dog bone samples were made with holes at each end with a gage length of 10 and 20 mm, and a cross section of approximately 3.5 mm x 1.3 mm.

Cuboid samples for in-situ experiments were also pressed with a uniaxial Carver press with the sample binder burn-out step as dog-bone samples. A pre-sintering step was also done at 900°C for 1 hour. This was done for added structural integrity of in-situ samples, due to the additional handling of the sample required for these experiments.

Figure 2.1: Example of dog-bone shaped ceramic green body after pressing

2.2 Experimental Set-Up at CSU Boulder

Initial flash sintering experiments were carried out in collaboration with Prof. Rishi Raj's research group at their laboratory in CSU Boulder. The ends of the dog-bone samples were lightly coated with platinum past (SPI Supplies) to ensure a good electrical contact. The sample was than suspended inside a vertical tube furnace using platinum wires hooked into the holes at the ends of the dog-bone sample. The platinum wires also served as electrodes and were connected to a DC high voltage power supply (Glassman). The voltage and current were monitored and controlled with a Keithley digital multimeter and computer running a custom MATLAB program. An industrial camera (Imaging Source) equipped with an IR filter lens (Edmund Optics KG-3) was also connected to the computer to take still images and video during the flash sintering process.

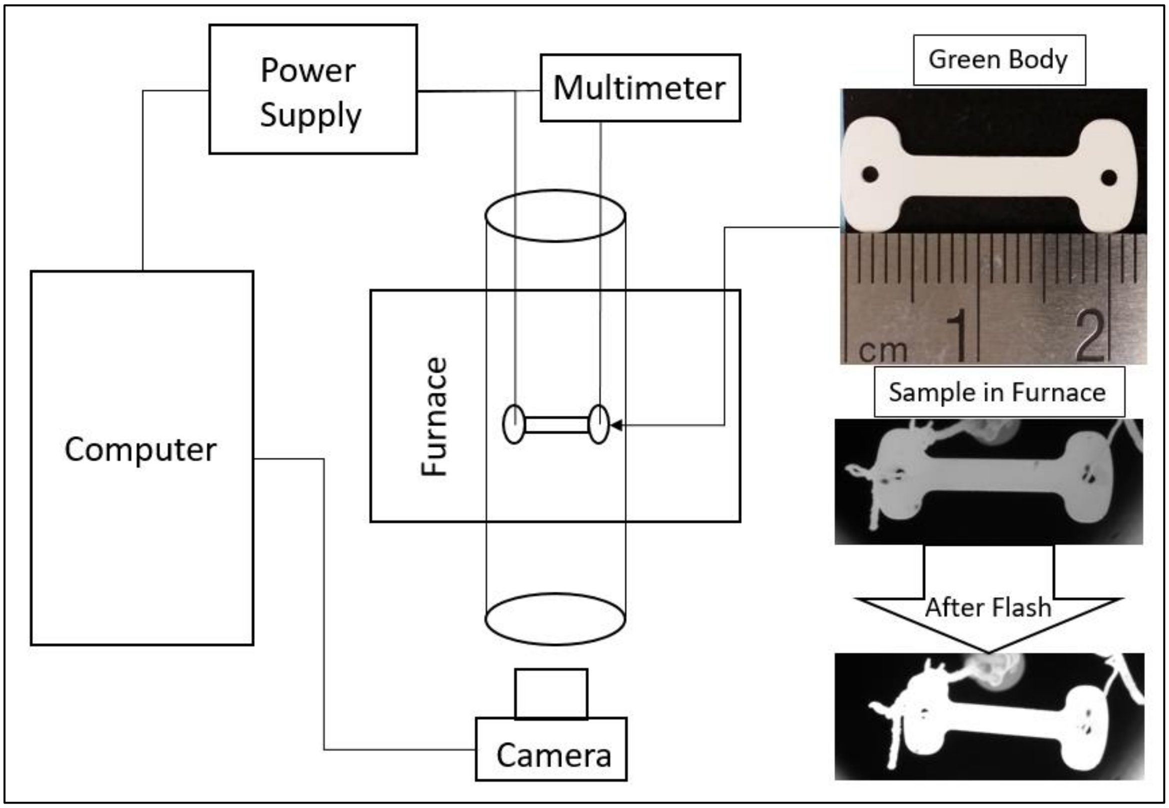

Figure 2.2: Diagram of the experimental set-up at CSU Boulder

2.3 Experimental Set-Up at UC Irvine

After initial experiments at the Raj lab, a flash sintering set up was built at UC Irvine based on the set up at CSU Boulder. At UC Irvine, a horizontal tube furnace (ATS Series 3420) is used for easier sample loading. The ends of the dog-bone sample are coated with platinum paste (SPI Supplies) and attached to platinum leads at each end of the dog-bone. The platinum leads are than connected to Kanthal wires that serve as electrodes. The Kanthal wires are insulated from each other inside of individual alumina tubing. An alumina support system was also fabricated to support the electrodes inside of the horizontal tube furnace. The same type of hardware as the set up at CSU Boulder is used at UCI in terms of high voltage DC power supply (Glassman), digital multimeter (Keithley), camera (Imaging Source), and IR filter (Edmund). All the hardware is connected to a computer with a modified version of the MATLAB program from CSU Boulder to run the flash sintering experiments and to collect data.

2.4 In-Situ Experimental Set-Up

2.4.1 Argonne National Laboratory

In-situ experiments at Argonne National Laboratory (ANL) were conducted at beamline 33BMC of the Advance Photon Source (APS). Platinum wires were wrapped around both ends of the length of a cuboid sample, and platinum paste (SPI Supplies) was applied to ensure good electrical contact. A thin sliver of platinum paste (1 mm wide) was applied to one side of the samples to measure the sample temperature.

The platinum wires were connected to a power supply (Sorenson) and a digital multimeter (Keithley). The samples were heated inside a quadrupole lamp furnace (QLF).[48] All experiments were conducted at furnace temperature held constant at 1250°C.

The sample was placed on an alumina sample holder for stability and was then positioned in the hot zone of the furnace. The QLF was also configured to allow for the incident x-ray beam to travel through the sample and the diffracted beam to impinge on a Pilatus 100K 2D image plate detector (DECTRIS). The wavelength of the X-ray beam was set to 0.7749 Å (16 kV) for all the in-situ experiments. Due to the physical size of the detector, the angular collection range of the detector was 4°.

2.4.2 Brookhaven National Laboratory

In-situ experiments at Brookhaven National Laboratory (BNL) were done at the National Synchrotron Light Source II (NSLS-II). A monochromatic beam of wavelength 0.18668 Å (corresponds to beam energy of 66.415 keV) was used at X-ray powder diffraction (XPD) beamline 28ID. The sample was attached to an alumina rod, with platinum wires, which also sever as electrodes to apply field. After wrapping the platinum wire at the sample ends, the gage length left on the sample was 4 mm. Platinum paste (SPI Supplies) was applied near the wires for better electrical contact. Platinum paste was also applied to a small section of the gauge area of the sample to be used as a standard for the calculation of the sample temperature during flash sintering. The sample was then placed in the hot zone of a quadrupole lamp furnace set to 1250°C. The lamp furnace was configured in such a way as to allow the incident X-ray beam to fall on the sample and the diffracted beam to fall on an amorphous silica-based flat panel detector (Perkin-Elmer). An electric field was applied with a DC power supply (Sorensen). Current flowing through the sample was monitored through a digital multimeter (Keithley).

CHAPTER 3: INITIAL STUDY ON FLASH SINTERING OF THREE-PHASE COMPOSITES

3.1 Abstract

Three-phase ceramic composites constituted from equal volume fractions of α-Al2O3, MgAl2O4 spinel and cubic 8 mol% Y2O3-stabilized ZrO2 (8YSZ) were flash-sintered under the influence of DC electric fields. The temperature for the onset of rapid densification (flash sintering) was measured using a constant heating rate at fields of 50-500 V/cm. The experiments were carried out by heating the furnace at a constant rate. Flash sintering occurred at a furnace temperature of 1350°C at a field of 100 V/cm, which dropped to 1150°C at a field of 500 V/cm. The sintered densities ranged from 90-96%. Higher electric fields inhibited grain growth due to the lowering of the flash temperature and an accelerated sintering rate. During flash sintering, alumina reacted with the spinel phase to form a high-alumina spinel solid solution, identified by electron dispersive spectroscopy and from a decrease in the spinel lattice parameter as measured by X-ray diffraction. It is proposed that the solid solution reaction was promoted by a combination of electrical field and Joule heating.

3.2 Experimental Procedures

The sample was held at 600°C for 1 hour to burn out the binder. Next the electric field was applied, and the furnace was heated at a constant rate of 10°C/min. The flash was signaled by a rapid increase in conductivity and the power supply was switched to current control when the current reached a preset limit (called Stage II). The sample establishes a quasi-steady state of flash under current control (Stage III); this state was held for 30 seconds, when power was turned off and the furnace allowed to cool down. Current limit values were selected from experience with flash sintering experiments with other oxides.[49]

The final density of sintered samples was measured using the Archimedes method. Gauge sections of sintered samples (between the two electrode ends) were polished and thermally etched at 1150°C for 30 minutes (or 1100°C for 30 minutes for samples flash sintered at 1150°C) and coated with iridium for SEM analysis. Grain size analysis and microstructure characterization was conducted using SEM/EDS (FEI Magellan XHR SEM with Oxford EDS Detector) and XRD (Rigaku SmartLab XRD).

3.2 Results and Discussion

3.3.1 Temperature Ramp Flash Sintering

The linear shrinkages under different applied DC voltages with a current limit of 25 mA/mm^2 and a furnace temperature ramp of 10°C/min are shown in Figure 3.1. The field and current conditions, the sintering temperature, the final density, and the final grain size are summarized in Table 3.1. The flash temperature decreases with higher applied electric field, consistent with earlier experiments.[22]

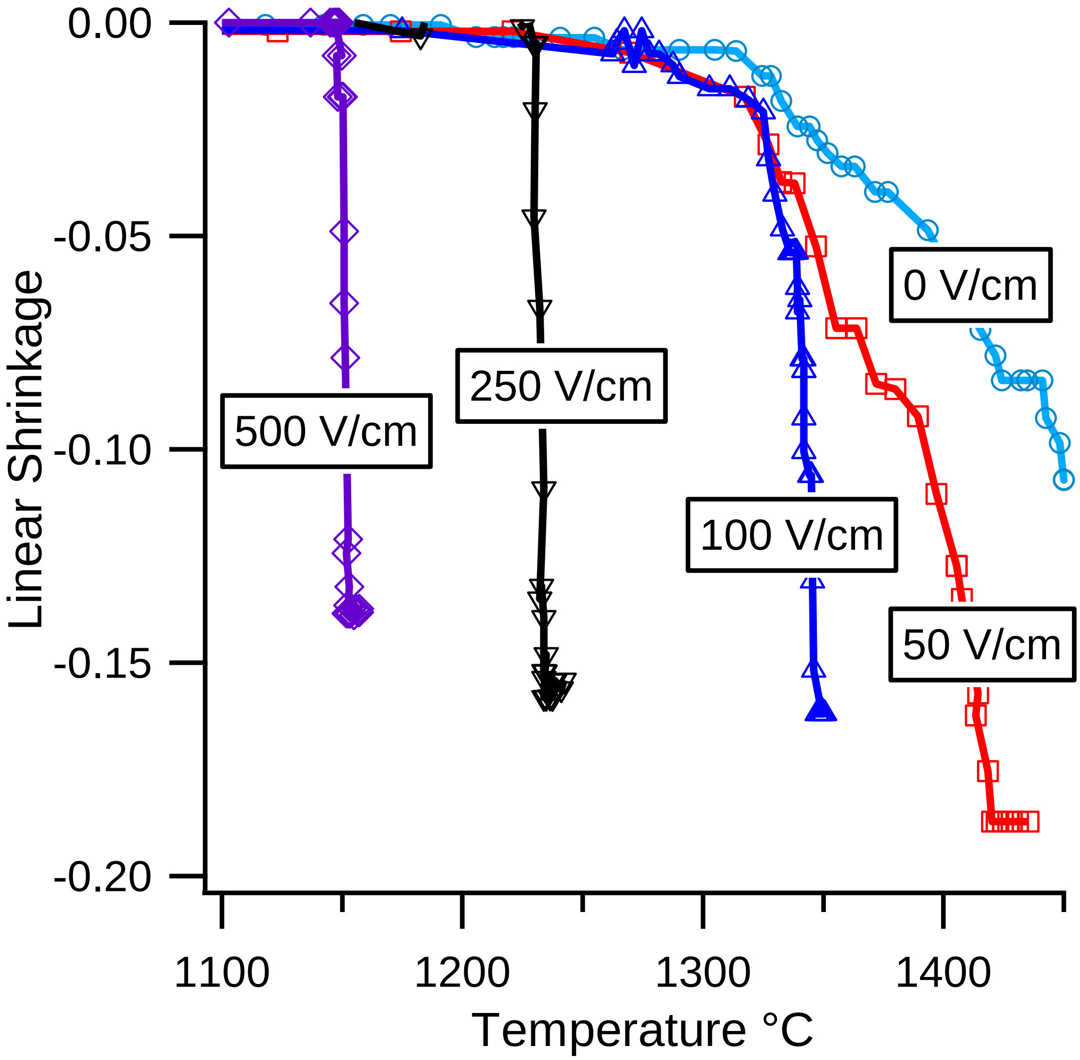

Figure 3.1: Sintering effect of different applied electric fields with current controlled at 25 mA/mm^2

E-Field (V/cm)	Current (mA/mm^2)	Furn. T (°C)	Calc. Sample T (°C)	Density (%)	Grain Size (nm)
0	0	1450	1450	74	400
50	25	1430	1490	95	650
100	25	1350	1450	96	600
250	25	1230	1390	94	520
500	25	1150	1330	90	470
250	75	1230	1500	95	1500

Table 3.1: Experimental parameters, calculated blackbody radiation T, density, and grain size data

Conventional sintering, without an applied field shows that sintering progresses to only 74% density even at 1450°C. At low applied fields, for example 50 V/cm, a resultant density of 95% is obtained. At 100 V/cm sintering occurs partially in the flash mode, reaching a final density of 96%. At 250-500 V/cm, the abrupt onset of densification, which is a feature of flash sintering, can be seen. At 250 V/cm, the sample densifies within seconds at 1230°C with a density of 94%. At 500 V/cm flash sintering occurs at 1150°C with a final density of 90%. The actual sample temperature can be higher than the furnace temperature due to the power dissipated in the sample. The calculated sample temperature in Table 1 was derived from a model that relates the specimen temperature to power dissipation and black body radiation (Equation 1.1).[15]

$$\frac{T}{T_o} = [1 + \frac{1000W_V}{e_m \sigma T_o^4}\left(\frac{V}{A}\right)]^{1/4} \qquad (1.1)$$

where T is the specimen temperature, T_o is the furnace temperature, W_V is the power density expended in the specimen in units of mW mm^{-3}, e_m is the emissivity, $\sigma = 5.67 \times 10^{-8}$ W m^{-2} K^{-4} is the Stefan Boltzmann constant, and V/A is the volume to surface area of the specimen in units of mm. The validity of this model has been confirmed by in-situ measurements of thermal expansion at the Advanced Photon Source.[15, 27]

The power dissipation is calculated from the product of the applied electric field (V/cm) and current density (mA/mm^2). It is plotted as a function of furnace temperature in an Arrhenius plot in Figure 3.2. The three stages of flash sintering are represented on this plot. The linear power increase (corresponding to the activation energy) represents Stage I. The abrupt rise in power dissipation signals the onset of the flash, or Stage II.

Finally, Stage III is the shown by the quasi-steady state under current control; it was briefly held for 30 seconds and then the power to the specimen was turned off. The power density curve (Figure 3.2) shows the different behavior of samples that experience pure flash sintering (250V, 500V) and those with a combination of flash and fast sintering (100V, 50V). Samples there are flash sintered show a sudden deviation from linearity going from Stage I to Stage II. A more gradual transition is seen with the samples that do not undergo pure flash sintering as has been observed for other ceramic systems.[20, 50] Stage III is seen at the maximum power density, where the current control regulates a constant power applied to the sample. The lowering of the flash temperature with a higher applied field is also seen in Figure 3.2, as commonly observed for flash sintering.[49]

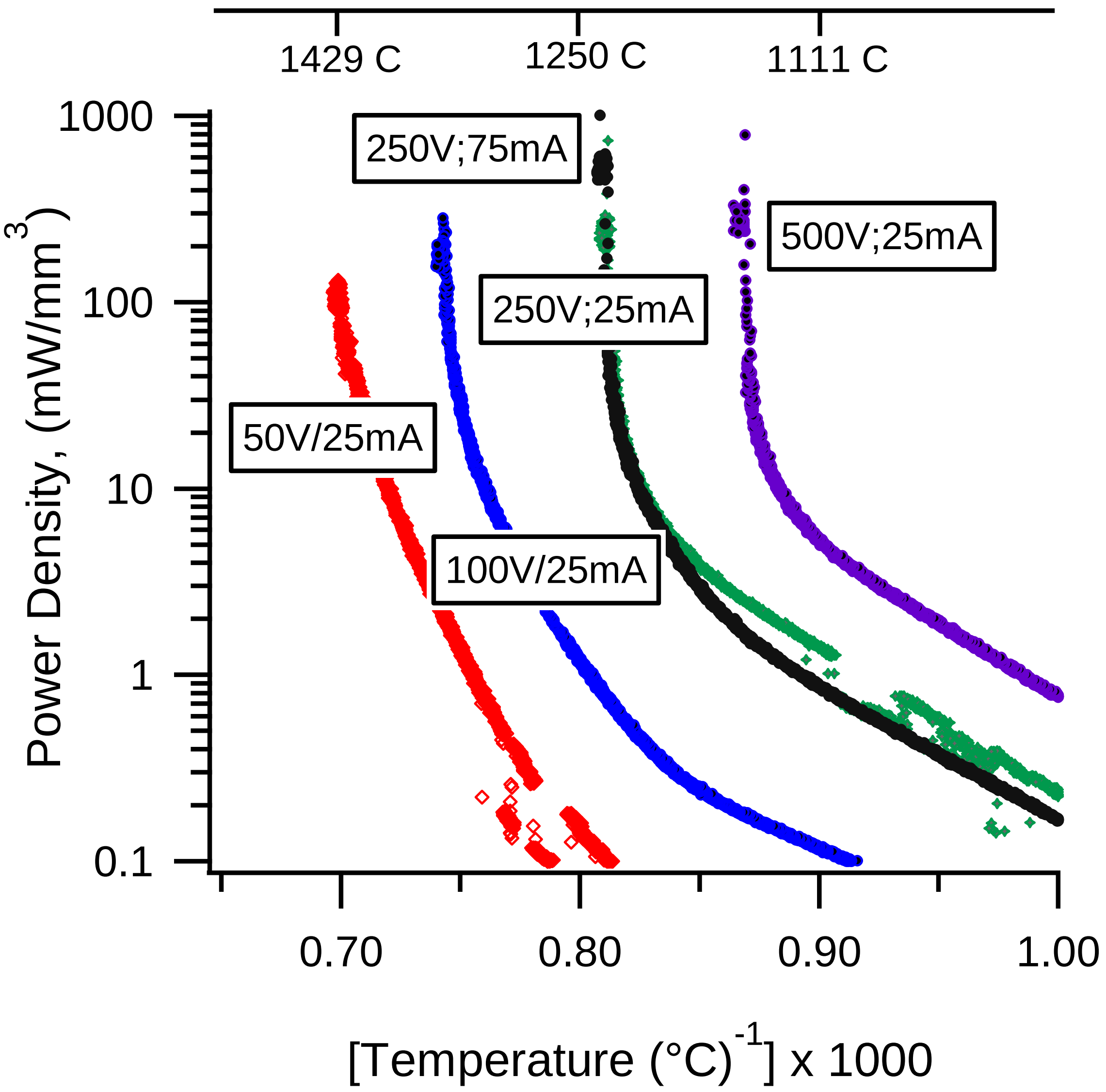

Figure 3.2: Arrhenius plot of the power dissipation with different applied electric fields and currents

The ability of flash sintering to quickly densify these samples at low temperatures should result in limited grain growth in the final microstructures of the samples.[50–52] Scanning electron micrographs of the composites sintered under different applied electric fields are shown in Figure 3.3-3.9. The darkest gray grains correspond to spinel, medium gray is alumina, and the light gray corresponds to 8YSZ. An average grain size is lowest for the highest field: 470 nm at a field of 500 V/cm and a current limit of 25 mA/mm^2.

3.3.2 Formation of High-Alumina Spinel

A higher current limit of 75 mA/mm^2 and 250 V/cm resulted in a very large grain size of 1.5 µm. At the same time alumina is absent in this specimen suggesting its dissolution into the spinel phase as solid solution. X-ray diffraction data shown in Figure 3.10 compare the results for the specimens obtained without the electric field as well as those sintered with 250 V/cm at 25 mA/mm^2 and at 75 mA/mm^2. At 75 mA/mm^2 the diffraction peaks from alumina are missing. The corresponding microstructure shown in Figures 3.9 and 3.9 also shows the absence of alumina grains. This composite is now approximately 1/3 8YSZ and 2/3 spinel.

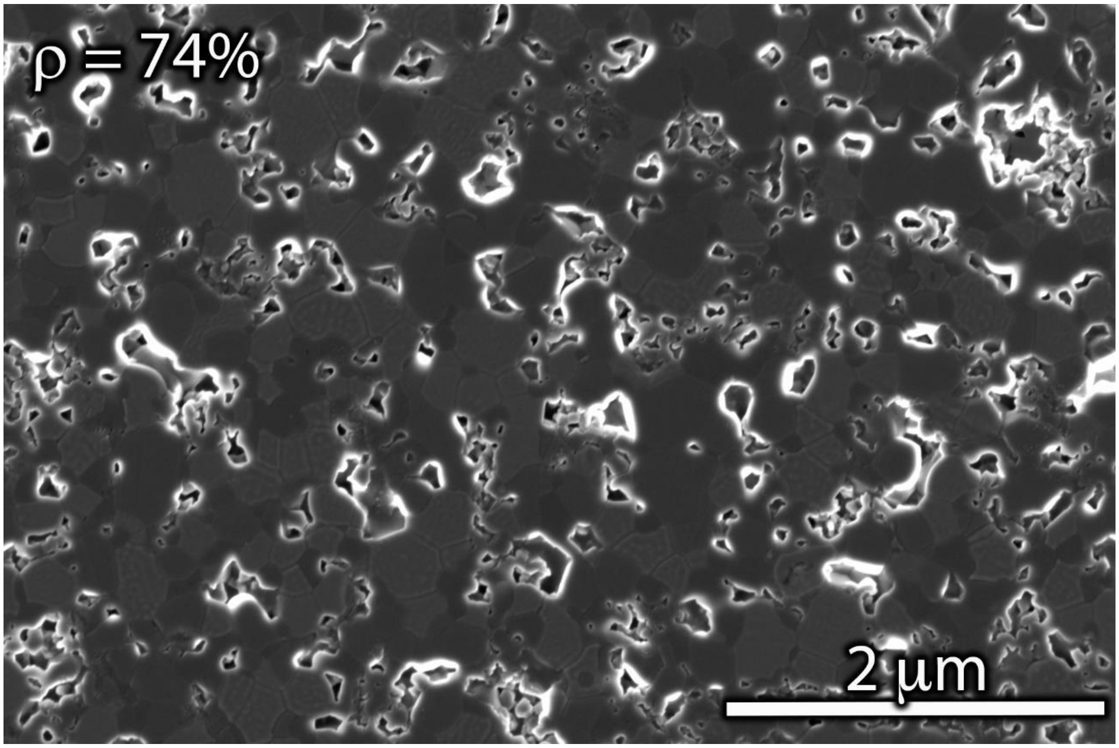

Figure 3.3: SEM micrograph of three-phase composite with no applied E-Field

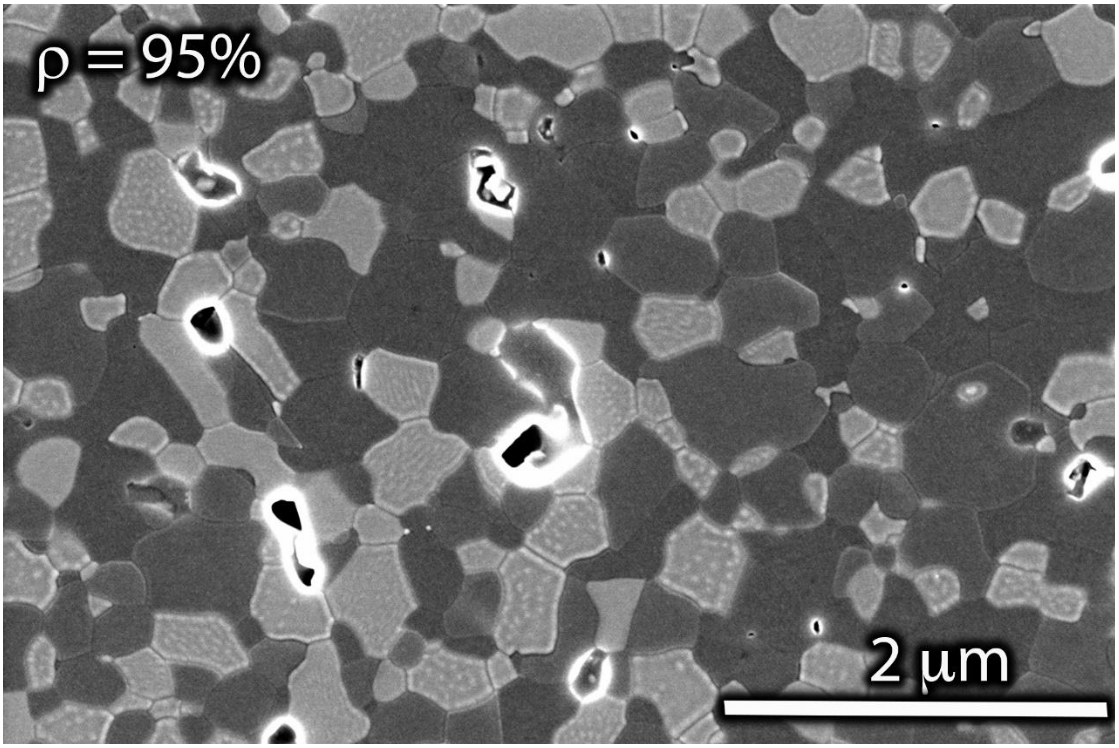

Figure 3.4: SEM micrograph of three-phase composite with an applied field of 50V; 25mA

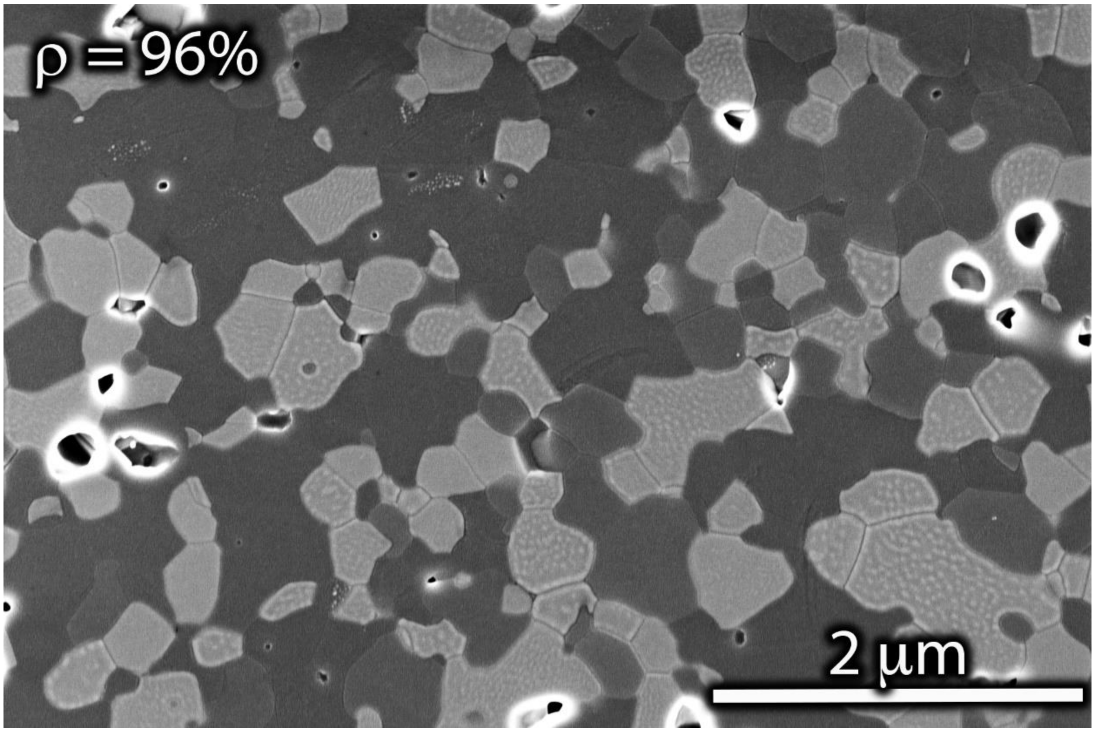

Figure 3.5: SEM micrograph of three-phase composite with an applied field of 100V; 25mA

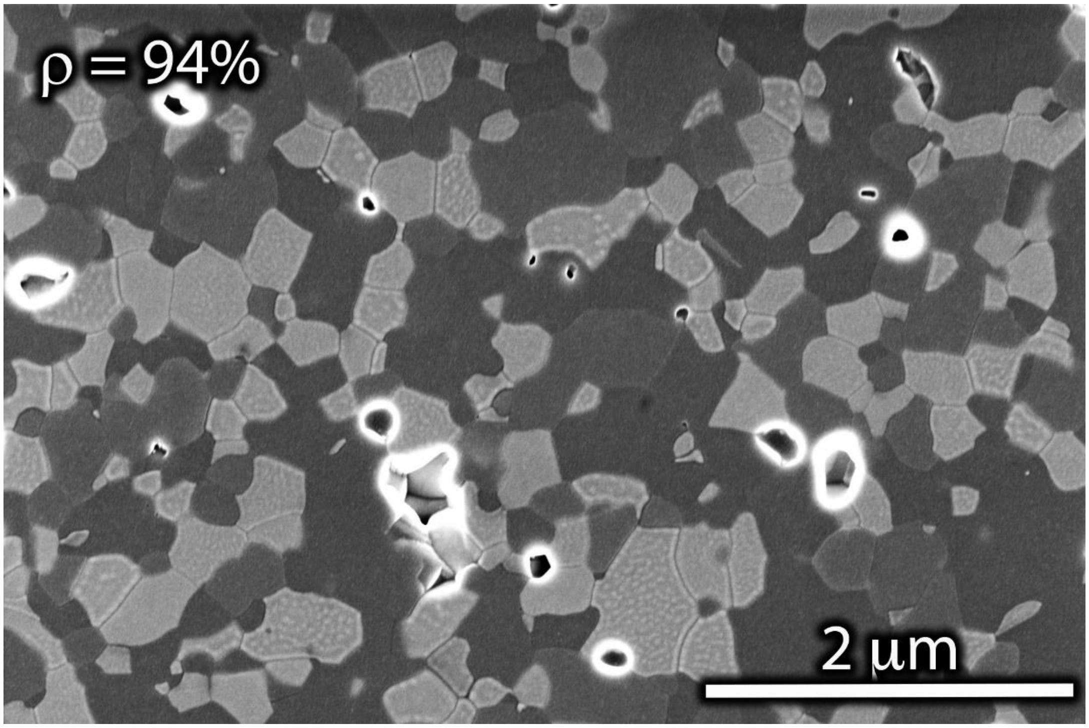

Figure 3.6: SEM micrograph of three-phase composite with an applied field of 250V; 25mA

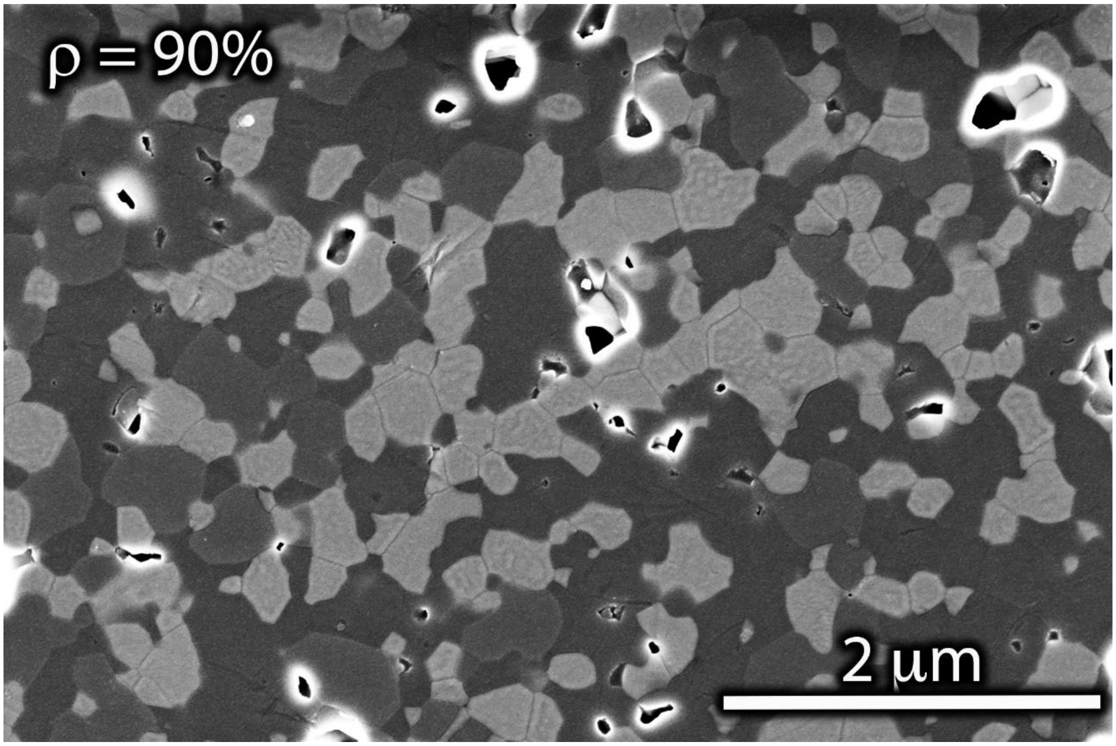

Figure 3.7: SEM micrograph of three-phase composite with an applied field of 500V; 25mA

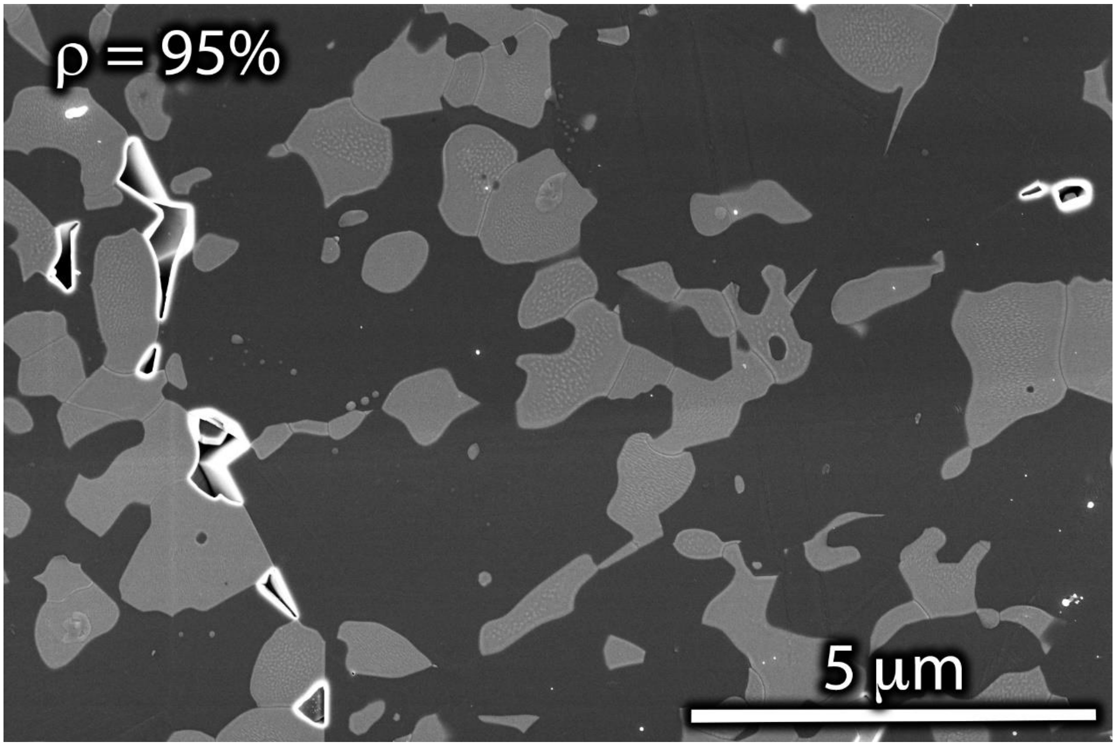

Figure 3.8: SEM micrograph of three-phase composite with an applied field of 250V; 75mA

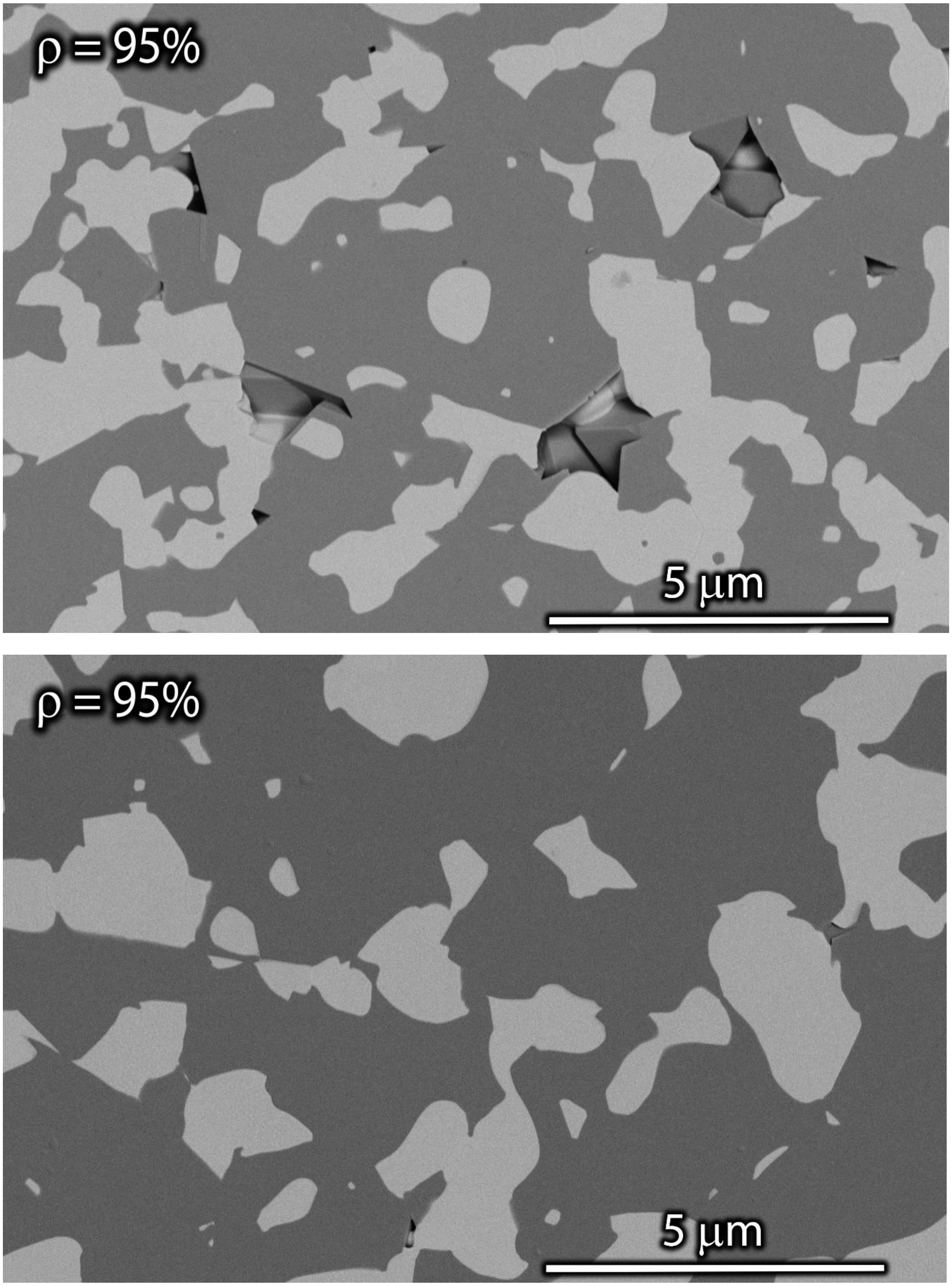

Figure 3.9: Backscatter SEM images of three-phase composite with an applied field of 250V; 75mA

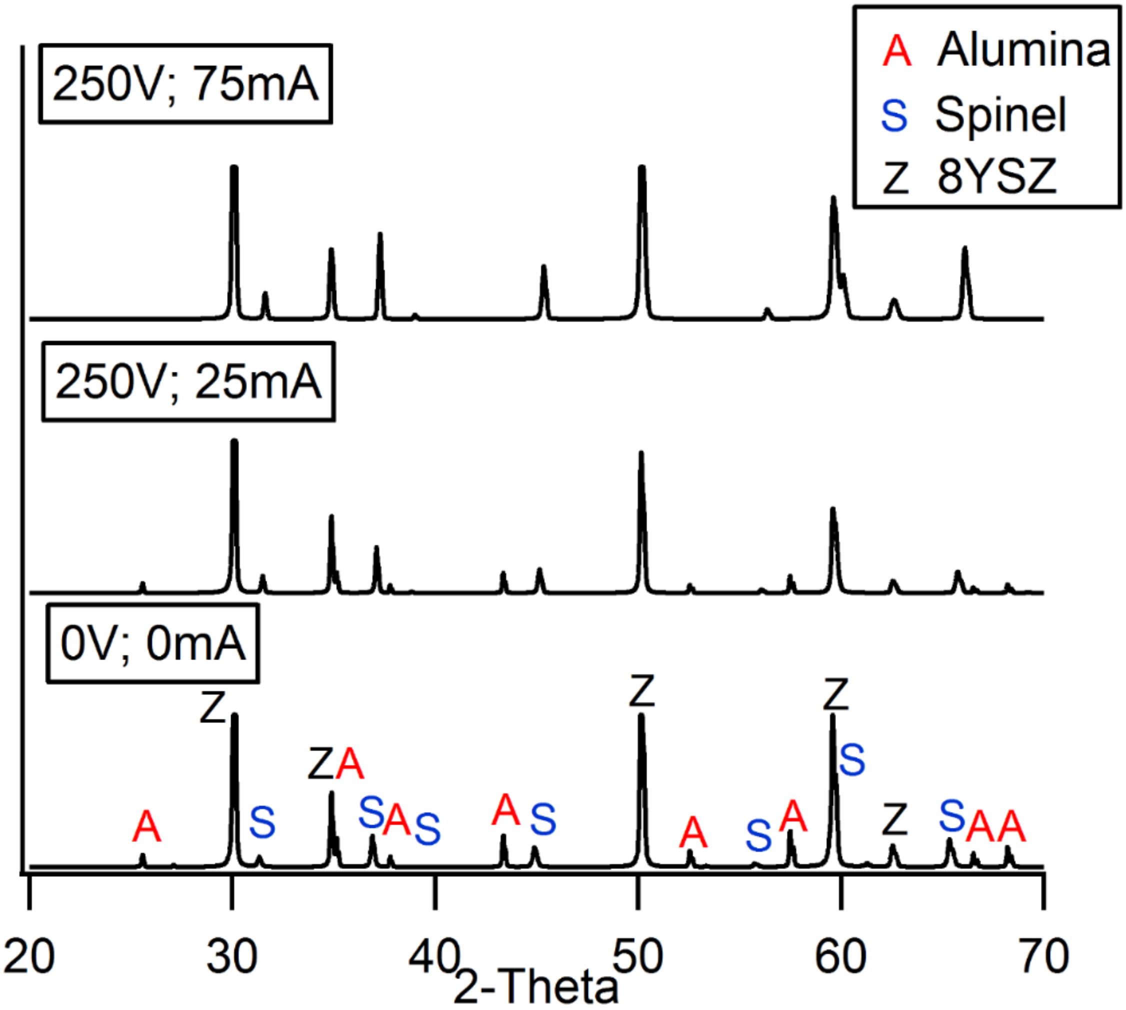

Figure 3.10: XRD patterns of the comparison of increasing current density

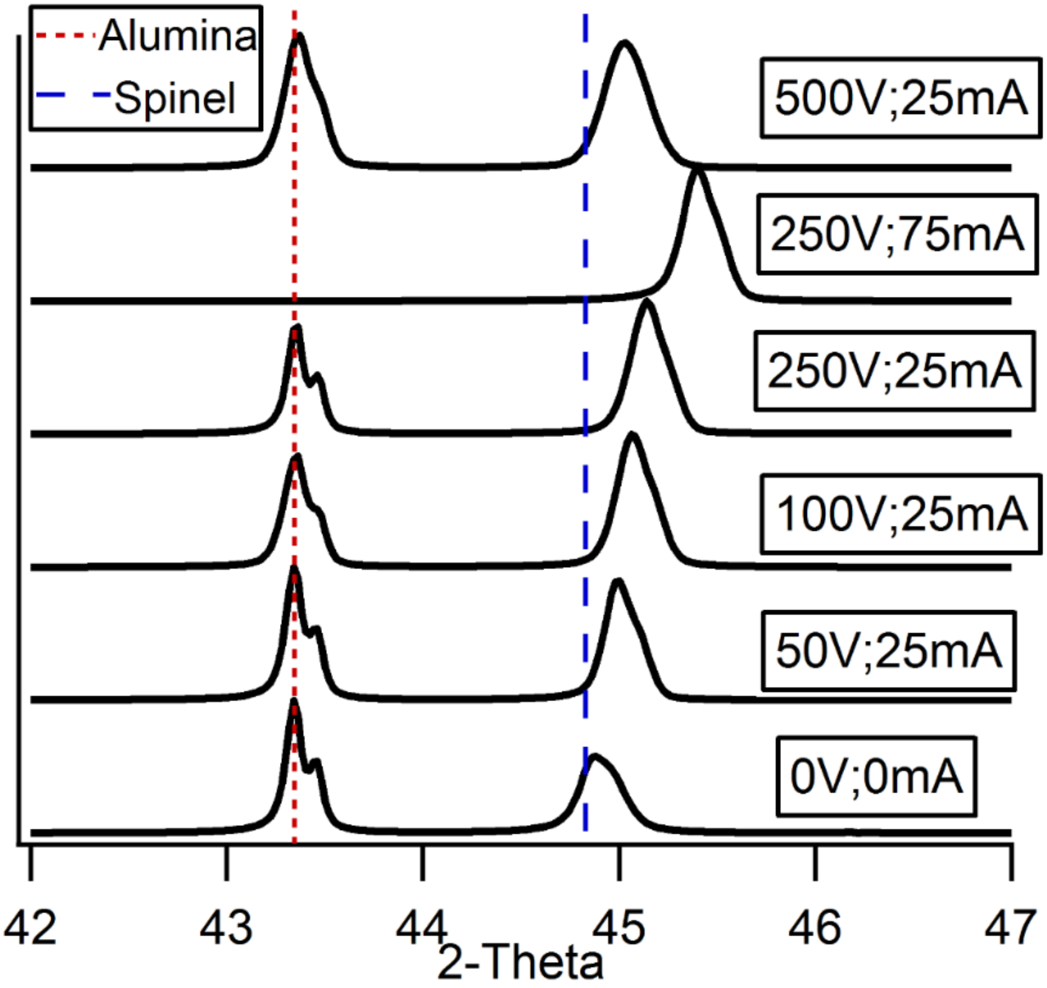

Figure 3.11: XRD patterns of the spinel peak shift with increasing current density

Figure 3.11 shows that the XRD peaks from the spinel phase are systemically shifted to higher 2Θ angles, which indicates a reduction of the lattice spacing in the spinel crystal structure expected in non-stoichiometric spinel solid solution when Mg^{2+} is replaced by Al^{3+}.[53] Table 2 also shows that in instances where the alumina is retained, the lattice parameter for spinel remained essentially unchanged. Figure 3.12 shows the relationship between Al/Mg ratio and the lattice parameter determined by XRD.

Sample	8YSZ Lat. Par. (Å)	Al_2O_3 Lat. Par. (Å)	$MgAl_2O_4$ Lat. Par. (Å)	EDS Atomic Al/Mg	EDS $MgAl_2O_4$ Composition
$MgAl_2O_4$ *(1500°C, 12 h)*	------	------	a = 8.083	2.2±0.1	MgO • 1.1 Al_2O_3
3-Phase *(1500°C, 12 h)*	a = 5.142	a = 4.761 c = 12.998	a = 8.068	3.0±0.2	MgO • 1.5 Al_2O_3
0V; 0mA *(1450°C, 30s)*	a = 5.143	a = 4.759 c = 12.992	a = 8.075	------	------
50V; 25mA *(1430°C, 30s)*	a = 5.142	a = 4.760 c = 12.995	a = 8.054	2.8±0.2	MgO • 1.4 Al_2O_3
100V; 25mA *(1350°C, 30s)*	a = 5.144	a = 4.756 c = 12.994	a = 8.044	3.2±0.2	MgO • 1.6 Al_2O_3
250V; 25mA *(1230°C, 30s)*	a = 5.143	a = 4.761 c = 12.999	a = 8.031	3.6±0.2	MgO • 1.8 Al_2O_3
500V; 25mA *(1150°C, 30s)*	a = 5.136	a = 4.758 c = 12.984	a = 8.057	3.1±0.1	MgO • 1.6 Al_2O_3
250V; **75**mA *(1230°C, 30s)*	a = 5.138	------	a = 7.988	6.2±0.4	MgO • 3.1 Al_2O_3

Table 3.2: Lattice parameters and compositions of conventionally and field assisted sintered samples listed with calculated temperatures from Table 3.1

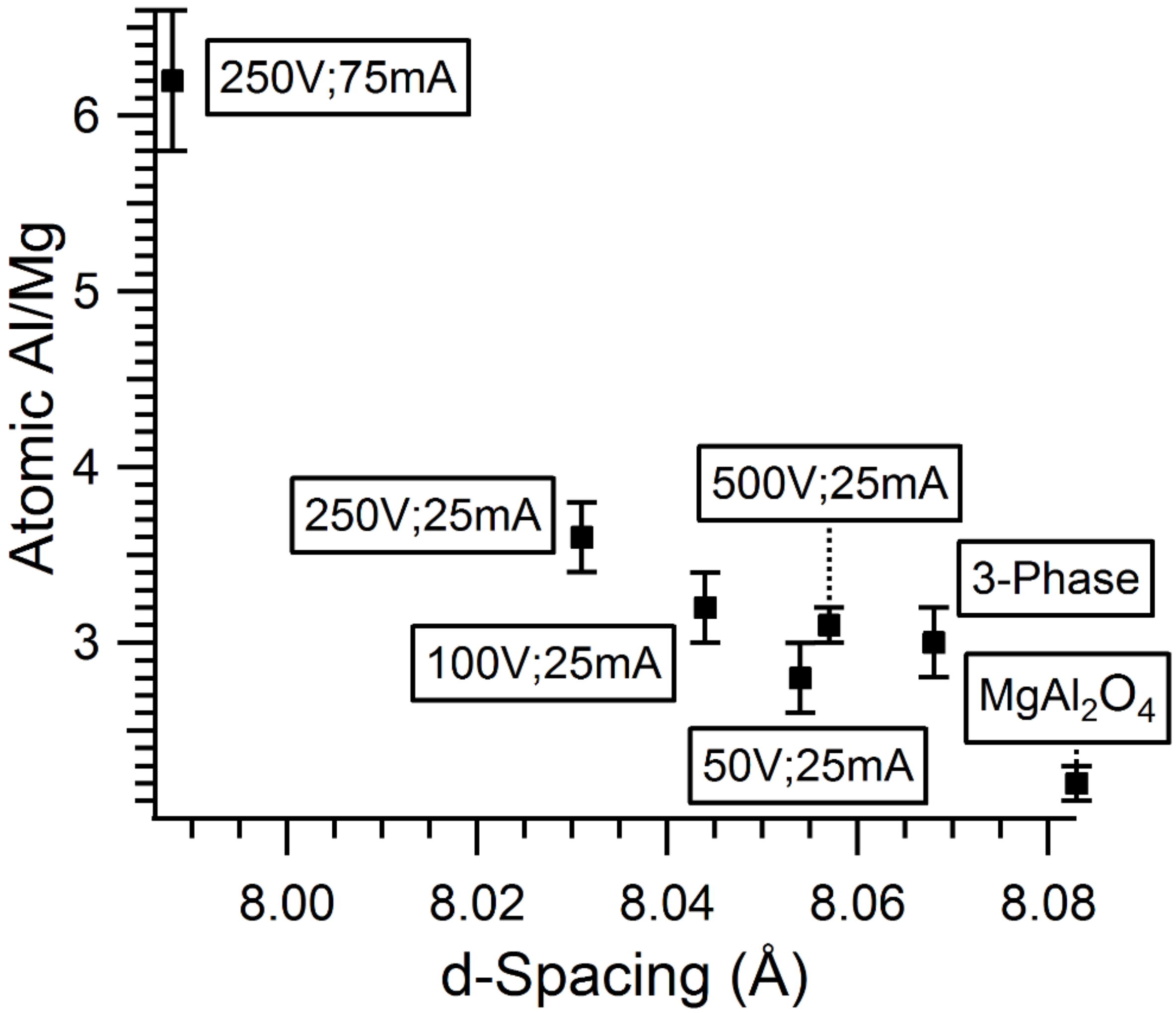

Figure 3.12: Lattice parameter as a function of atomic % Al/Mg

The Al/Mg ratio in the spinel grains was measured by EDS analysis of all samples. EDS analysis on conventionally sintered single-phase spinel using the same powders as for the three phase samples, shows that the starting spinel was close to being stoichiometric, MgO•1.1 Al_2O_3. For conventionally sintered single-phase spinel, the lattice parameter as measured by XRD matches the PDF file 00-021-1152. The conventionally sintered three-phase material has a slight increase in the Al/Mg ratio, MgO•1.5 Al_2O_3. which could be due to dissolution of alumina in the spinel after sintering for 12 hours at the high temperature of 1500°C. Under 250 V/cm at 25 mA/mm^2 the spinel composition deviates significantly from the starting nearly stoichiometric composition; it is now $MgO\bullet1.8\ Al_2O_3$. At a current density of 75 mA/mm^2 the composition is further enriched in alumina to $MgO\bullet3.1\ Al_2O_3$. The decrease in lattice parameter of spinel correlates with EDS measurements of higher alumina content in solid solution and with higher current density (Figures 3.11 and 3.12). The case of 500 V/cm at 25 mA/mm^2 is an exception since here the Al/Mg ratio and the spinel lattice parameter is observed to decrease relative to 250 V/cm at 25 mA/mm^2, which may be a result of the much lower flash temperature at this field.

The phase diagram in Figure 3.13 shows that the solubility of alumina in spinel increases with temperature.[54] Accordingly, from thermodynamic equilibrium the spinel composition is expected to be $MgO\bullet1.5Al_2O_3$ at 1500°C, which matches the composition measured in the conventionally sintered specimen that had been held for 5 hours at 1500°C. In contrast, for the case of 250 V/cm and 25 mA/mm^2, where the specimen temperature during the flash is estimated to be only 1390°C, EDS analysis yields a much higher alumina content, $MgO\bullet1.8\ Al_2O_3$.

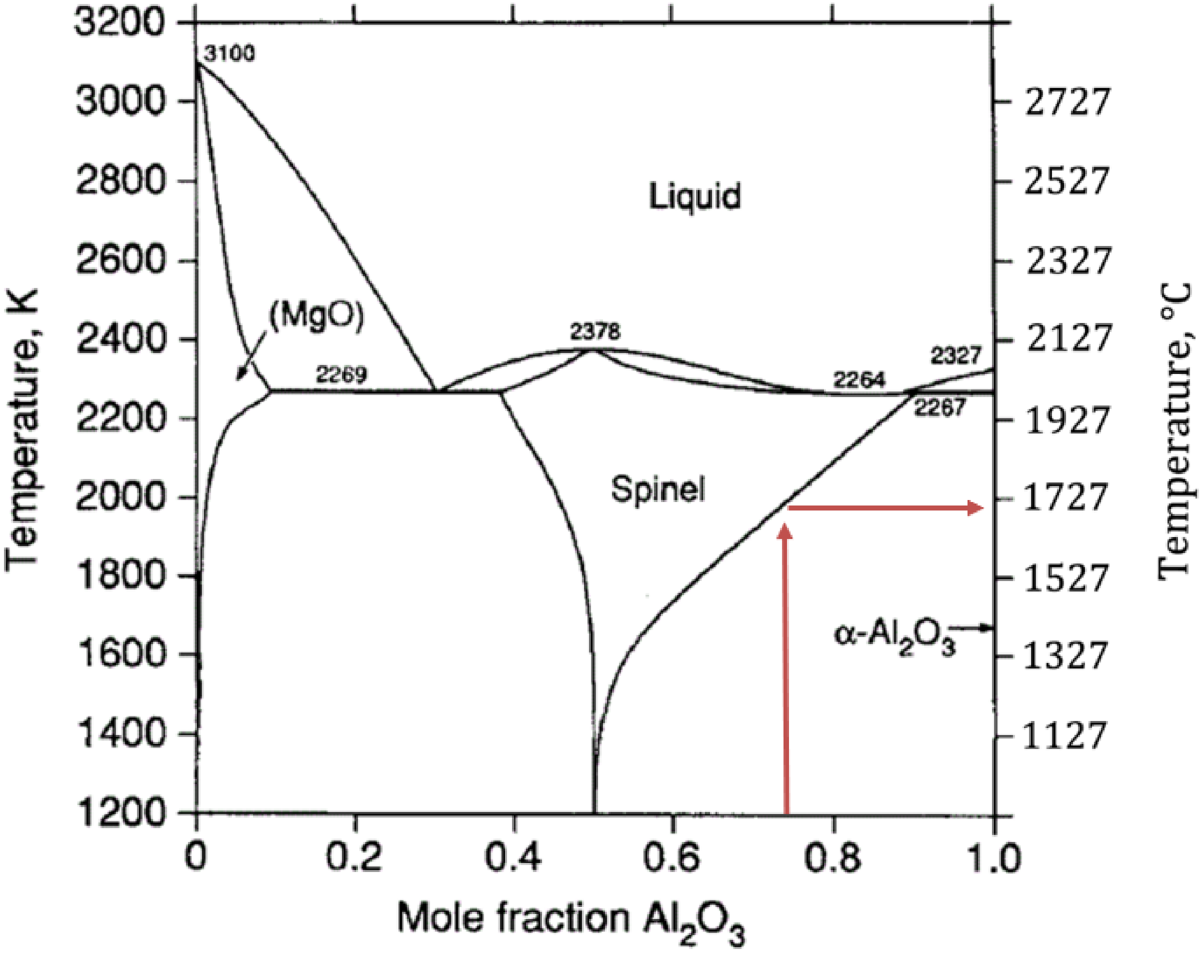

Figure 3.13: MgO – Al2O3 equilibrium phase diagram (modified from Hallstedt[54]). Temperature for formation of MgO•3Al$_2$O$_3$ is highlighted

At 250 V/cm and 75 mA/mm^2, when the calculated temperature of the specimen would have reached 1500°C but for only 30 seconds, the spinel composition is MgO•3Al$_2$O$_3$, which is hugely different than the prediction from the phase diagram. The phase diagram predicts this composition of the solid solution to be possible only at 1700°C, highlighted in the phase diagram in Figure 3.13. If all the alumina is consumed to produce a non-stoichiometric spinel, this would correspond to an Al$_2$O$_3$/MgO molar ratio of 0.80/0.20 on the phase diagram in Figure 3.13 with a single-phase spinel conversion temperature of

1800°C. Therefore, we attribute the formation of single-phase spinel at a sample temperature of 1500°C within 30 seconds to the electric field effect of flash sintering.

Currently the role of 8YSZ in the flash sintering of the three-phase samples are unknown. Deviations in the 8YSZ lattice parameters (Table 3.2) are seen in the 500V; 25mA and 250V; 75mA samples. This phase may need to be present in a minimum concentration to promote flash sintering. Previously published research on binary compositions of tetragonal zirconia (TZP) and alumina demonstrated that flash sintering is enhanced by the addition of TZP, which is attributed to increased conductivity from the presence of the zirconia phase.[20, 55]

The spinel microstructures in Figures 3.8 and 3.9 has some features reminiscent of a melt, but according to the phase diagram melting would require temperatures above 2000°C. Enhanced creep is expected under high electric fields[22] but creep due to intergranular liquid phase formation should also be considered. Eutectic liquid phases can form at high temperatures (≥ 1715°C for Al_2O_3-Y_2O_3-ZrO_2[56] and ≥ 1807°C for Al_2O_3-MgO-ZrO_2[57]). However, no pockets of residual amorphous intergranular phases were observed. It is possible that there were some loss of MgO from the spinel[58] during flash sintering in the sample where only solid solution spinel was found but no alumina phase, since the measured composition of MgO•3.1 Al_2O_3, corresponds to Al_2O_3 molar fraction of 0.76, whereas the starting powders contained 0.80 molar Al_2O_3.

3.4 Conclusions

Flash sintering of a three-phase composites constituted from equal volume fractions of alumina, spinel, and 8YSZ under a DC electric field produced samples with > 90% density in a few seconds at furnace temperatures of 1150-1430°C. The temperature for flash sintering dropped from 1350 to 1150°C as the electric field was increased from 100 V/cm to 500 V/cm. The transition to flash occurred at a power density of 6-20 mW/mm^3 regardless of the electric field. Higher fields led to a smaller grain size by lowering the flash temperature; an average grain size of 470 nm at a field of 500 V/cm and current density of 25 mA/mm^2 was obtained. Increasing the power density to 600 mW/mm^3 by increasing the current density to 75 mA/mm^2 at a field of 250 V/cm resulted in dramatic grain growth as well as the dissolution of alumina to form a solid solution of spinel of composition $MgO \bullet 3Al_2O_3$ in just 30 seconds.

CHAPTER 4: IN-SITU STUDIES ON FLASH SINTERING OF THREE-PHASE COMPOSITES

4.1 Abstract

In-situ X-ray diffraction measurements at Argonne National Laboratory (ANL) shows that α-Al_2O_3 and $MgAl_2O_4$ react nearly instantaneously and completely, and nearly completely to form single-phase high-alumina spinel during voltage-to-current type of flash sintering experiments. The initial sample was constituted from powders of α-Al_2O_3, $MgAl_2O_4$ spinel, and cubic 8 mol% Y2O3-stabilized ZrO_2 (8YSZ) mixed in equal volume fractions, the spinel to alumina molar ratio being 1:1.5. Specimen temperature was measured by thermal expansion of the platinum standard. These measurements correlated well with a black body radiation model, using appropriate values for the emissivity of the constituents. Temperatures of 1600-1736°C were reached during the flash, which promoted the formation of alumina-rich spinel. In a second set of experiments the flash was induced in a current rate method where the current flowing through the specimen is controlled and increased at a constant rate. In these experiments we observed the formation of two different compositions of spinel, $MgO \bullet 3Al_2O3$ and $MgO \bullet 1.5Al_2O_3$, which evolved into a single composition of $MgO \bullet 2.5Al_2O_3$ as the current continued to increase. In summary, flash sintering is an expedient way to create single-phase, alumina-rich spinel. A follow up in-situ experiment was done at Brookhaven National Laboratory (BNL). Using the higher in-situ scan rate at BNL, the solid solution reaction of alumina and spinel was observed to occur < 1 second.

4.2 Experimental Procedure

At ANL data was recorded in total scan mode or local scan mode. In total scan mode, the detector traverses the full range of 2Θ. In local scan mode, the detector remains fixed at a specific 2Θ angle and captures the diffracted peaks with 4°. Local scan mode allows for more rapid scans (one scan per 3 seconds). Due to the fast sintering times of flash sintering, in-situ data could be collected only in the local scan mode. PDF files for cubic 8YSZ (# 00-030-1468), spinel (# 00-021-1152) and alumina (# 01-070-7346) were converted to the synchrotron radiation wavelength and used for peak identification and indexing.

The shift in the (111) platinum peak was measured in the total scan mode and converted into specimen temperature using the standard values for the thermal expansion of platinum.[59] This baseline temperature calibration was obtained by heating the sample to different temperatures without applying an electric field. The calibration curve is shown in Figure 4.1. The sample temperature during flash sintering was determined from this curve. Note that a platinum standard was necessary because of the evolution of different phases, with different lattice parameters[15, 39].

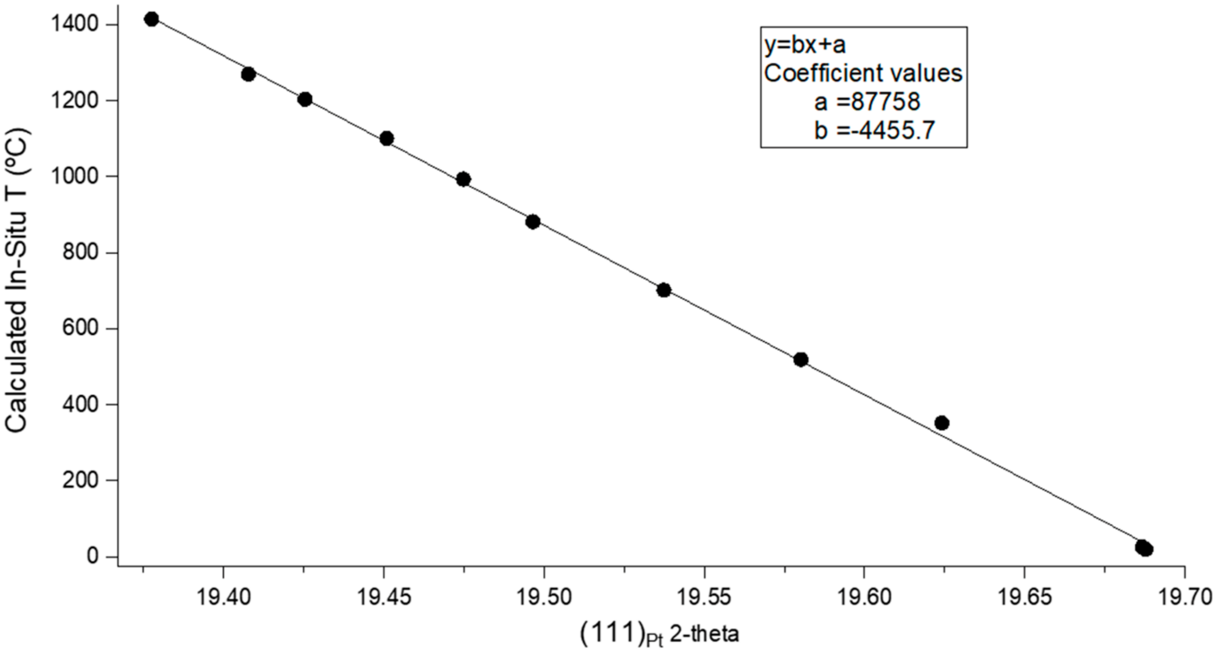

Figure 4.1: The calibration of the specimen temperature measured by the shift of the (111) peak of platinum

Flash sintering experiments at APS began by heating the furnace with the sample in position for 5 minutes to allow for equilibration of the sample temperature at 1250°C. Before the onset of flash sintering, at 1250°C 8YSZ has the highest electrical conductivity (0.52 S/cm) of the three phases. This is followed by spinel (5 x 10-4 S/cm), and alumina (2 x 10-5 S/cm).[3, 60, 61] Two categories of flash experiment were conducted. The first set of experiments utilized a voltage control to current limiting profile. The magnitude of the electrical fields and the current limit for these experiments are given in Table 4.1.

In the second set of experiments, a current ramping profile was used. The current was increased at a constant rate of 25 mA/min until it reached the current density of 85 mA/mm^2. In these current ramping experiments, the flash sintering process is slower which allows more detailed analysis of the spinel phase transformation. Table I list the parameters for these experiments. The diffraction data in the total scan mode, was taken before and after the flash. In the case of the experiments done in local mode, in-situ data at a scan rate of one scan per 3 seconds was done.

A follow up experiment was done at BNL with the same flash sintering conditions used at ANL for current ramping experiments (Figure 4.1). Due to the faster scanning rate at BNL, full 2Θ scans were able to be done with a scan rate of one scan per second.

Experiment Type	**Field (V/cm)**	**Current (mA/mm^2)**	**Flash Profile**
ANL (Total Scan)	450	75*	Current Limiting
ANL (Local Scan)	450	85*	Current Limiting
ANL (Local Scan)	450	(max current) 85	Current Ramping
BNL	450	(max current) 85	Current Ramping

Table 4.1: List of experiments conducted at ANL and BNL

4.3 Results and Discussion

4.3.1 Full Scan Experiments at ANL

The total-scan diffraction patterns for the current limiting profile taken before and after flash sintering are shown in Figure 4.2. The scan before flash sintering shows the three starting phases. However, the alumina peaks are absent in the scan taken after flash sintering. At the same time the spinel peaks are more intense and shifted to the right suggesting a decrease in the lattice parameter.

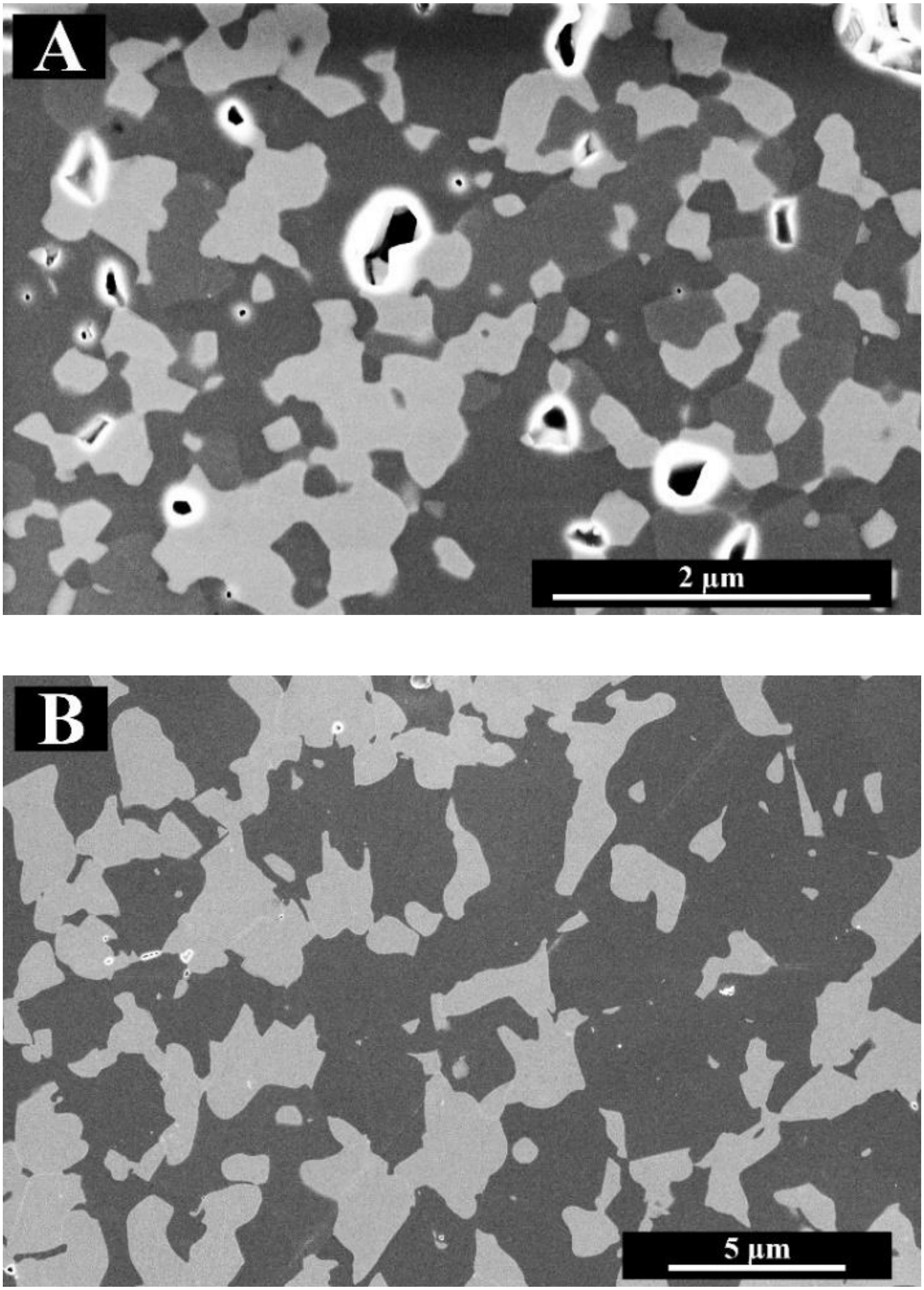

Figure 4.2: SEM microstructure of three-phase composites flash sintered with a current limiting profile (A) 250V/cm; 25mA/mm^2 (B) 250V/cm; 75mA/mm^2

A shift in the zirconia peaks is also seen and thought to be due to the effect of the dopants.[62] The XRD data in Figure 4.3 matches previous observations, where high alumina spinel was formed during flash sintering.[63]

The in-situ data for the local scan experiment is shown in Figure 4.4. The 2Θ range for the local scan was chosen so that peaks from all three phases, as well as the platinum (111) peak could be included. Note that the dissolution of alumina and formation of high-alumina spinel occurred within one scan, that is within 3 seconds, between the second and the third scan. The formation of high-alumina spinel also corresponds to a large jump in temperature measured with the platinum standard, 1405°C to 1736°C (as described later). In the current ramping profile, residual amounts of alumina can still be seen in Figure 4.4, but the bulk of the alumina was consumed in forming the high-alumina spinel. Video of the in-situ data can be found in the supporting information published by Kok et al.[64]

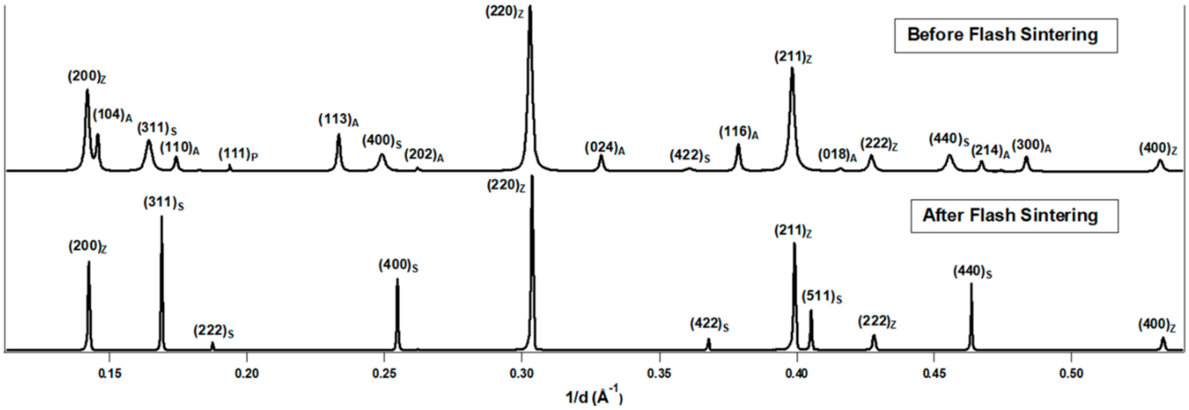

Figure 4.3: Full 2Θ (total scan) XRD pattern from before and after flash sintering at 450 V/cm; 75mA/mm^2 done at ANL

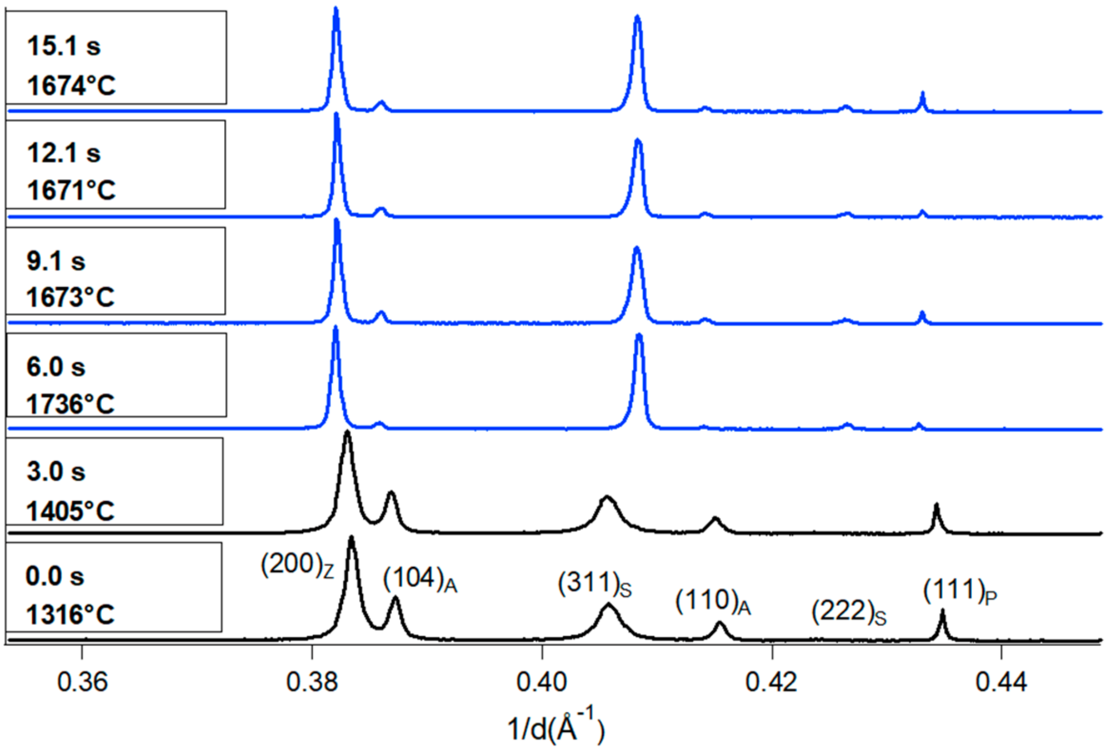

Figure 4.4: In-situ synchrotron XRD pattern obtained at current ramping profile with a limited 2Θ (local scan) at ANL

4.3.2 Current Ramp Experiments at ANL and BNL

In contrast to the current limiting experiments where the sintering occurs quickly at the onset of the flash, the process occurs more slowly in current ramping experiments where the current is injected and increased at a constant rate. Figure 4.5 shows the power density curves for the live experiments; they illustrate the difference between the flash sintering profiles for current limiting and currenting ramping experiments. In current limiting experiments the powder density rises quickly at the onset of the flash and reaches a plateau as the power supply is switched to current control. In current ramping experiments the power dissipation spikes at the onset of the flash and then continues to rise as the current is increased.

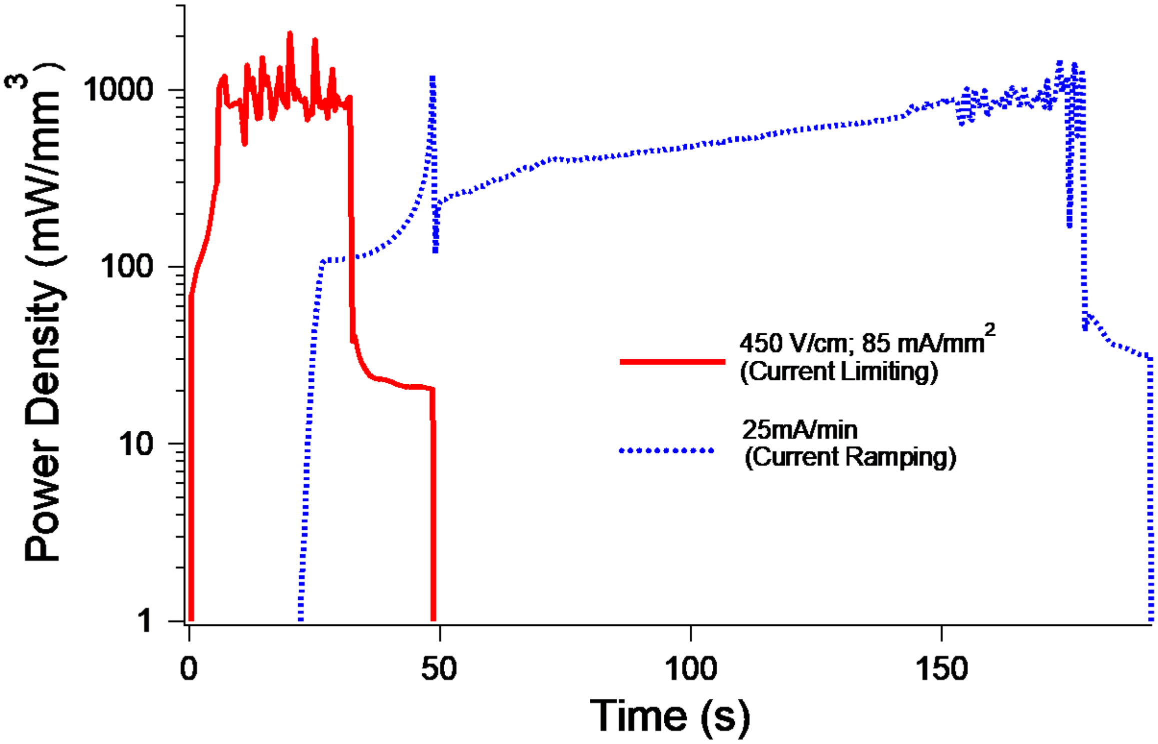

Figure 4.5: Power density curve of current limiting and current ramping flash sintering profiles

The current ramping experiment slows down the spinel phase transformation, as shown by the data in Figure 4.6. The onset of the flash is indicated again by a large increase in temperature of 1384°C to 1526°C (the measurement of the temperatures is described in more detail in the following section), between the scans at 45.5 seconds and 48.6 seconds. As the current increases, the (311) spinel peak splits into two distinct peaks. The intensity of the right peak begins to decrease with time and increasing current density, with the left peak shifting to the right. The double peak eventually evolves into a single (311) spinel peak of the high-alumina spinel phase. Again, a small amount of residual alumina remains.

The temperature profiles obtained from the platinum standard are discussed in the following section.

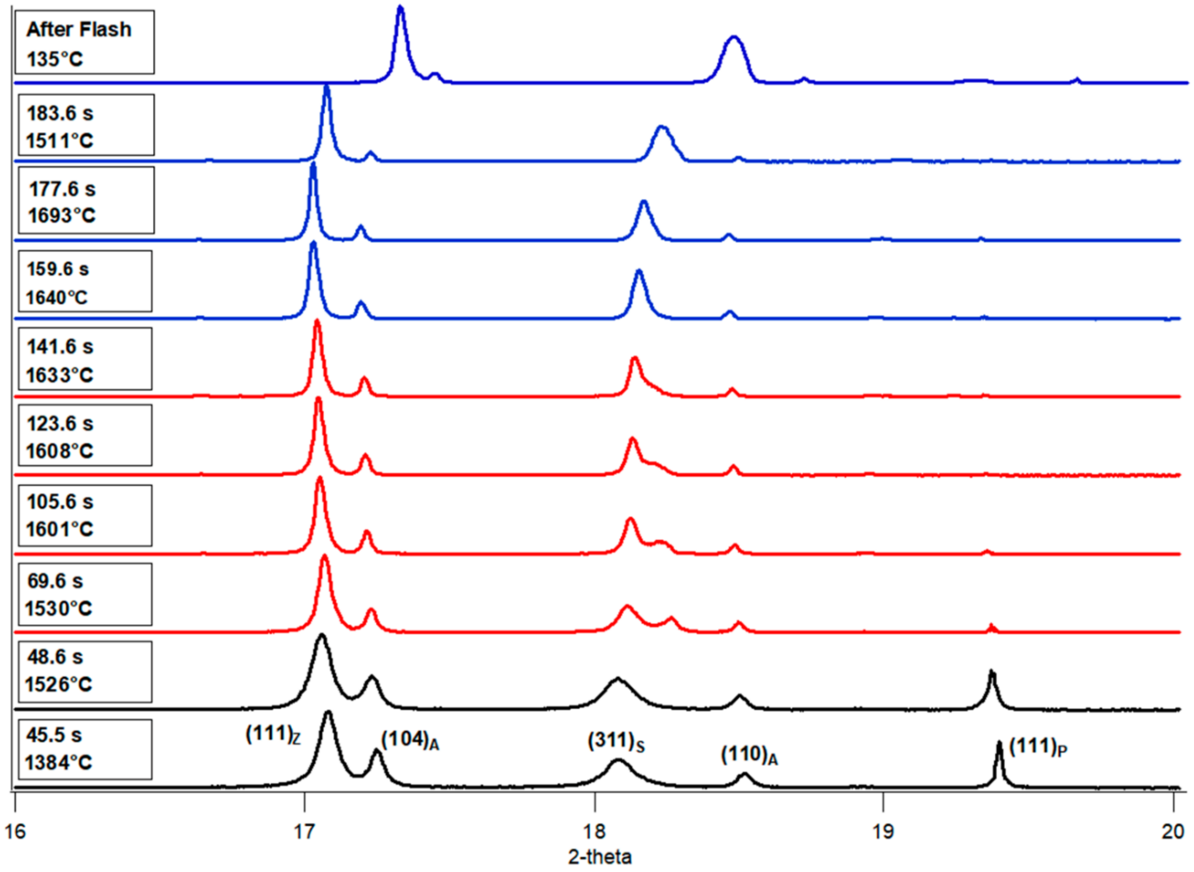

Figure 4.6: Selected in-situ synchrotron XRD patterns obtained under Type B current rate controlling flash conditions

The in-situ experiment carried out at BNL shows that the formation of high-alumina spinel during the flash sintering of the three-phase composite occurs within 1 second between the voltage control stage to the onset of flash sintering (Figure 4.7). In the voltage control stage, there is an increase of the sample temperature as indicated by the shifting of the platinum standard peaks. At the onset of flash sintering, the platinum peaks are no longer detected. This is attributed to the brief melting of the platinum standard at the onset of flash. As the flash sintering progresses to the current control stage, the limiting of the Joule heating in this stage reduces the sample temperature enough so that the platinum standard re-crystalizes and the platinum peaks are again detected.

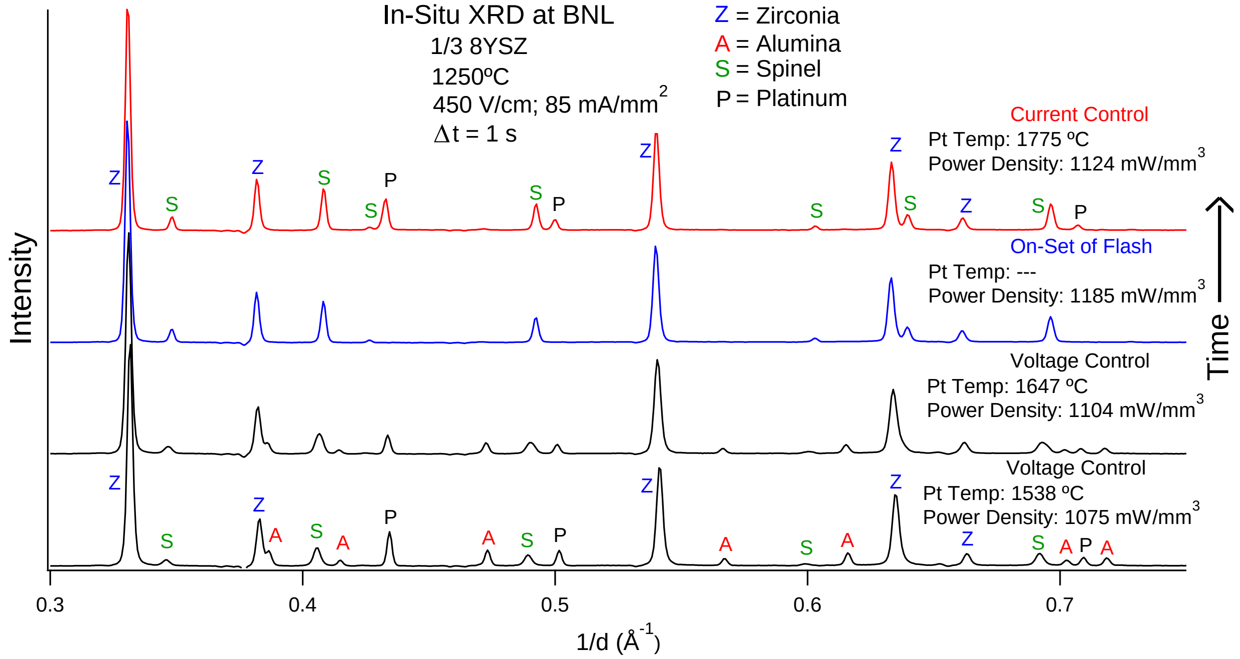

Figure 4.7: In-situ XRD experiments done at BNL (XRD scans shown before and after the on-set of flashing, with each scan being 1 second apart)

4.3.3 Measurements (Pt Standard.) and Black Body Radiation Estimate of Temperature

As shown with Jha et al, using a blackbody radiation equation (Equation 4.1) can be an effective method to estimate the sample temperature during flash sintering.[15]

$$\frac{T}{T_o} = [1 + \frac{1000W_V}{e_m \sigma T_o^4}\left(\frac{V}{A}\right)]^{1/4} \tag{4.1}$$

where T is the specimen temperature, T_o is the furnace temperature, W_V is the power density expended in the specimen in units of mW mm^{-3}, e_m is the emissivity, $\sigma = 5.67 \times 10^{-8}$ W m^{-2} K^{-4} is the Stefan Boltzmann constant, and V/A is the volume to surface area of the specimen in units of mm. In this section we report the best possible estimate of the specimen temperature by two methods, the black body radiation (BBR) model of Equation (1) and measurements of thermal expansion of the platinum standard.

Both methods have constraints. The BBR model applies only when the specimen is in the steady state, as is the case for current limiting experiments where the power density remains at a plateau. In the current ramping experiments where the power density is constantly increasing the steady state BBR model is not applicable since the electrical energy partitions in to specific heat and the radiation loss. Thus, the BBR model only is applied to the experiment where a current limiting profile is used.

The platinum standard method also has constraints since as shown in Figure 4.1 the calibration extends only up to about 1400°C since beyond that platinum paste begins to volatilize and the (111) peak becomes faint, as can be seen in Figure 4.6. High magnification of the peak at higher temperatures is shown in Figure 4.8. The dashed line shows the extrapolation of the calibration curve from Figure 4.1. The extrapolation extends to 1736°C, which is just below the melting point of Pt, 1768°C. These peaks are difficult to resolve, so the results presented for the temperatures estimated from them are subject to a degree of uncertainty. Nevertheless, these results are presented for the sake of being as complete as possible.

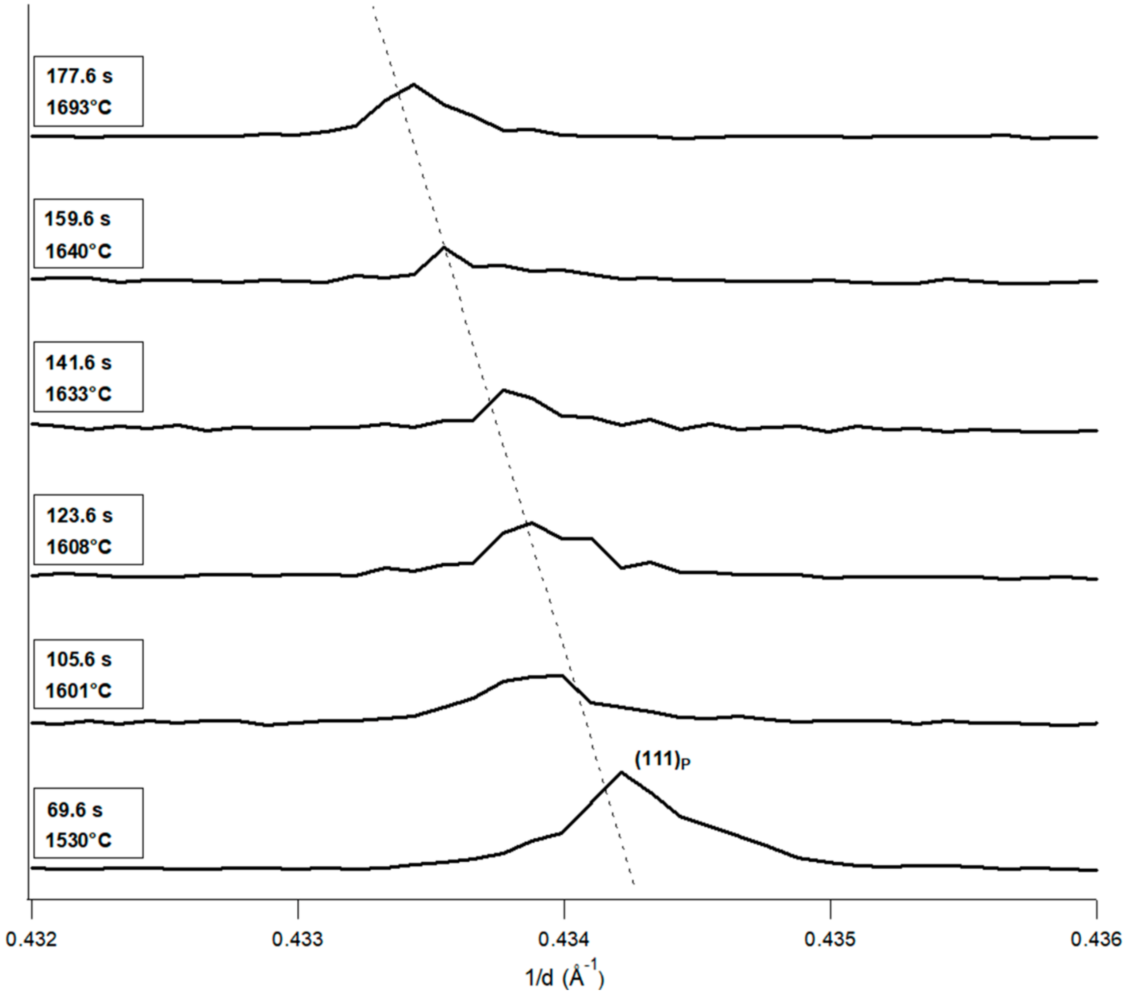

Figure 4.8: (111) Platinum peak shift and calculated temperatures during current ramping flash conditions

The application of the BBR model requires knowledge of the emissivity, which is both material and temperature dependent. For YSZ an emissivity value of 0.9 seems appropriate.[27] Literature values for the emissivity values[65, 66] for Al_2O_3 and $MgAl_2O_4$ were extrapolated to 1600°C; they were 0.47 for Al_2O_3 and 0.19 for $MgAl_2O_4$. Due to the large differences in the values for the three phases, the rule of mixtures and the inverse rule of mixtures was used to estimate the upper bound and lower bound for the emissivity of the composite; they were 0.52 and 0.35. A lower emissivity value predicts higher specimen temperature since it reduces the energy lost to black body radiation.

In the case of current limiting experiments, the BBR model is acceptable since the power density reaches a plateau indicating a steady state in the specimen temperatures. The estimated BBR temperature, using the emissivity values given just above, as well as the temperature estimated from the platinum standard are shown in Figure 4.9. The Pt-standard method predicts the sample temperature during the steady state of flash to lie between 1670-1736°C. These range falls within the upper and lower bounds calculated by the black body radiation using the higher and lower values of the emissivity.

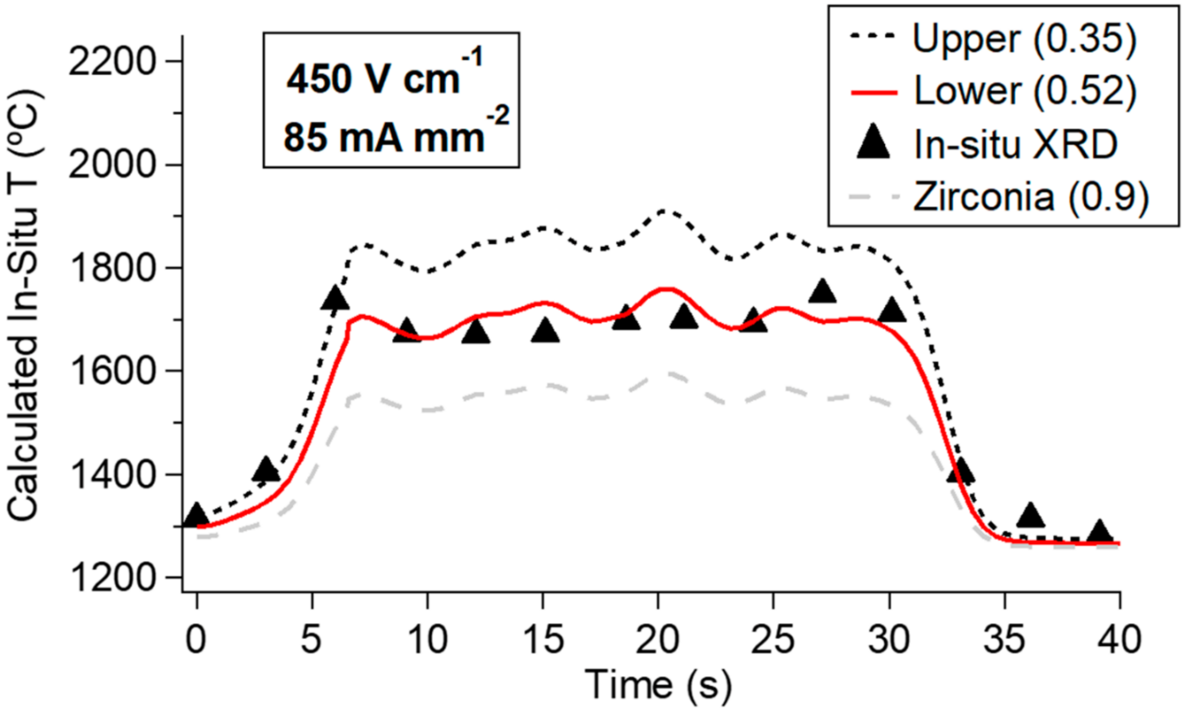

Figure 4.9: Calculated black body radiation temperatures compared with temperatures calculated from in-situ temperatures from the platinum standard. Calculated black body radiation temperatures with zirconia emissivity (0.9) is also shown for reference.

For comparison the prediction using emissivity of 0.9, the accepted value for zirconia, is also shown; it predicts lower specimen temperature. It is to be noted that the data for emissivity of various materials are not readily available and carry a significant degree of uncertainty.

The current ramping experiments have the advantage that the sample temperature rises more gradually, being controlled by the rate at which the current is increased. However, being a non-steady state process only the Pt-standard method is applicable. In Figure 4.6 the (111) Pt peak is seen to shift as the power density expended in the sample increases. The Pt peaks grow faint above ~1400°C, and the exploded view of the peaks, shown in Figure 4.8, which carries a degree of uncertainty, was used to estimate the specimen temperature.

The measurement of the specimen temperature by the Pt-standard method while the power density increases are shown in Figure 4.10. The data was obtained from successive local scans. In this plot we see that the specimen temperature rises from about 1485°C to 1525°C at the onset of the flash, and then continues to rise to about 1675°C until the end of the experiment. The dissolution of the α-alumina phase begins at about 1500°C with the development of the second peak for spinel, and is completed by about 1640°C. However, measurable amount of alumina is retained even after the experiment ends and the furnace is cooled down, as shown by the diffraction spectra in Figure 4.6.

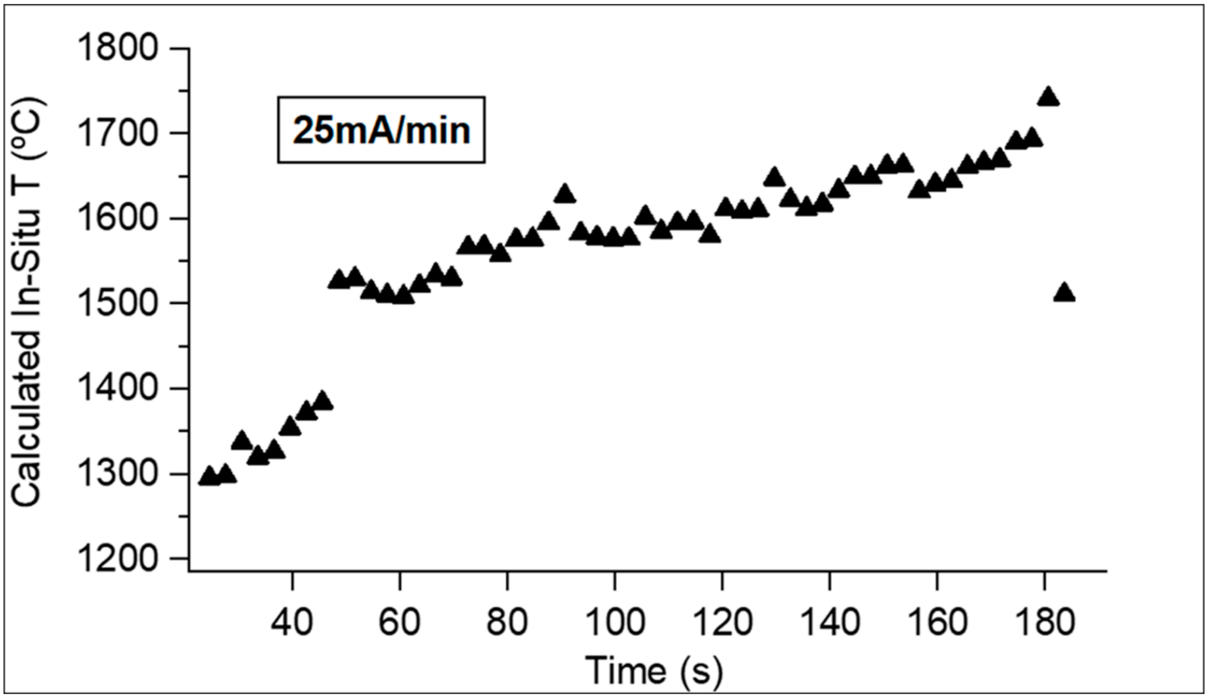

Figure 4.10: Calculated in-situ temperature from the platinum standard from current ramping experiment at ANL

The comparison between the evolution of the spinel phase is different in current limiting and current ramping experiments as shown by Figures 4.4 and 4.6. In the current limiting experiment, the transformation is faster and more complete (although some residual alumina remains) than in the current ramping experiment. Furthermore, the splitting of the spinel seen in current ramping is not seen in the current limiting experiment.

4.3.4 Kinetics of Phase Transformation

In this section the kinetics of the reaction is analyzed in terms of a previous study of the reaction between alumina and spinel to form non-stoichiometric spinel.[68]
Using Fick's second law and the high alumina spinel composition from previous data ($MgO \bullet 3Al_2O_3$), the reaction time could be calculated based on the grain size of spinel.[63]

This analysis is based upon Fick's second law (Equation 4.2) and shown as an illustrated schematic in Figure 4.11.

$$\frac{C_x - C_o}{C_s - C_o} = 1 - \operatorname{erf}\left(\frac{x}{2\sqrt{Dt}}\right) \qquad (4.2)$$

where we insert the following values for the parameters for the present work,

C_x = Conc. At x (0.75 mol% alumina)
C_o = Initial conc. at t = 0 (0.5 mol% alumina)
C_s = Surface con. at x = 0 (1.0 mol% alumina)
x = Distance (surface to middle of spinel grain)
D = Diffusion coefficient (1736°C)
t = Time

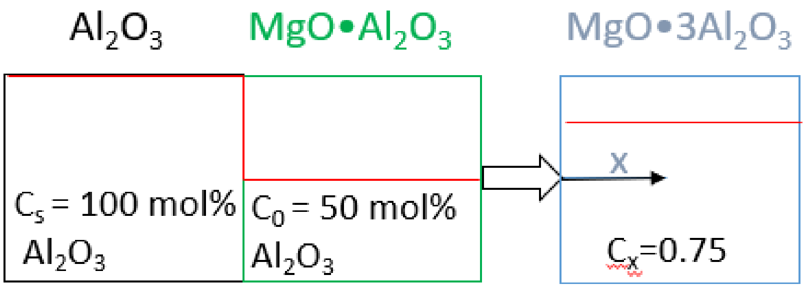

Figure 4.11: Diffusion schematic of the formation of high alumina spinel

The average particle sizes of the three-phase starting material was ~ 250 nm, but the average grain size of the high alumina spinel after flash sintering was determined from SEM analysis to be 1.5 μm. The reaction times, calculated from Equation 2, based on 0.5, 1.0, 2.0, and 3.0 μm spinel grain sizes are summarized in Table 4.2.

Initial Spinel Grain Size (μm)	**Calc. Reaction Time (s)**
3.0	5.6
2.0	2.5
1.0	0.6
0.5	0.2

Table 4.2: Reaction time to form high alumina spinel based on initial spinel grain size at a temperature of 1736°C

These results suggest that the temperature reached during flash sintering in this study may have been sufficient for the formation of high alumina spinel starting with a spinel grain sizes of 2 μm or smaller, with the caveat that the specimen temperature was estimated from faint and rather broad peaks of platinum as shown in Figure 4.8. It should be noted that this temperature estimation assumes that the applied electric field does not influence the grain growth kinetics during flash sintering. Both grain growth reduction and enhancement during flash sintering have been reported.[5, 29, 60, 69–71] The reaction time of formation of high alumina spinel in this study has already been determined to be 1 second or less though in-situ XRD at BNL. The purpose of calculating the reaction time with Fick's second law is to reaffirm that this reaction is possible within 1 second with the temperatures determined from the in-situ XRD measurements. This does not preclude the possibility that the electric field influences diffusion and is just an approximation.

4.3.5 High-Alumina Spinel Compositions

The current ramping experiments at ANL, was distinguished by the evolution of two adjacent peaks for (311) spinel (Figure 4.6). Eventually the two peaks merged into a single peak before the end of the experiment. Due to the transient nature of the two (311) spinel peaks, the spinel composition associated with these peaks was determined from EDS results of bulk experiments in which samples of different high alumina spinel compositions were formed (Figure 4.12). The lattice parameter of the high alumina spinels associated with the transient spinel peaks were then adjusted for temperature and were determined to have a composition of $MgO \bullet 3.0Al_2O_3$ (7.9947 Å) and $MgO \bullet 1.5Al_2O_3$ (8.0476 Å). This suggests that two separate compositions of non-stoichiometric spinel formed initially. As the current was increased, the two stoichiometries converged into $MgO \bullet 2.5Al_2O_3$ (8.0046 Å).

Formation of alumina-rich spinel is due to Al^{3+} occupying Mg^{2+} sites in the spinel structure, but the mechanism by which this defect is charged balanced is under debate.[72, 73] The defect compensation maybe due to Al^{3+} vacancies:

$$(4\mathrm{Al_2O_3} + 3\mathrm{Mg}_{\mathrm{Mg}}^{\mathrm{x}} + \mathrm{Al}_{\mathrm{Al}}^{\mathrm{x}} \rightarrow 3\mathrm{Al}_{\mathrm{Mg}}^{\mathrm{o}} + \mathrm{V}_{\mathrm{Al}}^{\prime\prime\prime} + 3\mathrm{MgAl_2O_4})$$

or by Mg^{2+} vacancies:

$$(4\mathrm{Al_2O_3} + 3\mathrm{Mg}_{\mathrm{Mg}}^{\mathrm{x}} \rightarrow 2\mathrm{Al}_{\mathrm{Mg}}^{\mathrm{o}} + \mathrm{V}_{\mathrm{Mg}}^{\prime\prime} + 3\mathrm{MgAl_3O_4}).$$ [74, 75]

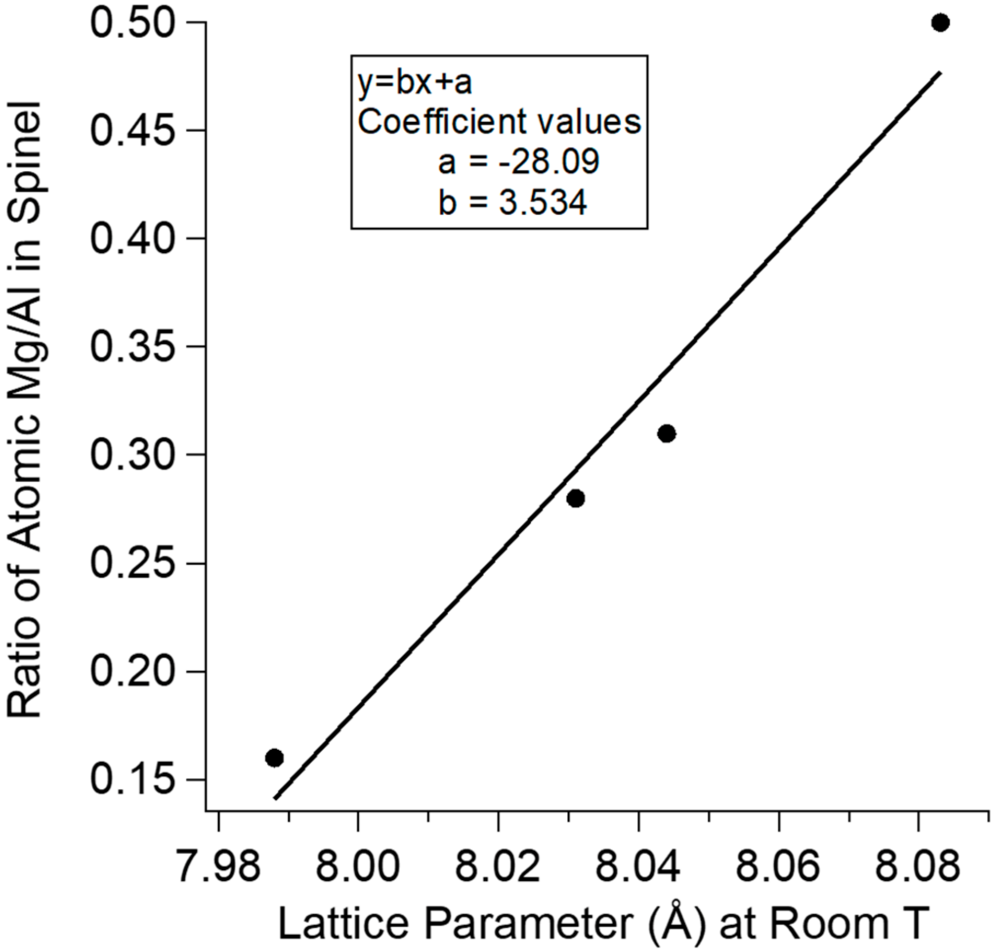

Figure 4.12: EDS results of atomic Mg/Al in Spinel in samples of high alumina spinel of various compositions

Cation incorporation energy calculations have shown that neither mechanism is thermodynamically preferred over another, so that both may occur together.[72] Flash sintering has been observed to result in the generation of defects in other flash sintered materials.[28, 76] The formation of non-stoichiometric spinel has also been found to be controlled by the generation of defect clusters.[73] These defects may explain the formation of alumina-rich spinel when flash sintering the three-phase system of alumina, spinel and 8YSZ.

4.4 Conclusions

High-alumina spinel can be formed in 1 second during flash sintering of composites constituted from equal volume fractions of alumina, spinel and 8YSZ at high current density limits. Under current limiting experiments, with 450 V/cm and a current limit of 85 mA/mm^2, the specimen temperature estimated from the Pt standard rose up to 1736°C, when the sudden formation of the high-alumina spinel phase was seen. Kinetic analysis shows that it is possible to form high alumina spinel within three seconds at such high temperature. However, it should be noted that the Pt peak position at these very high temperatures has been estimated from faint and very broad peaks of (111) Pt in the diffraction spectrum.

The black body radiation equation for the estimation of the sample temperature requires the knowledge of reliable values for the emissivity. For example, a change in emissivity from 0.38 to 0.9 can create a spread of approximately 250^{o}C in the uncertainty in the estimate of the specimen temperature.

In the current ramping experiments, the phase transformation occurs more slowly than in the current limiting experiments. Thus, two compositions of alumina-rich spinel formed as intermediates ($MgO\bullet3Al_2O_3$ and $MgO\bullet1.5Al_2O_3$) during the initial stages of flash, seen in the current ramping experiment are not present in the voltage to current limiting experiment. However, the two peaks from the dual spinel phases evolved eventually into a homogeneous composition of $MgO\bullet2.5Al_2O_3$.

CHAPTER 5: THE EFFECT OF CURRENT CONTROL HOLD AND THE AMOUNT OF ZIRCIONA IN FLASH SINTERING

5.1 Abstract

Dense, fined grained (0.3 μm) three-phase composite of equal vol. % alumina, spinel and 8YSZ is produced by flash sintering at a field of 650 V/cm with a current control hold of 6 seconds at 50 mA/mm^2 and an isothermal furnace temperature of 1450°C. Longer current control holds result in grain growth, and then subsequent formation of a high-alumina spinel phase. Reduced amounts of 8YSZ in the composites revealed that the incubation time for flash sintering is increased and demonstrates how 8YSZ may be used as a catalysis for flash sintering. Flash sintering two-phase alumina and spinel composites (without zirconia) required an extended incubation time and homogeneous sintering was difficult to obtain. Channeling of the current through the center of the sample in two-phase composites resulted in a gradient microstructure, with the grain size ranging from 150 μm in the center to 1 μm near the edges. Using only a trace amount of zirconia, a composite of MgO and spinel was flash sintered with no signs of channeling of the current.

5.2 Experimental Procedure

Composites of equal (1/3) volume percent 8YSZ-alumina-spinel, as well as samples of lesser amounts of 8YSZ (1/4, 1/6) and two-phase alumina-spinel composites were made. Samples flash sintered in isothermal laboratory experiments were done with a vertical tube furnace pre-heated to 1450°C. The applied electric field (650 V/cm) and current density (50 mA/mm^2) remained constant throughout all these experiments, but the Stage III hold times were varied to 6, 12, and/or 24 seconds for each sample.

A composite of two-phase MgO and spinel with trace amounts of 8YSZ was flash sintered at 1400°C with a field and current density of 1067 V/cm; 50 mA/mm^2 and hold time of 6 seconds. 8YSZ was introduced to the two-phase system by milling the MgO and spinel powders with zirconia media.

5.3 Results and Discussion

5.3.1 Current Control Holds

The power densities for the flash sintered samples containing equal (1/3) volume percent alumina-spinel-8YSZ with Stage III holds of 6, 12, and 24 seconds are shown in Figure 5.1. The room temperature XRD (Figure 5.2) also show that 8YSZ (PDF File: 00-030-1468), alumina (PDF File: 01-070-7346), and spinel (PDF File: 00-021-1152) are all present in each of the samples.

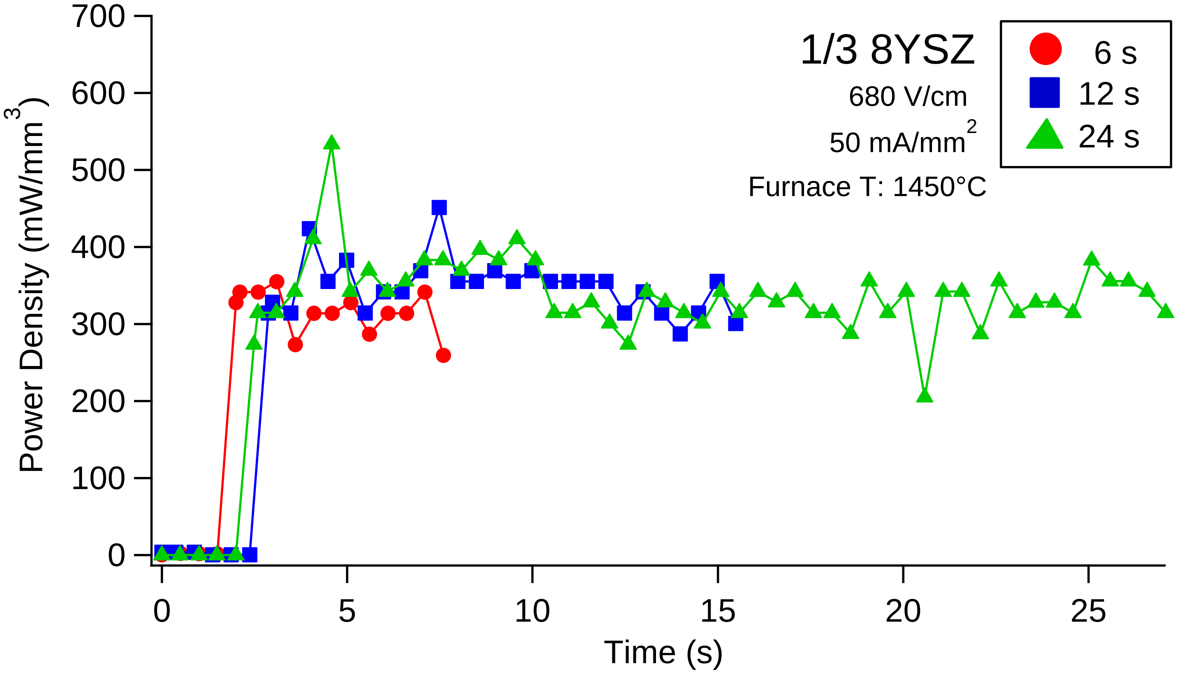

Figure 5.1: Power density vs time plot of flash sintered equal (1/3) volume percent 8YSZ-alumina-spinel composites at 6, 12, and 24 seconds

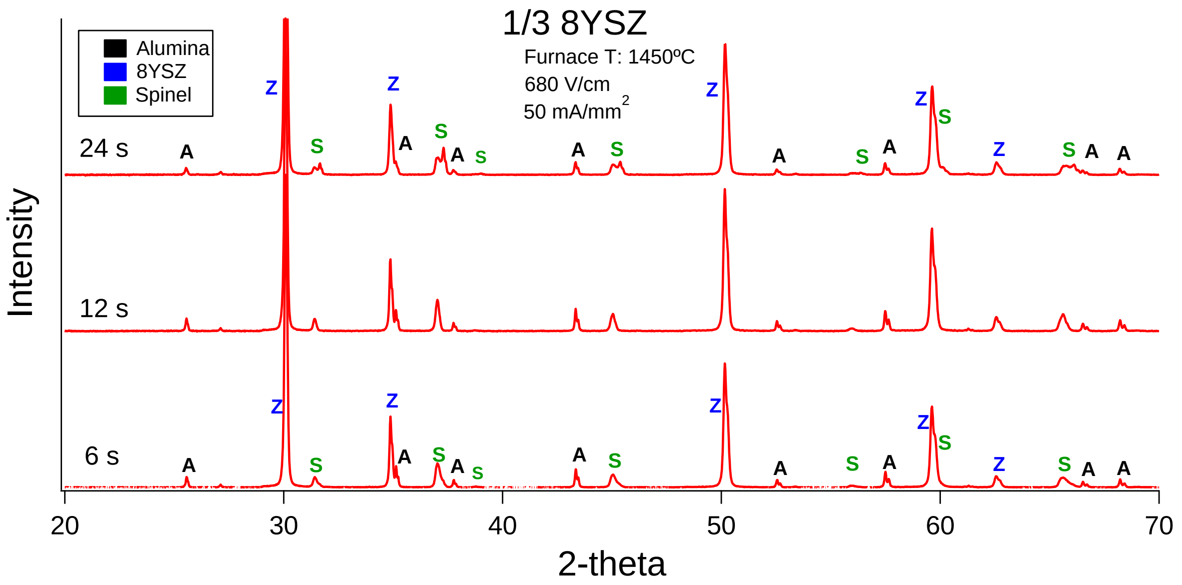

Figure 5.2 XRD patterns of equal (1/3) volume percent 8YSZ-alumina-spinel composites flash sintered at 650 V/cm and 50 mA/mm^2 with varying current control hold times

A high alumina spinel phase can be differed from stoichiometry spinel peaks their 2Θ positions. Alumina rich spinel are represent in XRD by spinel peaks but shifted to a higher 2Θ, due to the smaller d-spacing of the high-alumina spinel phase compared to stoichiometry spinel.[63] At a Stage III hold of 24 seconds, formation of a high-alumina spinel phase begins to occur along with residual stoichiometry spinel. This is seen in the doubling of each spinel peak for the sample with a 24 second Stage III hold. Figure 5.3-5.6 shows the SEM microstructure of the three-phase samples flash sintered with a current control hold of 6, 12, and 24 seconds. SEM of the 24 second sample (Figure 5.5 and 5.6) confirms the formation of high alumina spinel.

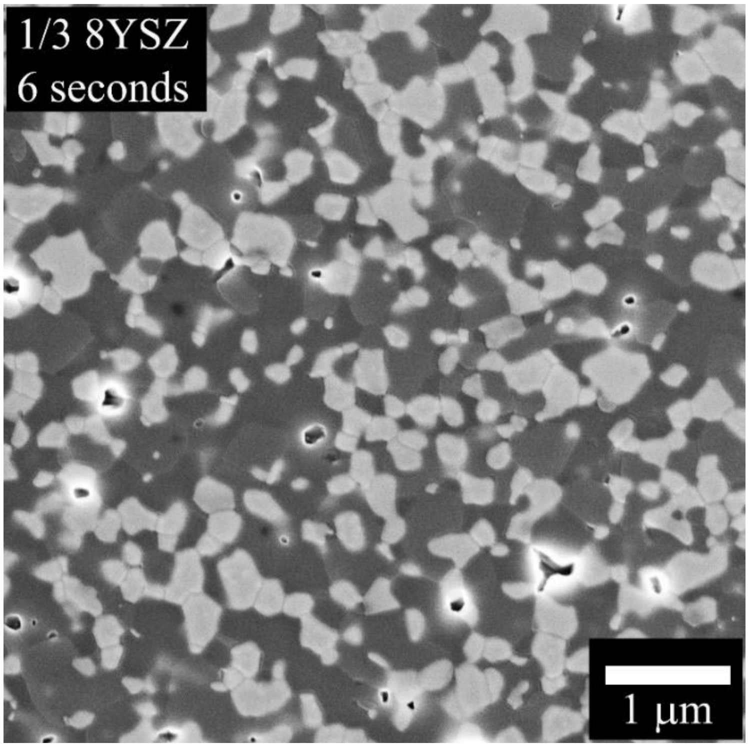

Figure 5.3: SEM of flash sintered, equal (1/3) volume percent alumina, spinel and 8YSZ composite with current control hold of 6 seconds

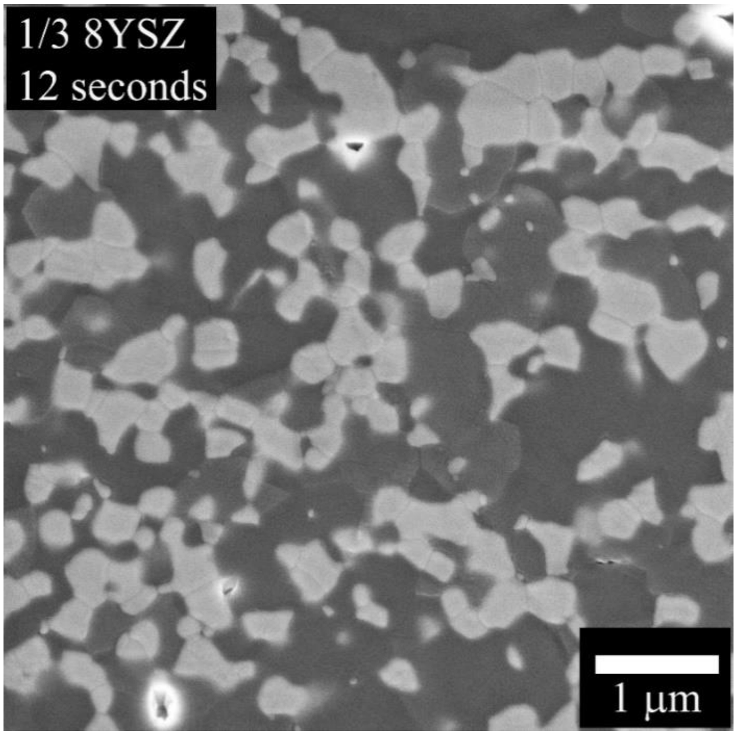

Figure 5.4: SEM of flash sintered, equal (1/3) volume percent alumina, spinel and 8YSZ composite with current control hold of 12 seconds

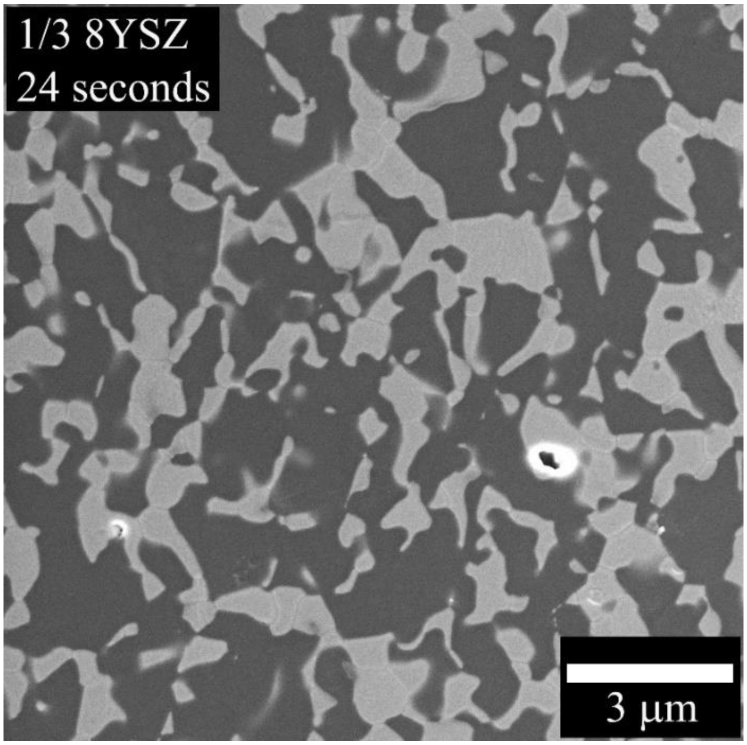

Figure 5.5: SEM of flash sintered, equal (1/3) volume percent alumina, spinel and 8YSZ composite with current control hold of 24 seconds (low magnification)

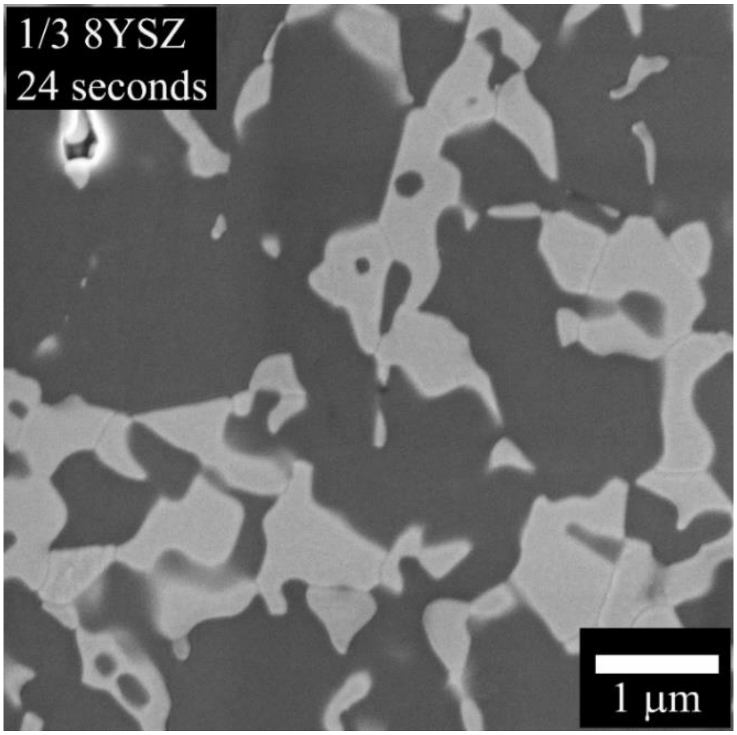

Figure 5.6: SEM of flash sintered, equal (1/3) volume percent alumina, spinel and 8YSZ composite with current control hold of 24 seconds (high magnification)

The results highlighted in Table 5.1 illustrate that limiting the current control hold can be used tailor the final grain size and the alumina content of the spinel composition. In the sample where the current hold is limited to 6 seconds (Figure 5.3), an average grain size of 0.3 μm is observed. As the current hold is increased to 12 seconds (Figure 5.4), the average grain size increases to 0.5 μm. Finally, with a current hold of 24 seconds, the average grain size is further increased to 1.5 μm and the formation of alumina rich spinel begins (Figures 5.5 and 5.6).

Composition	*Stage III Hold t (s)*	*P. Density (mW/mm^3)*	*Th. Density (%)*	*Grain Size (μm)*
1/3 8YSZ	6	350	97	0.3 ± 0.1
1/3 8YSZ	12	300	97	0.5 ± 0.2
1/3 8YSZ	24	350	92	1.5 ± 0.5
1/4 8YSZ	24	300	92	1 – 5 ± 0.5 – 1.0
1/6 8YSZ	24	300	95	1 – 7 ± 0.5 – 1.5
Alumina-Spinel	24	300 – 400	94	Center: 150 ± 27 Edge: 0.8 ± 0.2

Table 5.1: Stage III hold, power density, Archimedes density, and grain size of isothermal (1400°C) flash sintering experiments with a field of 650 V/cm; 50 mA/mm^2

5.3.2 Varying Amounts of Zirconia during Flash Sintering

The onset of flash sintering occurs instantly, without an incubation period, with the applied electric field of 650 V/cm; 50 mA/mm^2 with a composite of equal volume (1/3) alumina-spinel-8YSZ (Figure 5.7). As the amount of 8YSZ is decreased to 1/4 volume percent in the composites, an incubation period of ~10 seconds is now observed before the on-set of flash sintering. As the zirconia content is further decreased to 1/6 volume percent, a longer incubation period is required for flash sintering. The incubation time increased to over 2 minutes with a two-phase alumina and spinel system. XRD and SEM of these samples show that the formation of high alumina spinel continues to occur with decreasing amounts of 8YSZ (Figures 5.8, 5.9, and 5.10). The SEM of the alumina-spinel composite showed a gradient microstructure, with larger grains in the center of the gauge section (Figure 5.11). The power densities required to flash sinter each of the composites are listed in Table 5.1 in addition to the average grain size and Archimedes densities of the flash sintered samples. All composites flash sintered between 300-400 mW/mm^3. A wide-ranging average grain sizes were produced in this study, depending on the Stage III hold times and composite composition. Densities of all samples were above 90% theoretical density.

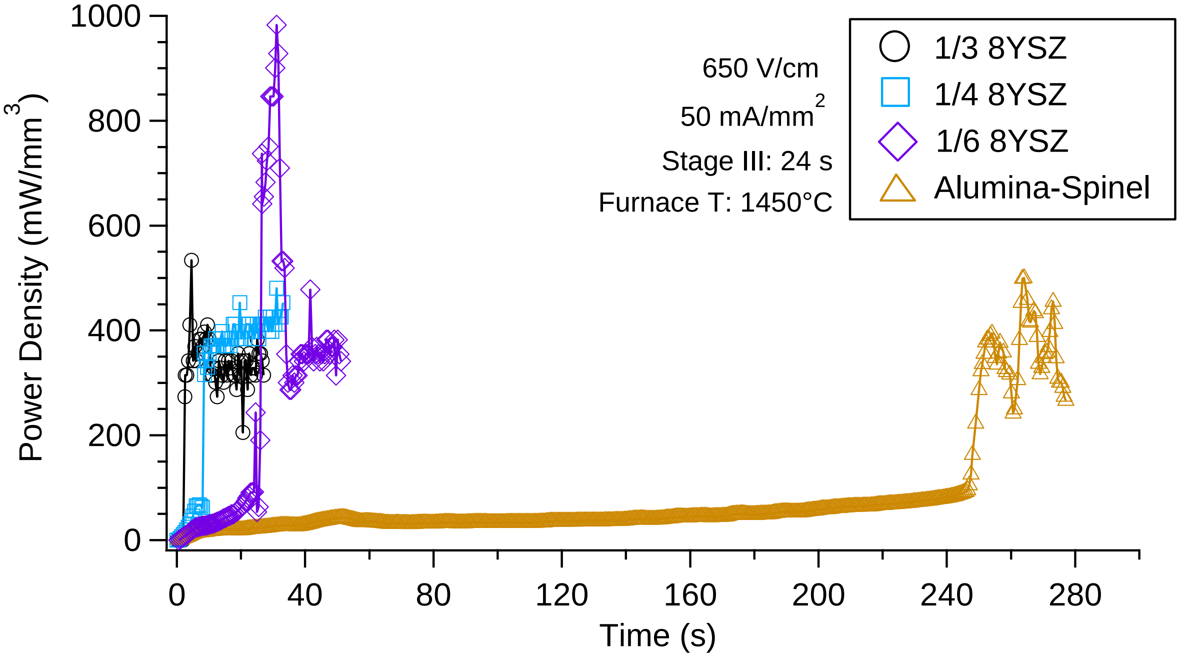

Figure 5.7: Power density vs time plot of various composites with reducing amounts of 8YSZ

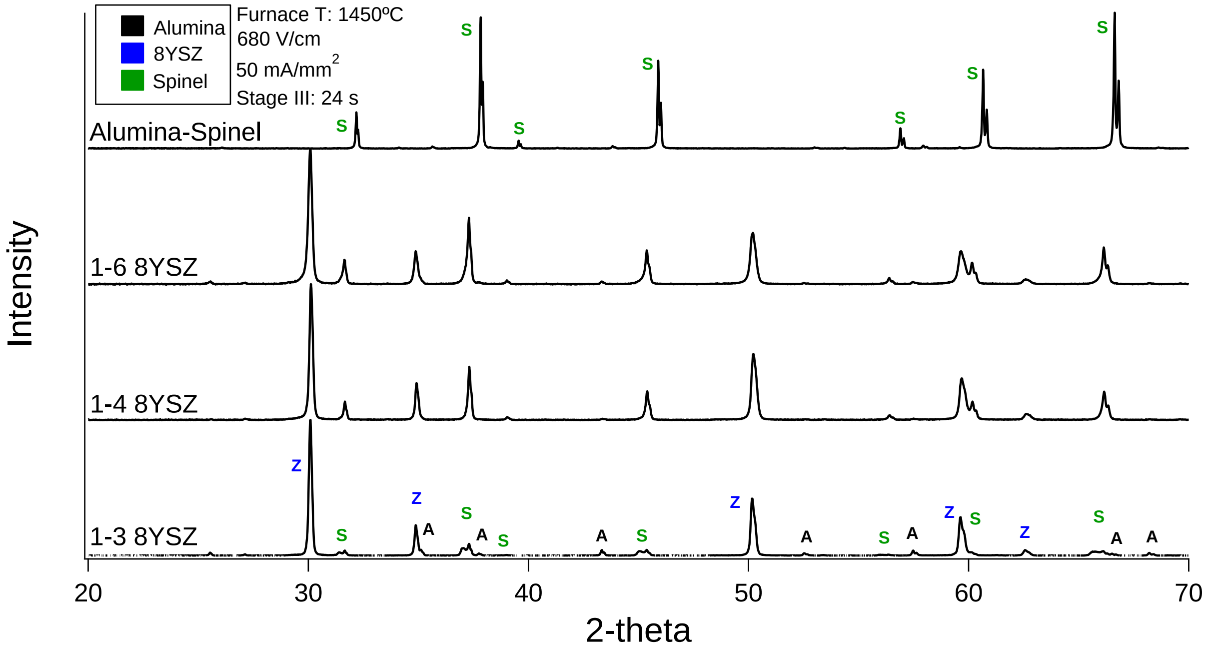

Figure 5.8: XRD patterns of equal (1/3) volume percent, 1/4, and 1/6 volume fraction 8YSZ-alumina-spinel and two-phase alumina-spinel composites after flash sintering with a 24 second current control hold time

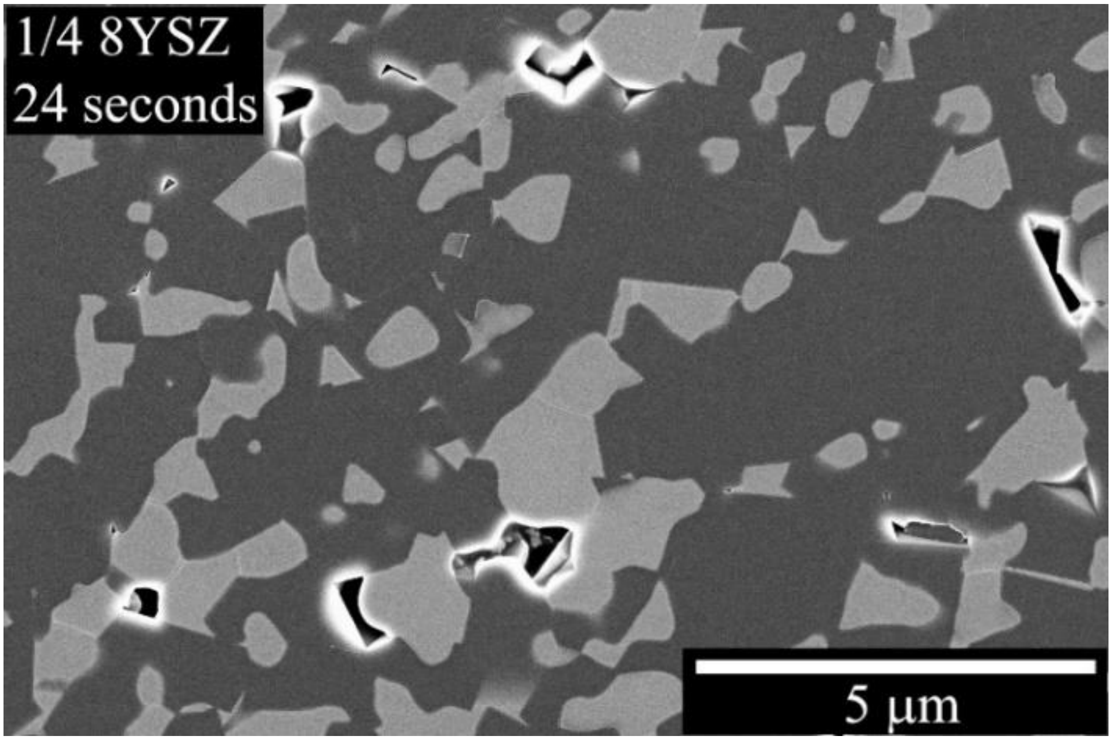

Figure 5.9: SEM of three phase composite with 1/4 8YSZ held in Stage III current hold for 24 seconds at a current density of 50 mA/mm^2

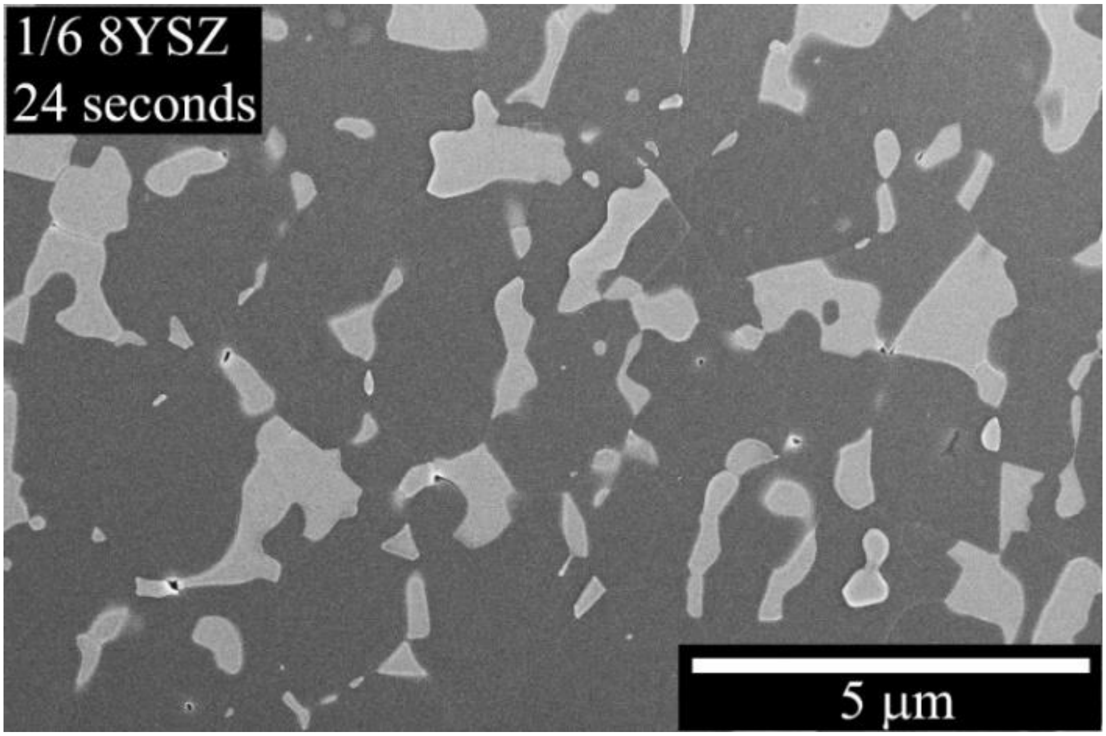

Figure 5.10: SEM of three phase composite with 1/6 8YSZ held in Stage III current hold for 24 seconds at a current density of 50 mA/mm^2

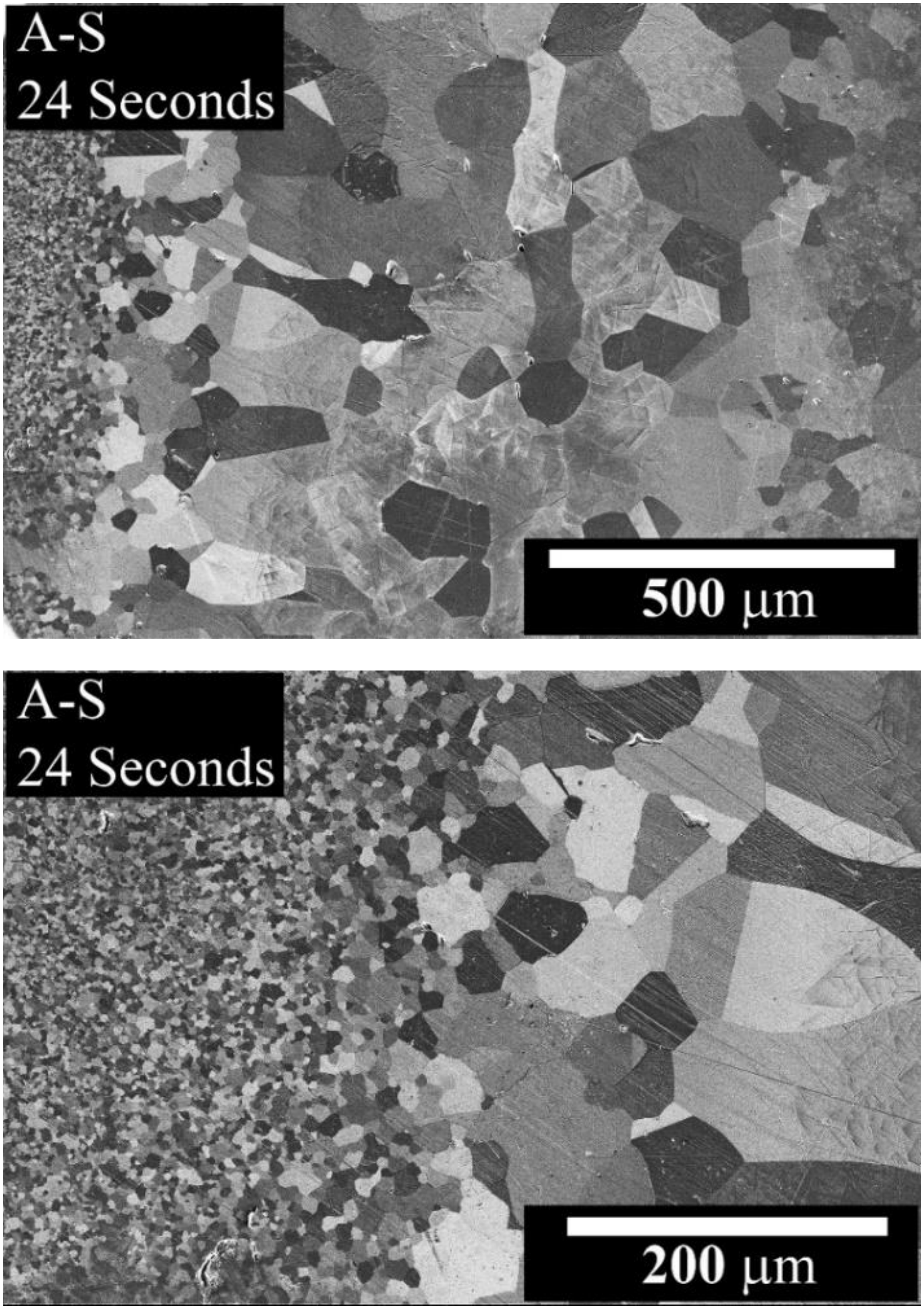

Figure 5.11: SEM images of alumina-spinel composite held in Stage III current hold for 24 seconds showing gradient microstructure in the center of the gauge section

The result of varying the amount of 8YSZ in the three-phase composite (Figure 5.7) suggest that 8YSZ can be used as a catalysis for the onset of flash sintering. The composition of alumina-spinel was able to be flash sintered, but with an incubation time of over 4 minutes. As 1/6 volume percent 8YSZ is added to the two-phase system, the incubation is reduced to less than 30 seconds. The trend of decreasing incubation time continues as the content of 8YSZ is increased to 1/4 volume percent. As the amount of 8YSZ is increased to 1/3 volume percent, the onset of flash occurs almost instantaneously. Without the inclusion of 8YSZ, the long incubation time can be attributed to the formation of a conductive pathway as the green body begins to sinter at the set furnace temperature of 1450°C. With the addition of 8YSZ, the ability of zirconia to catalysis flash sintering is credited to the higher conductivity of 8YSZ compared to alumina and spinel.[3, 60, 61]

Flash sintered alumina-spinel composites showed signs of extensive current channeling though the specimen's gauge section. Blackening was observed in the sample after flash sintering, similar to the results seen in flash sintering of single phase alumina and titania.[29, 77] This has been attributed to electrochemical blackening, in which partial reduction of sample occurs during flash sintering under large current densities and current holds.[29, 30] In flash sintered samples of single phase, spinel, alumina, and zirconia; a gradient microstructure is also observed between the two electrodes.[29, 60, 71, 78] This non-uniform densification has been attributed to migration of charge species during flash sintering (by formation of excess cation vacancies), interactions with the platinum electrodes, and differential heating and cooling at the each ends of the electrode contacts.[29, 60, 71, 77–79] Although a gradient microstructure is also observed throughout the gauge section of the two-phase sample (Figure 5.11), the gradient of larger to small grains extents out from the center of the gauge section to the edges of the sample. This suggests a channeling of the current though the center of the sample with a thermal and/or field effect gradient occurring in the sample during flash sintering. For the results presented in this study, only this two-phase alumina and spinel composite showed this channeling effect. Although similar results were presented by Biesuz and Sglavo et al, with the flash sintering of pure alumina; and noted that the sharp transition seen with the large and small grains cannot be explain by a thermal gradient alone, since the large thermal gradient required would not be substantial at in an area of just a few microns.[29] Temperature gradients due to uneven current distribution during flash sintering have also been reported.[23] Nevertheless the role of the defect chemistry cannot be overlooked, since oxygen vacancies can be generated during flash sintering ultimately increasing conductivity.[28, 29, 80]

A two-phase composite of MgO and Spinel was flash sintered with trace amounts of zirconia introduced in the milling processed with zirconia media. This was done to probe the viability of the formation of magnesia rich spinel with flash sintering. Work done on flash sintering of pure spinel was difficult to achieve.[60] No published literature to date has been found on the flash sintering of MgO, and initial laboratory experiments were unsuccessful in flashing pure MgO. A small amount of zirconia was introduced to catalyze flash sintering as well as preventing current channeling. An ultra-fined grained microstructure is observed in the SEM images of the flash sintered two-phase MgO and Spinel composites (Figure 5.12). Archimedes density measurement also showed a high density of 98% theoretical density. XRD results shown in Figure 5.13 show that MgO is still present in the sample, with no formation of magnesia rich spinel.

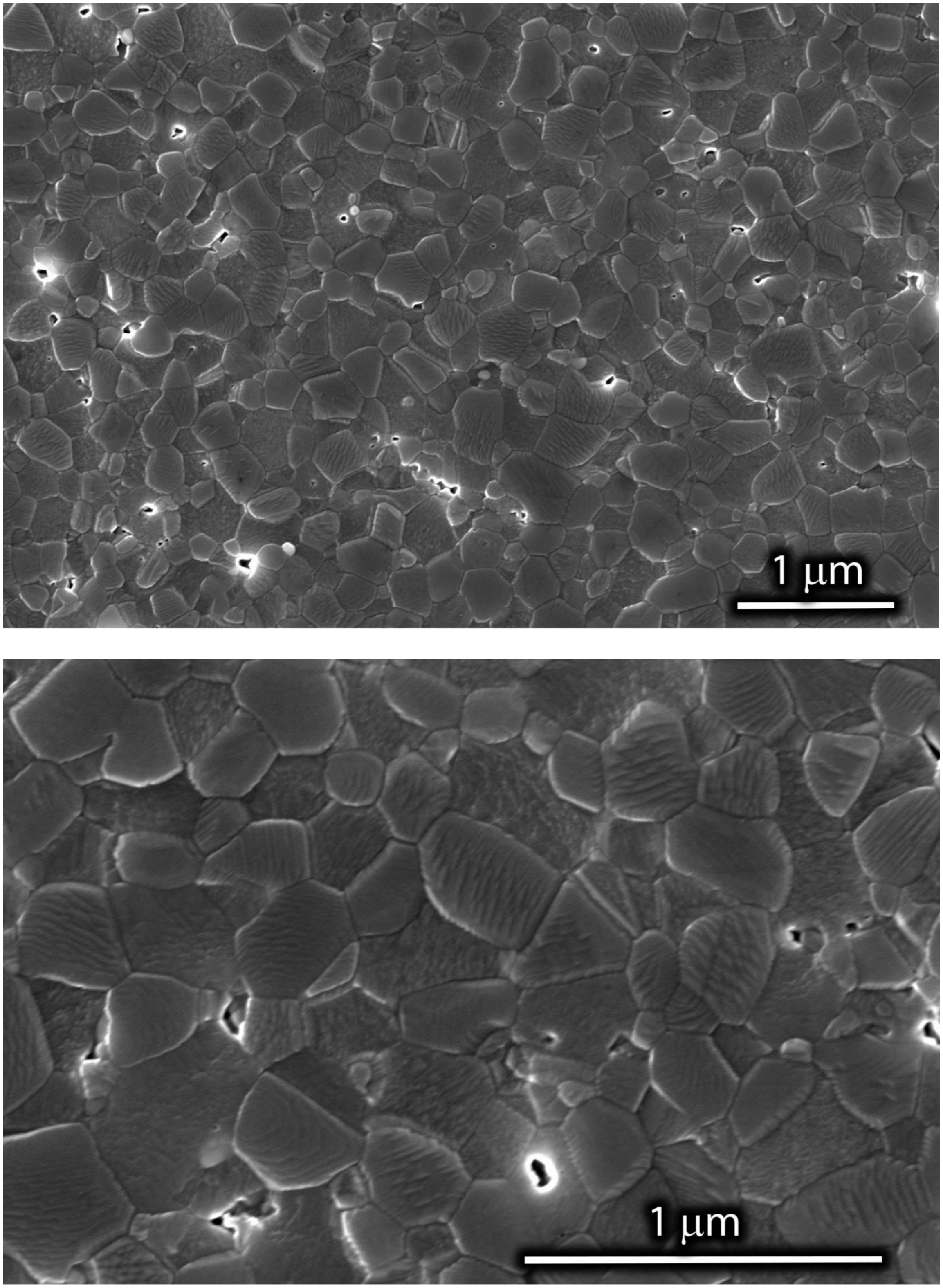

Figure 5.12: SEM images of two-phase MgO and Spinel composite after flash sintering

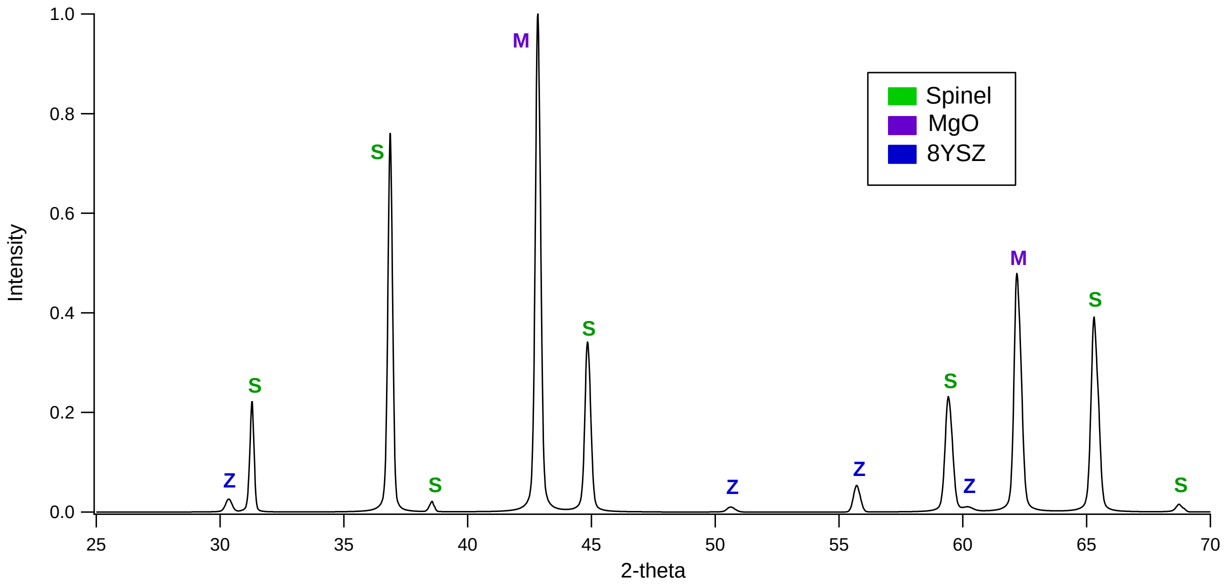

Figure 5.13: XRD of flash sintered two-phase MgO and Spinel Composite

5.4 Conclusions

Limiting the current control hold time during flash sintering of a three-phase (alumina, spinel and 8YSZ) composite allowed for rapid densification, while maintaining all three phases with minimal grain growth. With a current control hold time greater than 6 seconds, grain growth of the three-phase composite occurred, and will result in the eventual formation of a high-alumina spinel phase. Reducing the amount of 8YSZ in the three-phase composite increased the incubation time until the onset of flash sintering. Formation of high-alumina spinel (with a gradient microstructure) can also be achieved by flash sintering a two-phase composite of alumina and spinel. Flashing of a MgO and Spinel composite with trace amount of zirconia showed no phase reaction with a dense and ultra-fine grained microstructure.

CHAPTER 6: MECHANICAL PROPERTIES OF FLASH SINTERED CERAMICS

6.1 Abstract

Mechanical testing on flash sintered single and three phase composites were done. Flash sintered single phase 8YSZ showed no significant changes in mechanical properties when measuring for hardness, elastic modulus, and fracture toughness. Flash sintered three phase alumina, spinel, and 8YSZ did exhibit increased hardness, as well as unusually high elastic modulus and fracture toughness. The increased in hardness is attributed to point defect generations during flash sintered. The change in modulus and fracture toughness still need explaining and further mechanical characterization needs to be done.

6.2 Experimental Procedure

Flash sintering experiments were done with composites of three-phase (alumina, spinel, and 8YSZ) and two-phase (alumina-spinel), dog bone shaped samples. All flash sintering experiments were done at an isothermal condition of 1450°C with a horizontal tube furnace. Applied electric field, current density, and hold times were adjusted for each set of samples. Applied fields ranged from 650 - 800 V/cm, current densities were 1.5 - 50 mA/mm^2, and hold times were 6 seconds to 30 minutes.

Standard control sample of single phase, and three-phase samples were made from conventionally and two-step sintering to compare with mechanical testing results from flash sintered samples. Cylindrical shaped control samples were prepared by cold isostatic pressing at 380 MPa. Conventionally sintered samples were sintered at 1550C for 20 hours. Two-step sintered samples were first sintered at 1450°C for 6 minutes the furnace temperature was dropped to 1325°C for 5 hours. Two-step sintering was done in a creep testing furnace (ATS 2390, Butler, PA) to allow for a load of 35 MPa to be applied during the sintering process to further increased densification with minimum grain growth.

Hardness (H) and fracture toughness (K_C) was done using the Vickers indentation method with a micro hardness tester (Zwick Z 3212, Germany). After sintering, samples were polished and etched at 1200°C for 30 minutes. Samples were then indented with a load of 1 kg.

Hardness was calculated using the following equation:

$$H = \frac{F}{d^2} \qquad (6.1)$$

Where *F* is the indentation load, and *d* is the diameter of the indentation.

The elastic moduli were calculated with Knoop indentation using Marshall method:[81]

$$E = H\left(\frac{0.45}{\frac{1}{7.11} - \frac{W}{L}}\right) \qquad (6.2)$$

Where *H* is the hardness, *W* is the minor diagonal indent length, and *L* is the major diagonal indent length.

Finally, the fracture toughness was calculated with the equation:[82]

$$K_C = 0.016\left(\frac{E}{H}\right)^{\frac{1}{2}} \frac{F}{c^{\frac{3}{2}}} \qquad (6.3)$$

Where *E* is the elastic moduli, *H* = hardness, *F* = load, and *c* is the half diagonal crack length.

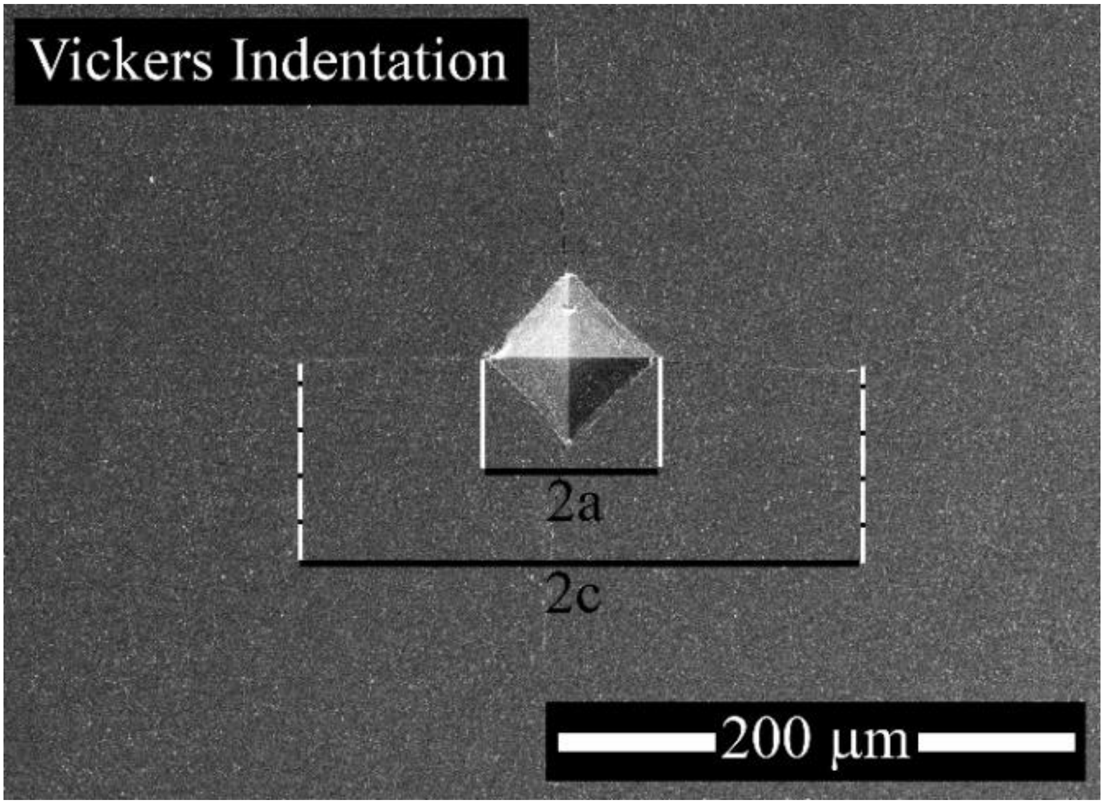

Figure 6.1: Examples of Vickers indentation

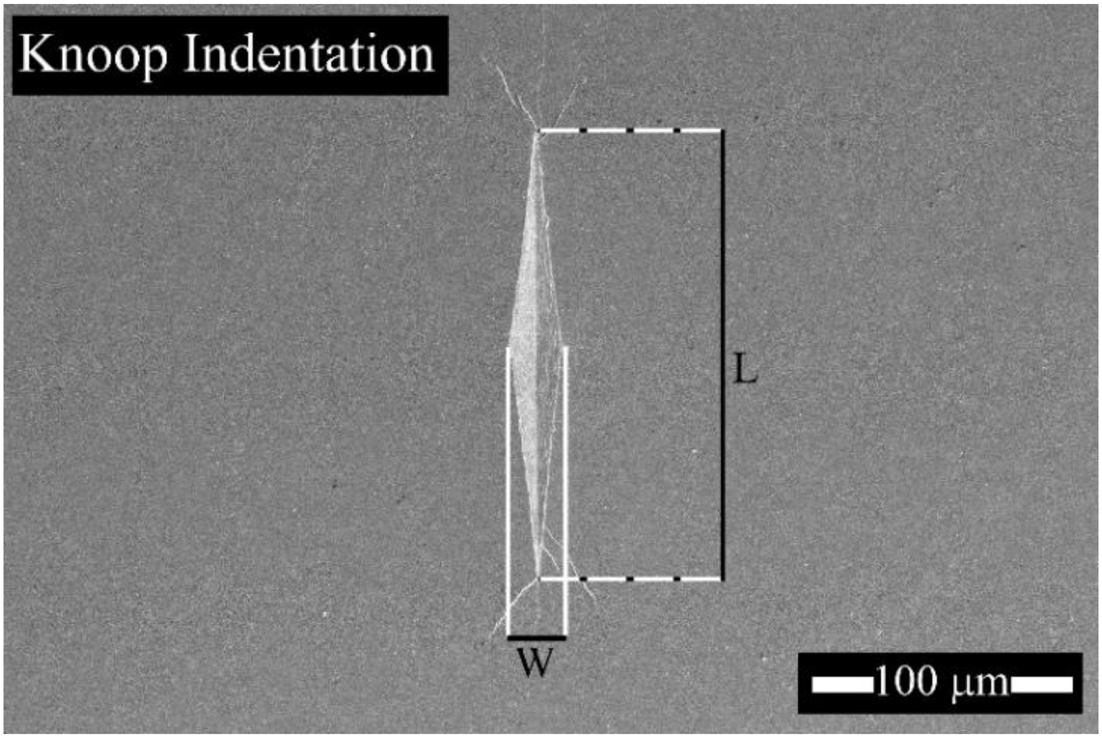

Figure 6.2: Examples of Knoop indentation

6.3 Results and Discussion

6.3.1 Single Phase 8YSZ

Experiments with single phase 8YSZ were done to determine the mechanical properties of flash sintered 8YSZ as well as the effect of extended current control holds. Flash sintering of single phase 8YSZ was done with a field of 680 V/cm and a current density of 50 mA/mm^2. Current control holds were limited to 6 minutes, 30 minutes, and 1 hour. Figure 6.3 shows the hardness values as a function of grain size of each of the flash sintered and conventionally sintered 8YSZ specimens. The SEM microstructure of each flash sintered sample as well as a standard conventionally sintered 8YSZ sample can be seen in Figure 6.3-66.

The large overall grain size of the 8YSZ conventionally sintered sample is expected because of the long sintering hold of 20 hours at 1550°C. As the current control hold times for the flash sintered 8YSZ samples are extended, the grain size is also increased (Figure 6.3). Current control holds of 30 minutes and 1 hour produced samples with overlapping grain sizes, but the trend shows that a longer current control hold will results in larger grains. A similar hardness value compared to the conventionally sintered 8YSZ sample is achieved with a current control hold of 30 minutes and 1 hour. The SEM microstructure of the flash sintered samples (Figures 6.5, 6.6, and 6.7) show a progression of densification as the current control hold is extended to 1 hour. Although a similar density is observed in the current control hold of 30 minutes compared to 1 hour, a reduction of larger pores can be observed in the 1 hour sample.

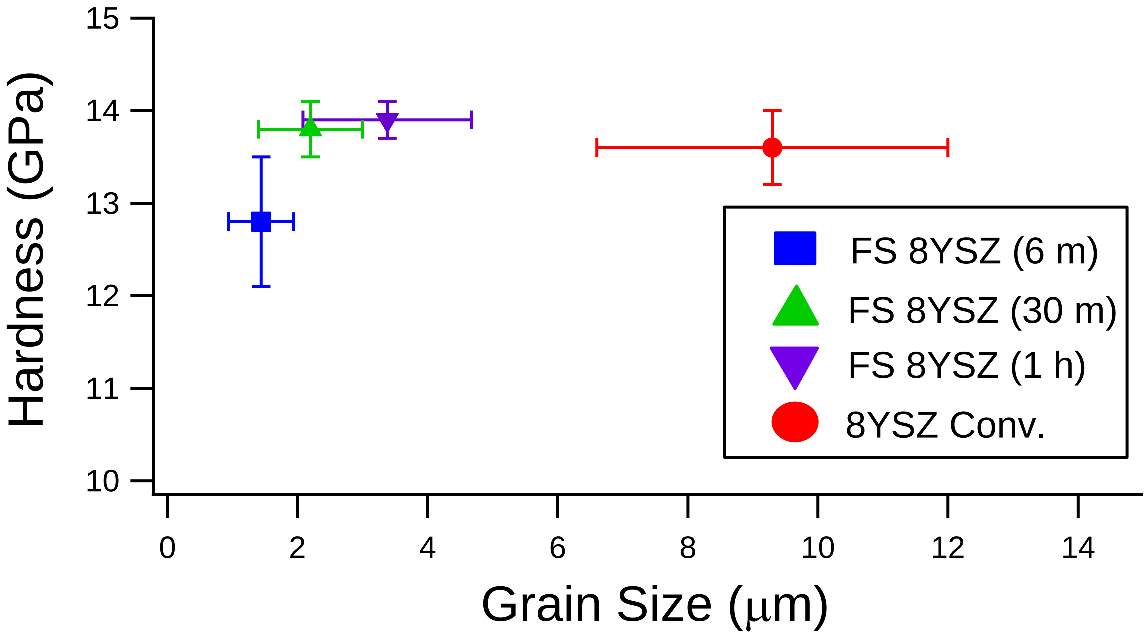

Figure 6.3: Hardness values of flash sintered and conventionally sintered 8YSZ

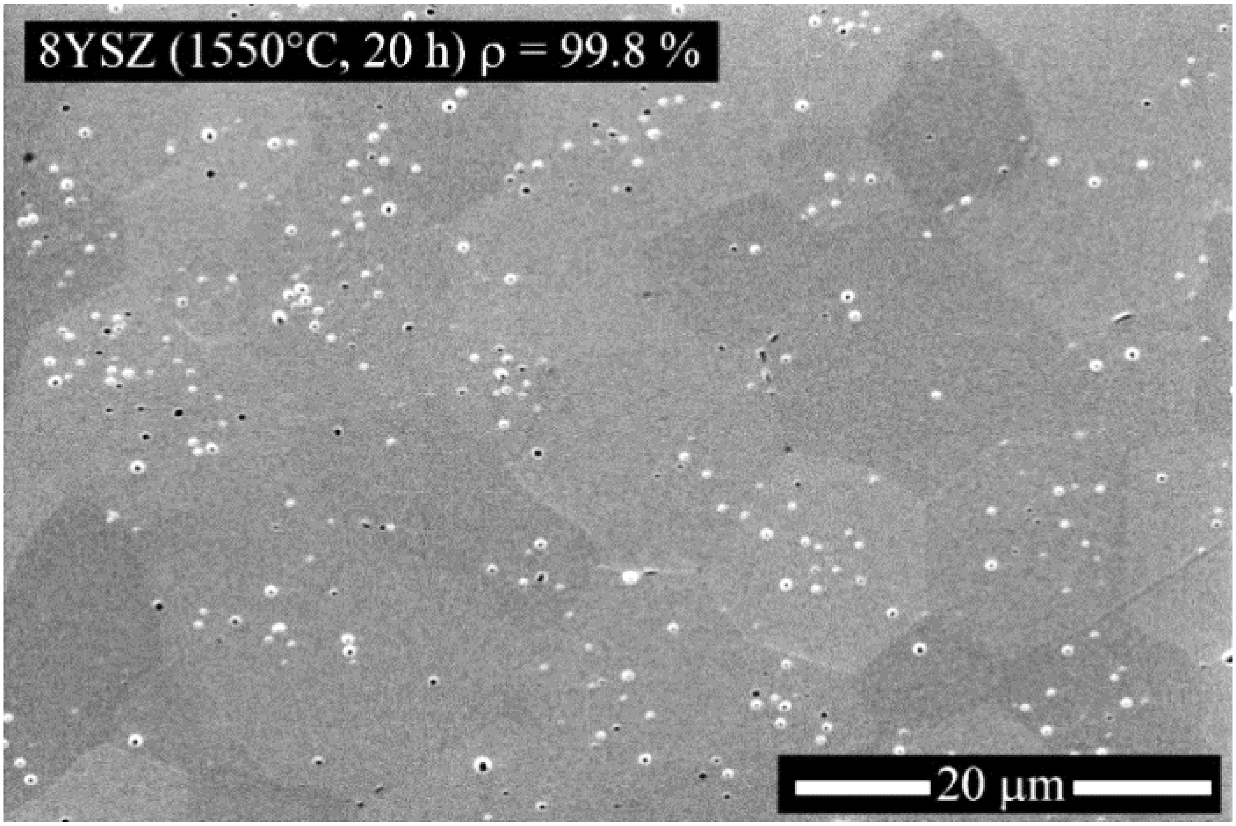

Figure 6.4: SEM microstructure of single phase 8YSZ conventionally sintered

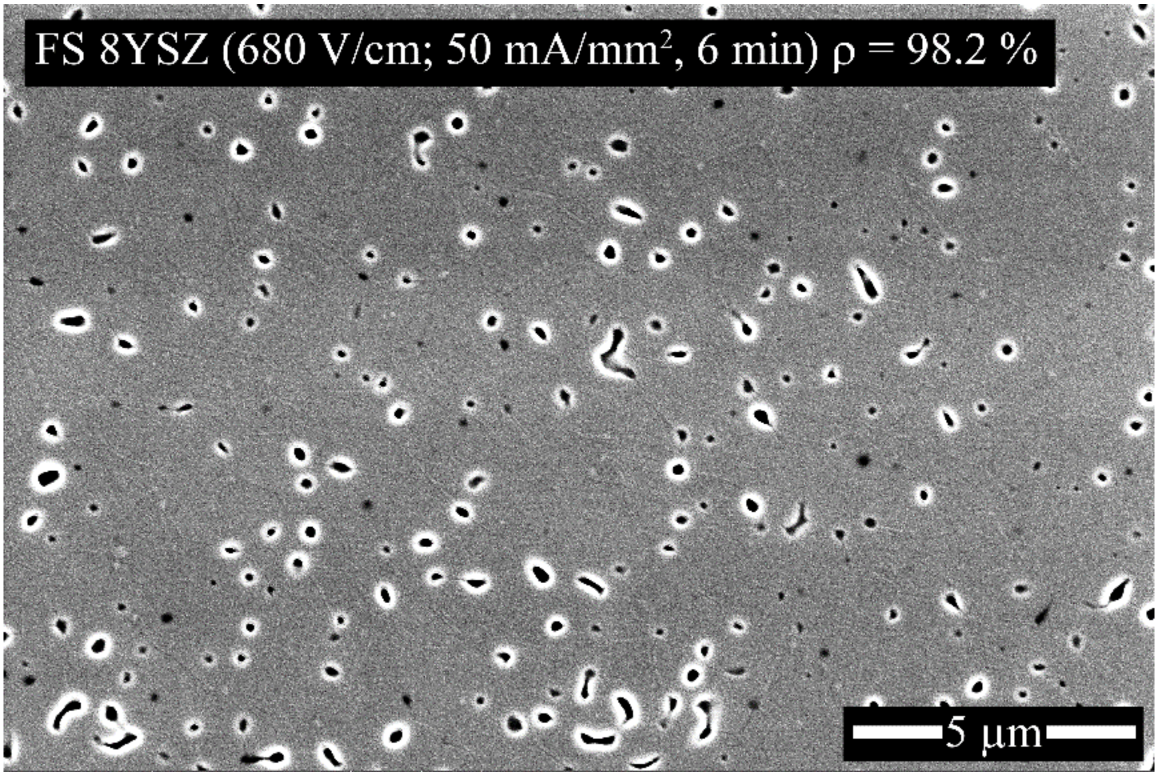

Figure 6.5: SEM microstructure of single phase 8YSZ flash sintered for 6 minutes

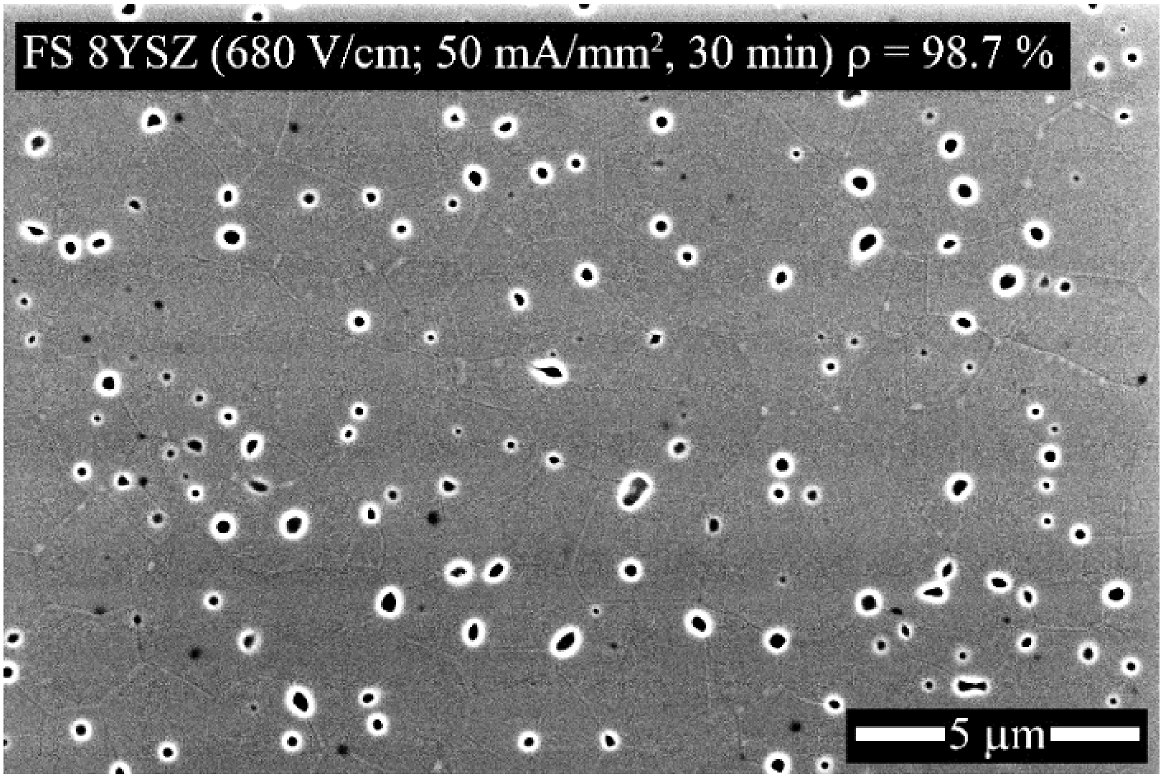

Figure 6.6: SEM microstructure of single phase 8YSZ flash sintered for 30 minutes

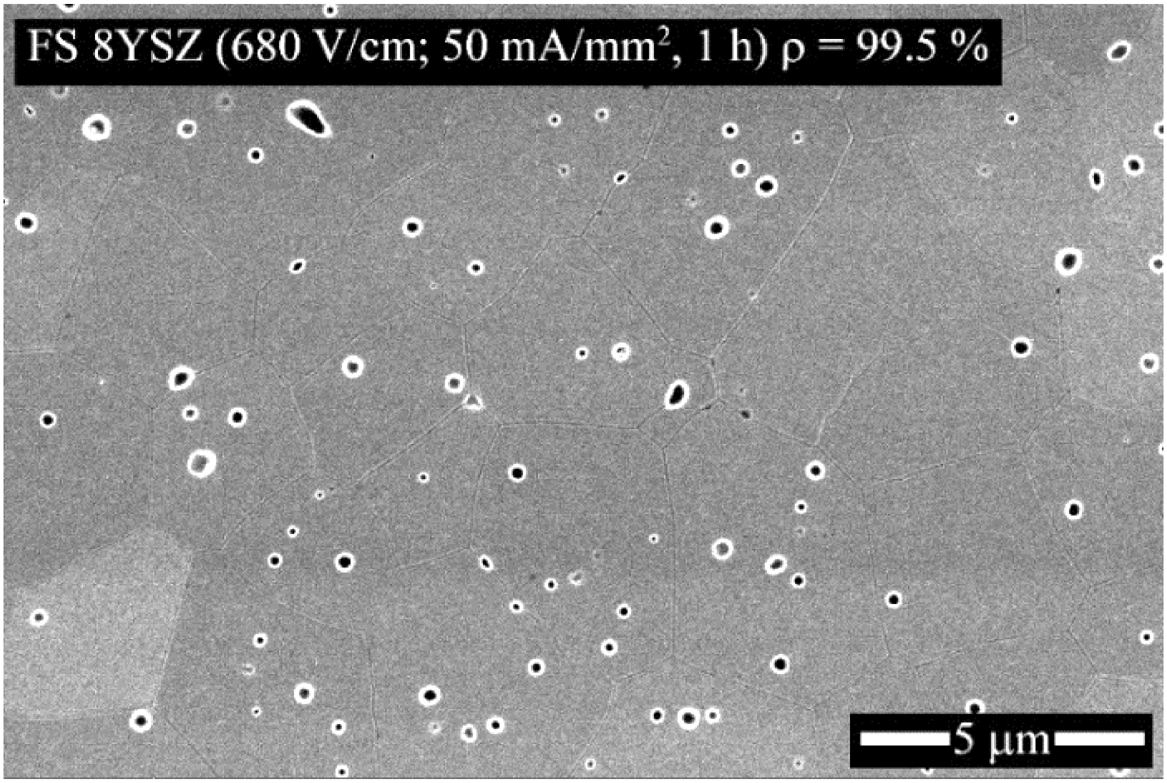

Figure 6.7: SEM microstructure of single phase 8YSZ flash sintered for 1 hour

The Vickers hardness, elastic moduli, and fracture toughness of the conventionally sintered 8YSZ is compared with the flash sintered sample that was held in current control for 1 hour in Figures 6.8, 6.9, and 6.10. Although there is a slight increase of each of the mechanical properties in the flash sintered sample, there is so significant change in the properties when accounting for the standard deviation in the measurements. Similar results were seen in 3YSZ in terms of fracture toughness measured by three point notched bend tests.[83]

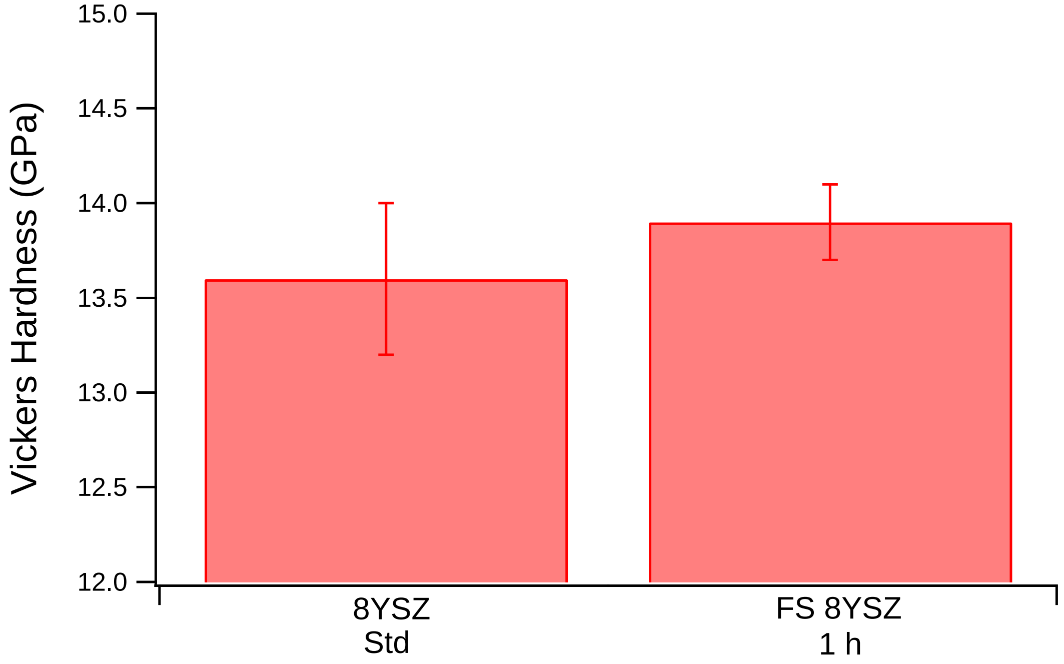

Figure 6.8: Vickers Hardness values for single phase 8YSZ

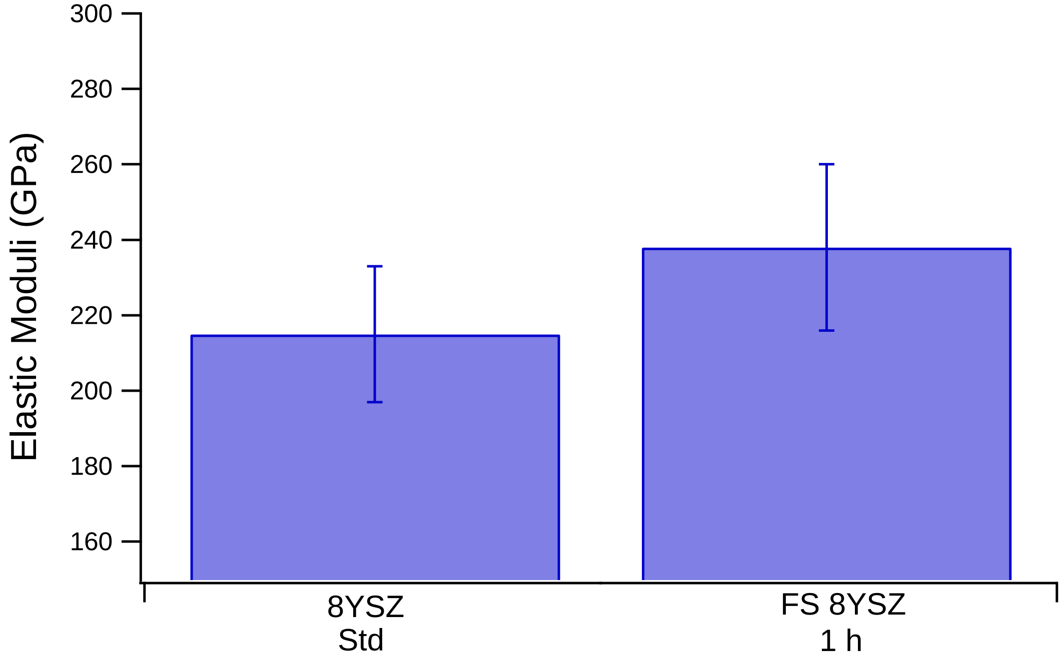

Figure 6.9: Elastic Moduli for single phase 8YSZ

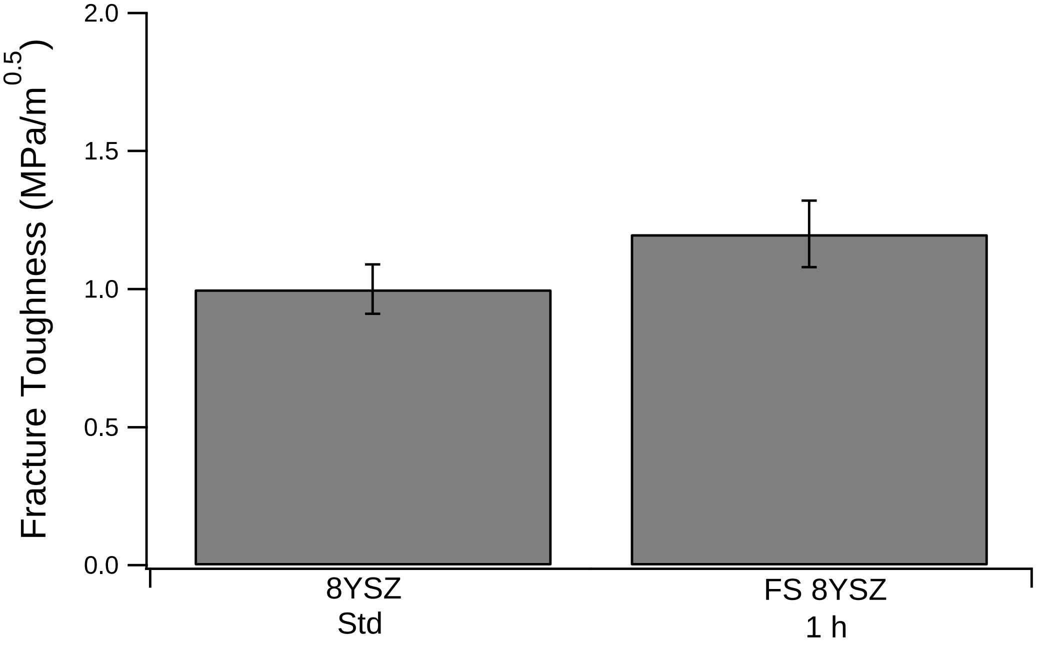

Figure 6.10: Fracture toughness for single phase 8YSZ

6.3.2 Alumina, Spinel, and 8YSZ Composites

Equal volume three-phase (alumina, spinel, 8YSZ) samples were conventionally sintered with an isothermal and two-step method. This was done to produce highly dense samples with different grain sizes for comparison with flash sintered three-phase samples. Flash sintering was again done at 650 V/cm and 50 mA/mm^2, but with a current control hold of 6 and 24 seconds. SEM microstructure of the three-phase samples are shown in Figures 6.11 - 6.14. Note the phase contrast of the induvial phases: alumina (medium grey), spinel (dark grey), and 8YSZ (light grey).

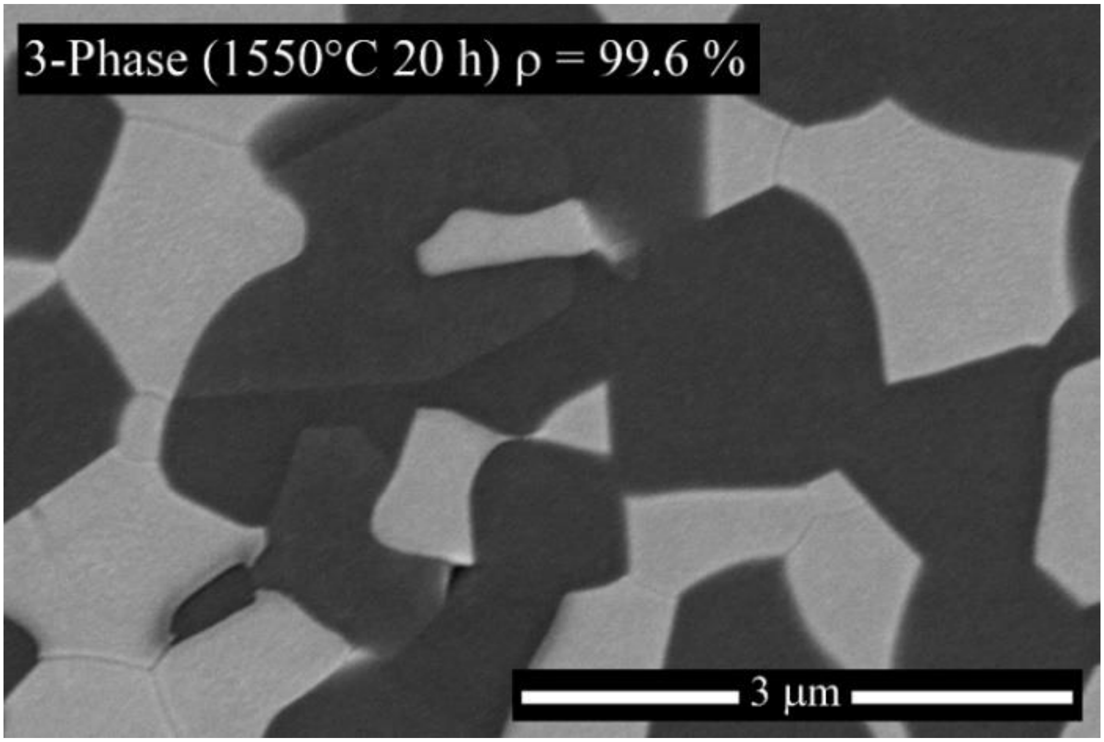

Figure 6.11: SEM microstructure of conventionally sintered three-phase composite

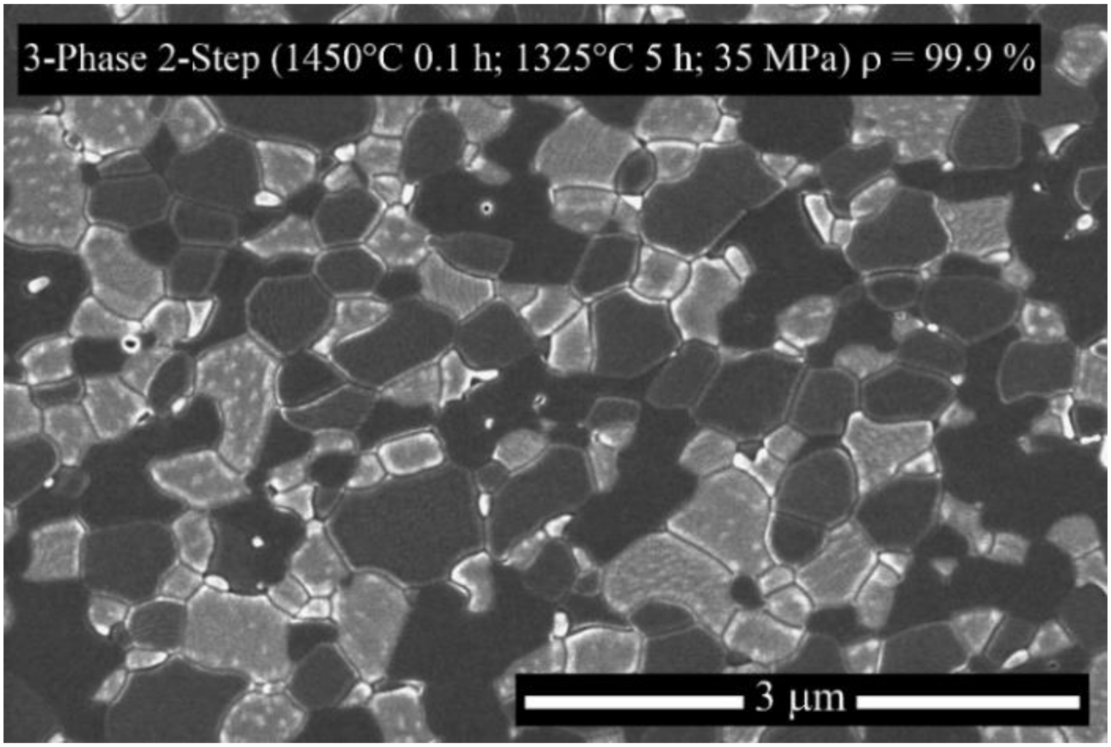

Figure 6.12: SEM microstructure of two-step sintered three-phase composite

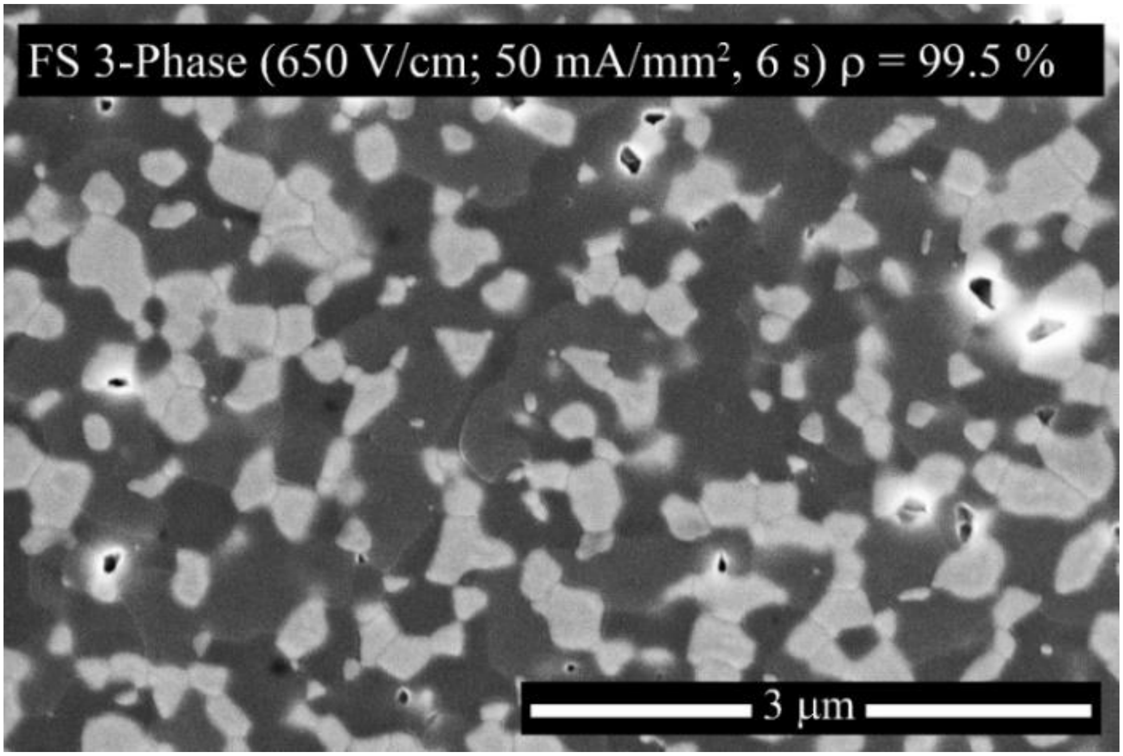

Figure 6.13: SEM microstructure of flash sintered three-phase composite held at 6 seconds

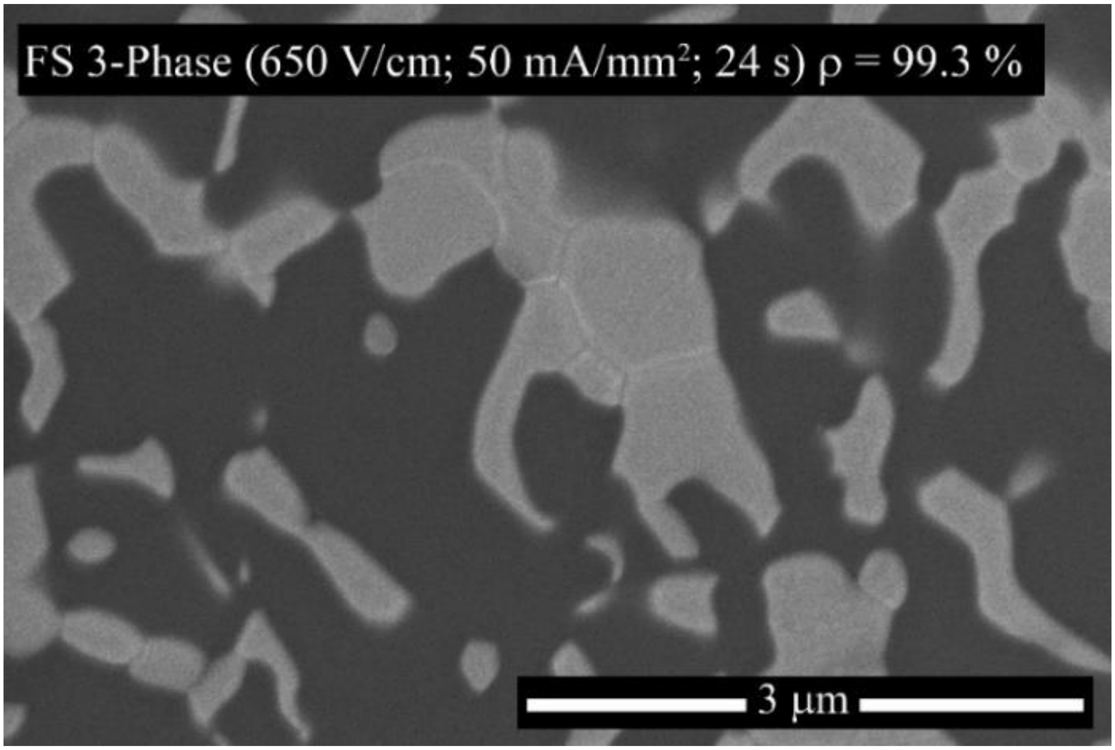

Figure 6.14: SEM microstructure of flash sintered three-phase composite held at 24 seconds

As previously reported with the flash sintering of a three-phase composite of Al_2O_3, $MgAl_2O_4$, 8YSZ, high alumina spinel forms with flash sintering with high current densities or extend current control holds.[63, 64] The SEM microstructure of the sample flash sintered at 24 seconds (Figure 6.14) shows this high alumina spinel phase. The XRD of the three-phase samples (Figure 6.15) confirm the formation of high alumina spinel in the flash sintered 24 seconds sample. This is seen as a shifting of the spinel peaks to a higher 2Θ angle.[63] A stoichiometry spinel peak at a 2Θ of 45° (PDF: 00-021-1152) is included in the XRD data to highlight the alumina rich spinel peak shifts.

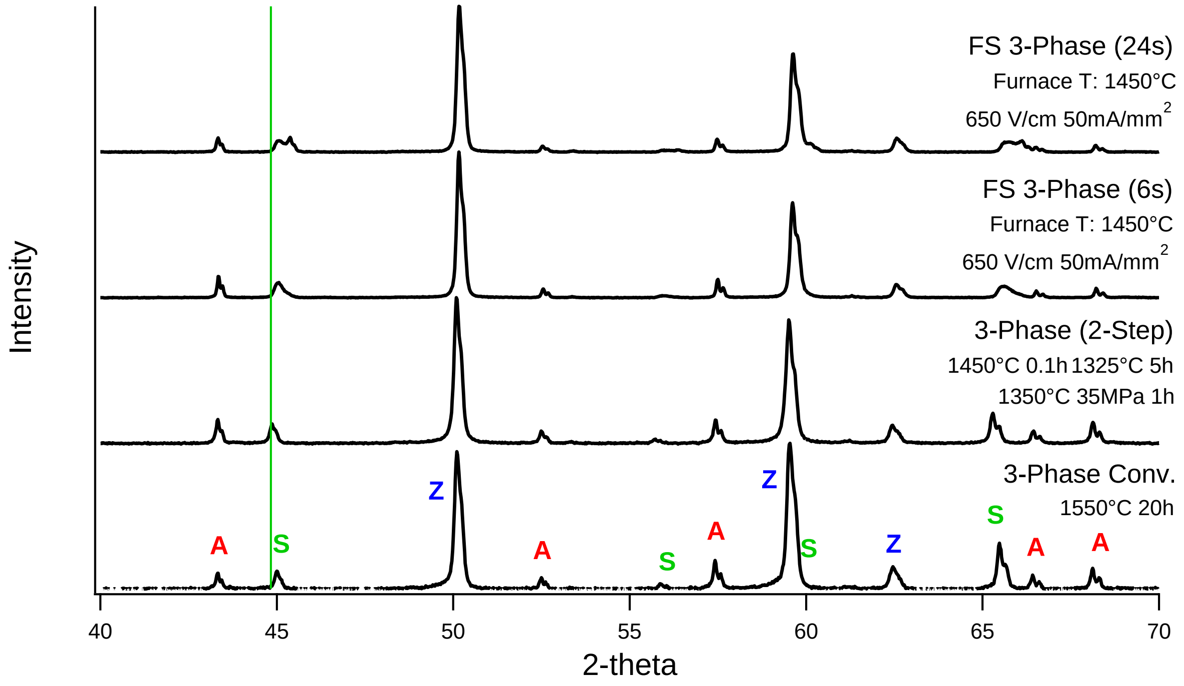

Figure 6.15: XRD of three-phase (A = alumina, S = spinel, Z = 8YSZ) conventionally, 2-step and flash sintered samples

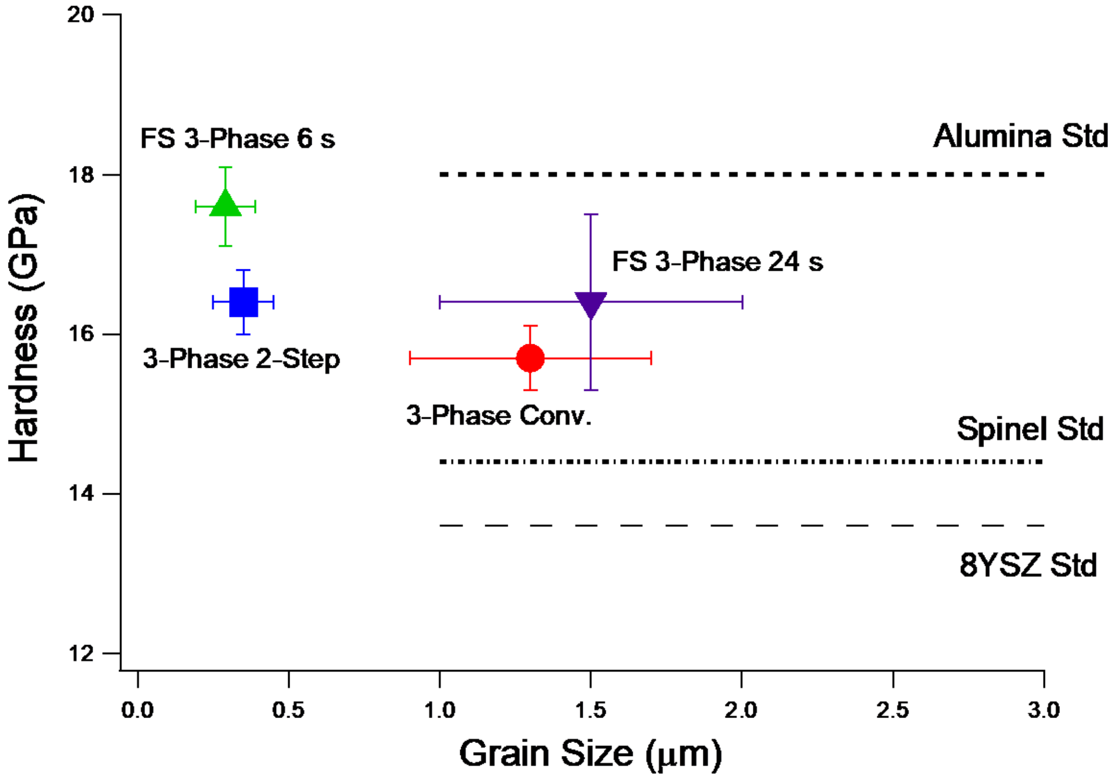

Figure 6.16: Hardness values of three-phase conventionally, 2-step, and flash sintered samples

It should be noted that the spinel becomes slightly non-stoichiometry in other three-phase samples except for the two-step sintered samples. This is due to a prolonged high temperature sintering in the standard sample and elevated sample temperature in the flash sintered 6 second sample. The hardness values of the three-phase samples are shown in Figure 6.16. The hardness values of single-phase samples of alumina, spinel, and 8YSZ are also included in Figure 6.16. The single-phase samples were prepared in the same manner (1550°C, 20 h) as the three-phase standard sample.

Using standard single-phase values taken experimentally with the same experimental set up is important due to the large scattering that can happen with indentation testing on ceramics.[84] Alumina has the highest hardness reported values, followed by spinel then 8YSZ.[10, 85, 86] This is trend is also seen in the experimental values seen with the single phase standard samples (Figure 6.16). It should also be noted that all the three-phase samples fall within the hardness values of expected from a three-phase composite containing alumina, spinel, and 8YSZ.

Comparing the flash sintered 6 second sample to the two-step sintered sample in Figure 6.15, a higher hardness is achieved with flash sintering. The same trend is seen for the large grained three-phase standard sample compared to the flash sintered 24 second sample in Figure 6.16. This is particular interesting since with the high alumina spinel present in the flash sintered sample at 24 seconds, a hardness decrease is expected.[87]

One of the proposed mechanisms of flash sintering is enhanced sintering due to defect generation, in particular Frankel pair defects.[28] This may explain the increase in hardness seen in the flash sintered three-phase samples. A known phenomenon that occurs with neutron irradiation is point defect hardening.[88, 89] An increase in hardening is seen due to point defects blocking dislocation movements. Point defect hardening has specifically been observed in alumina rich spinel.[90]

Bar graphs of the Vickers hardness values along with values the elastic moduli and fracture toughness for the three-phase samples are shown in Figures 6.17, 6.18, and 6.19 respectively. Accounting for the standard deviation in the measurements, the flash sintered sample held at current control at 6 seconds had the highest hardness value (Figure 6.17). There are many factors that can influence the hardness of these samples. An increase in hardness with fine grain sized ceramics is often attributed to the Hall-Petch relationship, with an decrease in grain size results in an increase in a hardness.[8] For this purpose, the two step sintering method was used for a proper comparison of the hardness for the flash sintered 6 second sample. The plot of the hardness vs grain size of the three-phase samples in Figure 6.15 show that the grain sizes between these two samples are almost identical. A study done on the comparison of the hardness values of alumina rich spinel to stochiometric spinel showed that a decrease in hardness is seen with a higher alumina content.[87] Never less this does not explain the increase in hardness seen with the flash sintered 6 second sample.

With defect chemistry being shown to be of growing importance in flash sintering, the idea of point defect hardening has to be considered when explaining the increase in hardness seen in the flash sintered 6 second sample. A proposed explaination of this increases in hardness is that with a flash sintering hold of just 6 seconds, the defects generated during the flashing event are not allowed to annel out. This results in a sample with a larger amounts of point defects compared to a sample that is allowed to flash for a longer hold time. Point defect hardening can also explain the results seen in 8YSZ, with flash sintering having no effect on the mechanical properties due to the inharent high defect concentrated strucutre of 8YSZ to begin with.

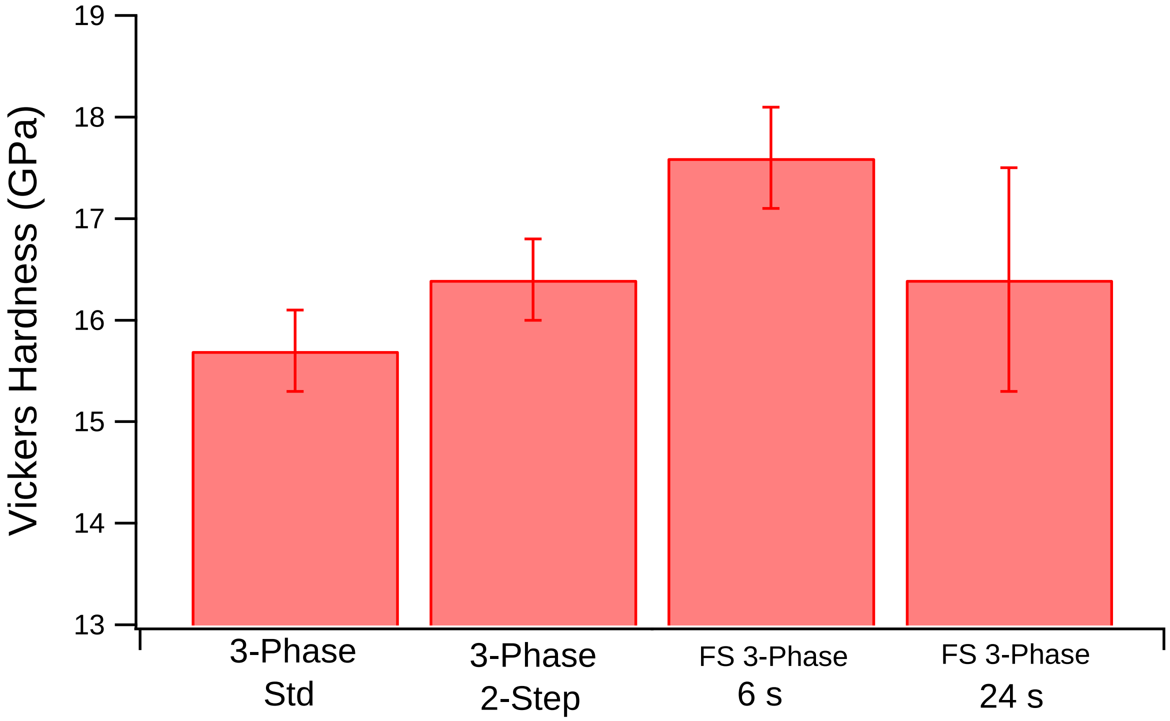

Figure 6.17: Vickers Hardness of three-phase composites

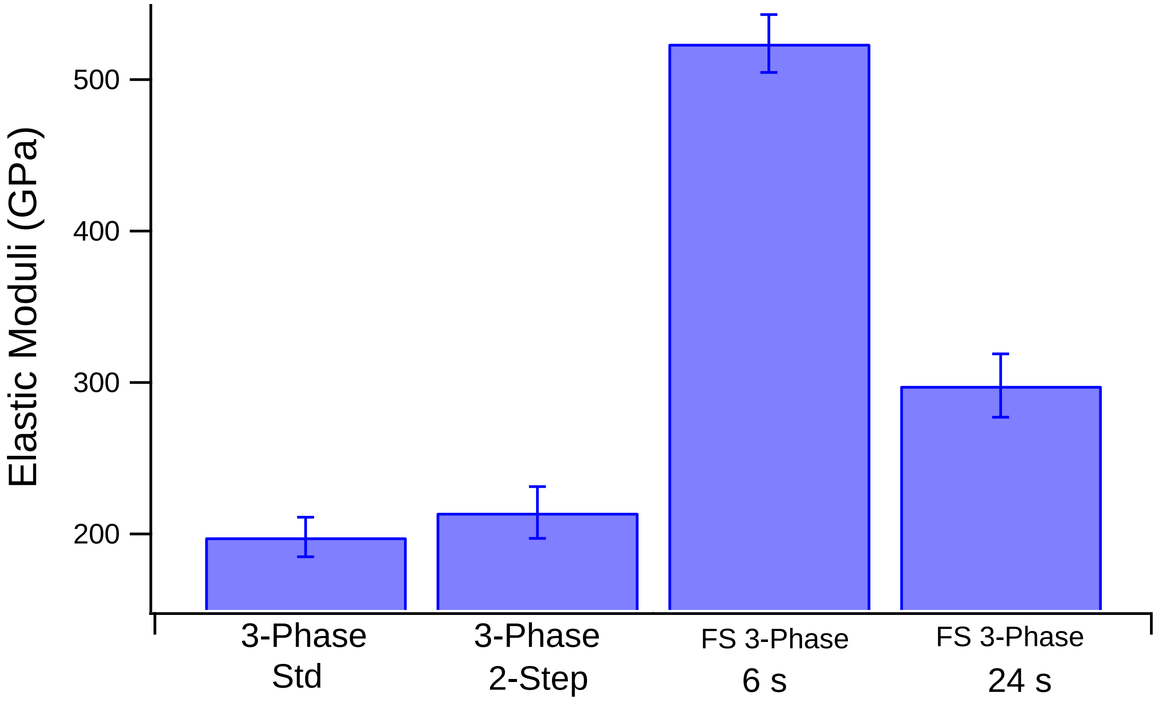

Figure 6.18: Elastic moduli of three-phase composites

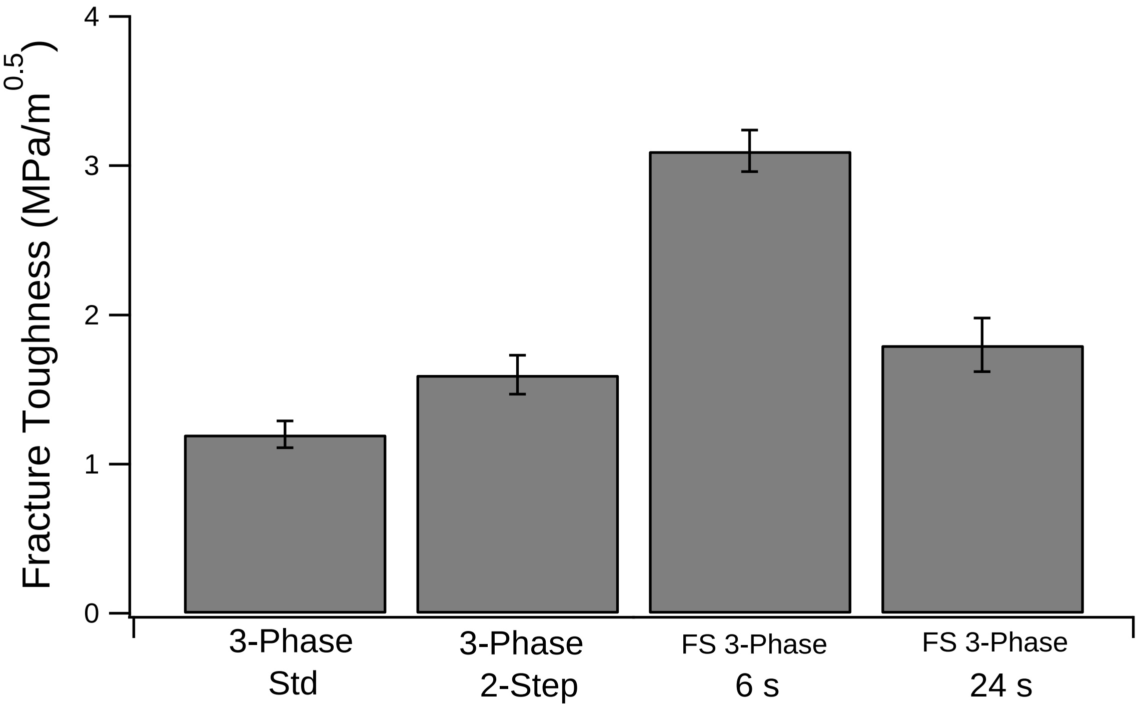

Figure 6.19: Fracture toughness of three-phase composites

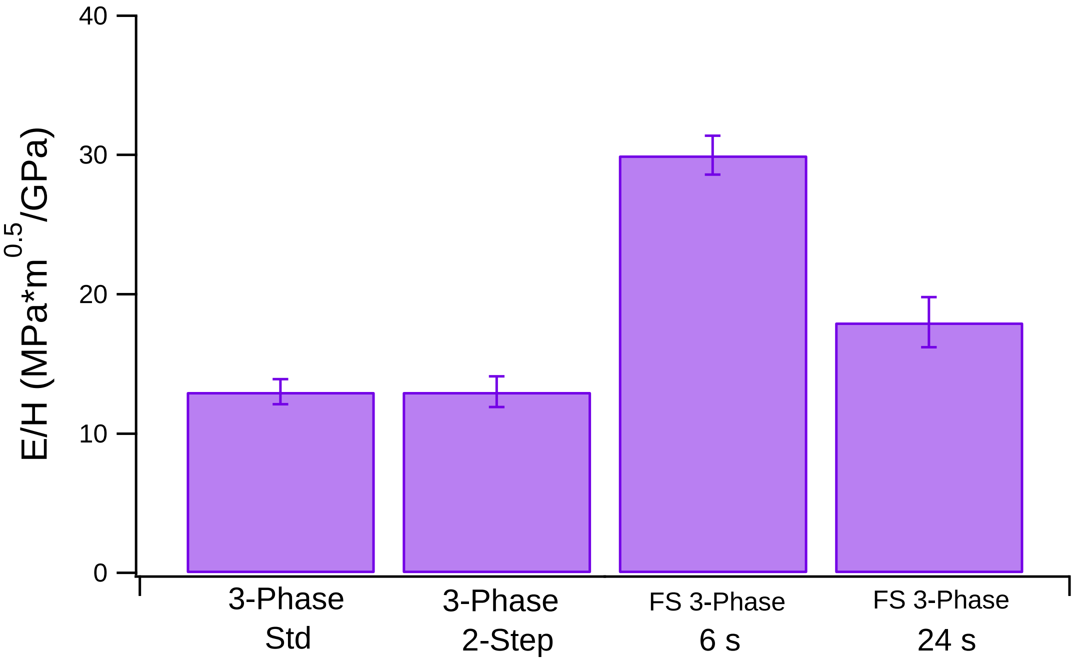

Figure 6.20: Ratio of the elastic moduli over Vickers hardness of the three-phase composites

Higher elastic moduli (Figure 6.18) and fracture toughness (Figure 6.19) for the flash sintered 6 second sample are also reported compared to all the other three-phase samples. This is a unexpected result since a decrease in elastic moduli is expected with an increase in point defects.[91–93] A plot of the ratio of elastic modulus over hardness is shown in Figure 6.20 to emphasizes the elastic modulus increase in the flash sintered 6 second sample. Comparing the Knoop (Figures 6.21 and 6.22) and Vickers (Figures 6.23 and 6.24) indentations on the three-phase flash sintered for 6 seconds and the two-step sintered sample, there is clearly a difference in mechanical properties. In the Knoop indentations, the flash sintered 6 second sample shows a higher elastic modulus with a larger indent left in the sample resulting from less recovery (higher stiffness). The increase in fracture toughness can also be see in the Vickers indent in the flash sintered 6 second sample, with smaller cracks generated compared to the two-step sintered sample.

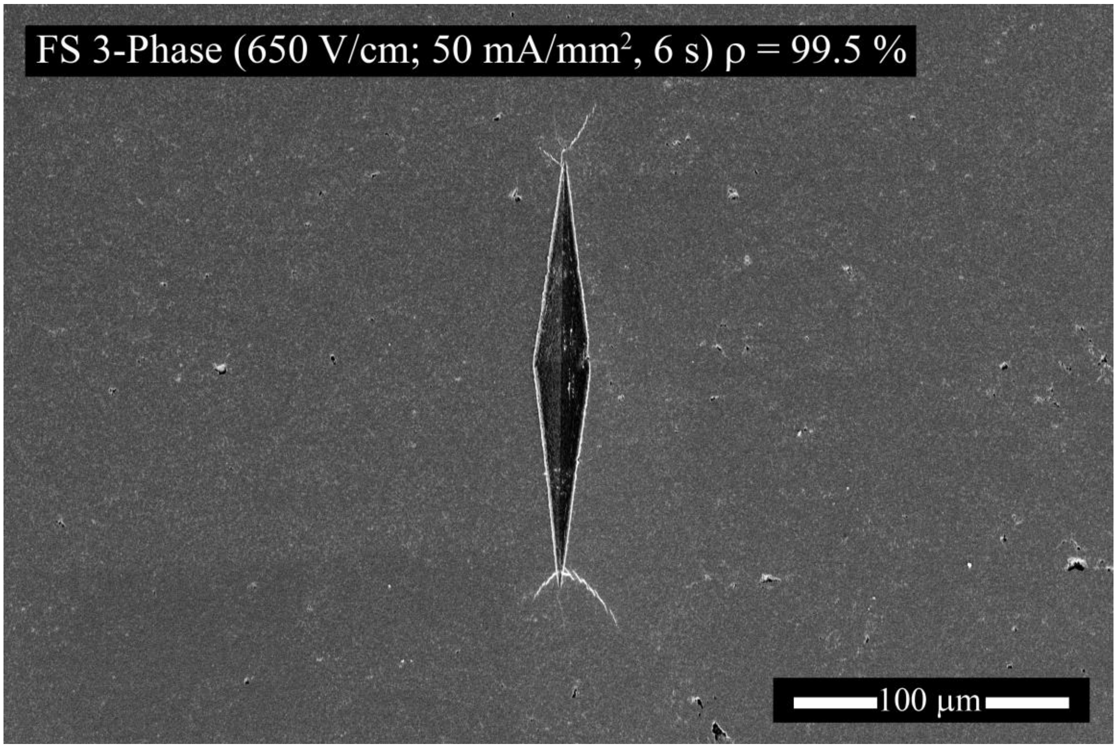

Figure 6.21: Knoop indentation on the three-phase sample flash sintered for 6 second

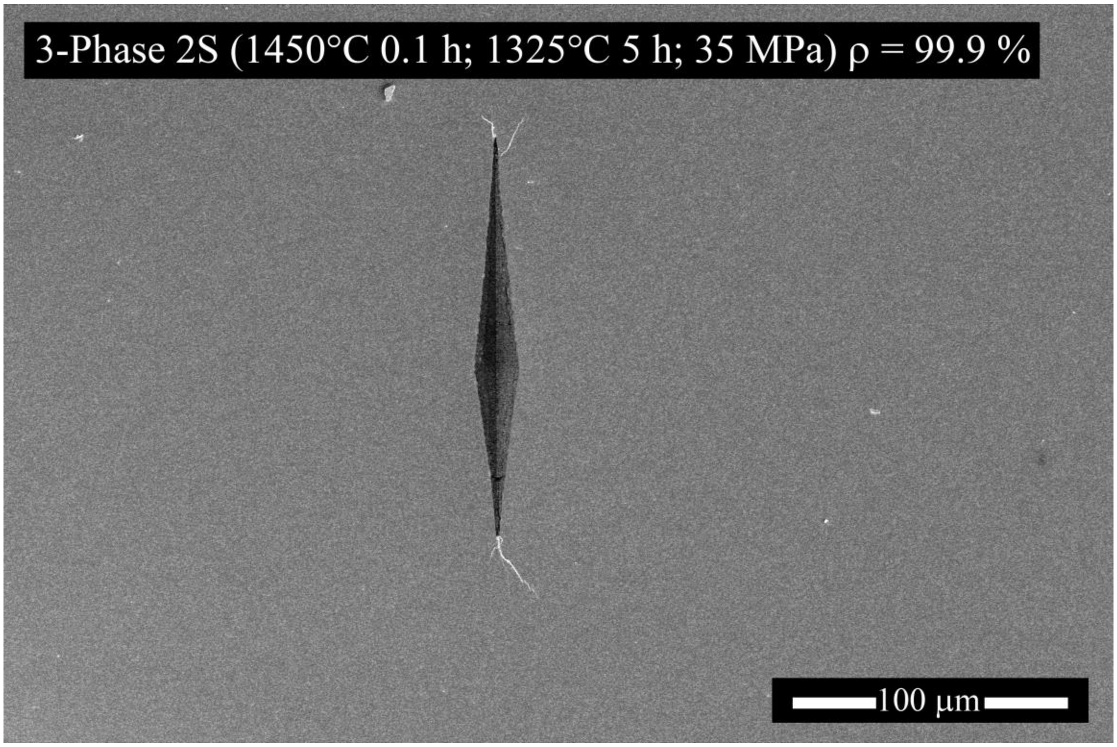

Figure 6.22: Knoop indentation on the three-phase, two-step sintered sample

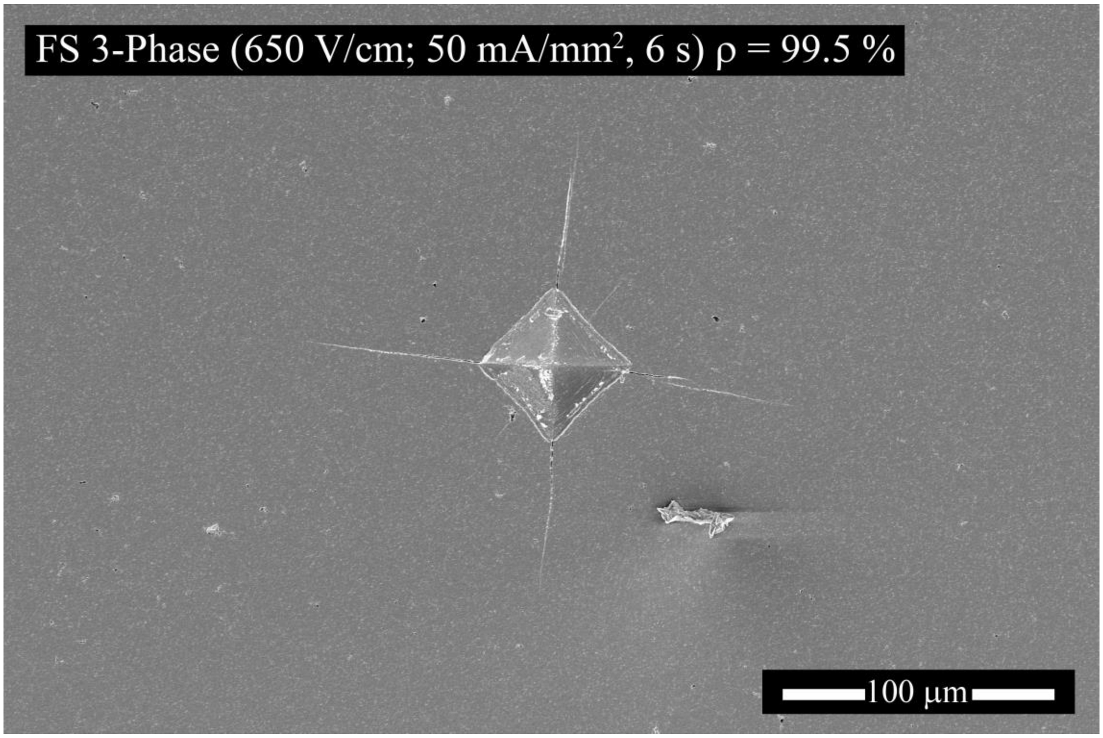

Figure 6.23: Vickers indentation on the three-phase sample flash sintered for 6 second

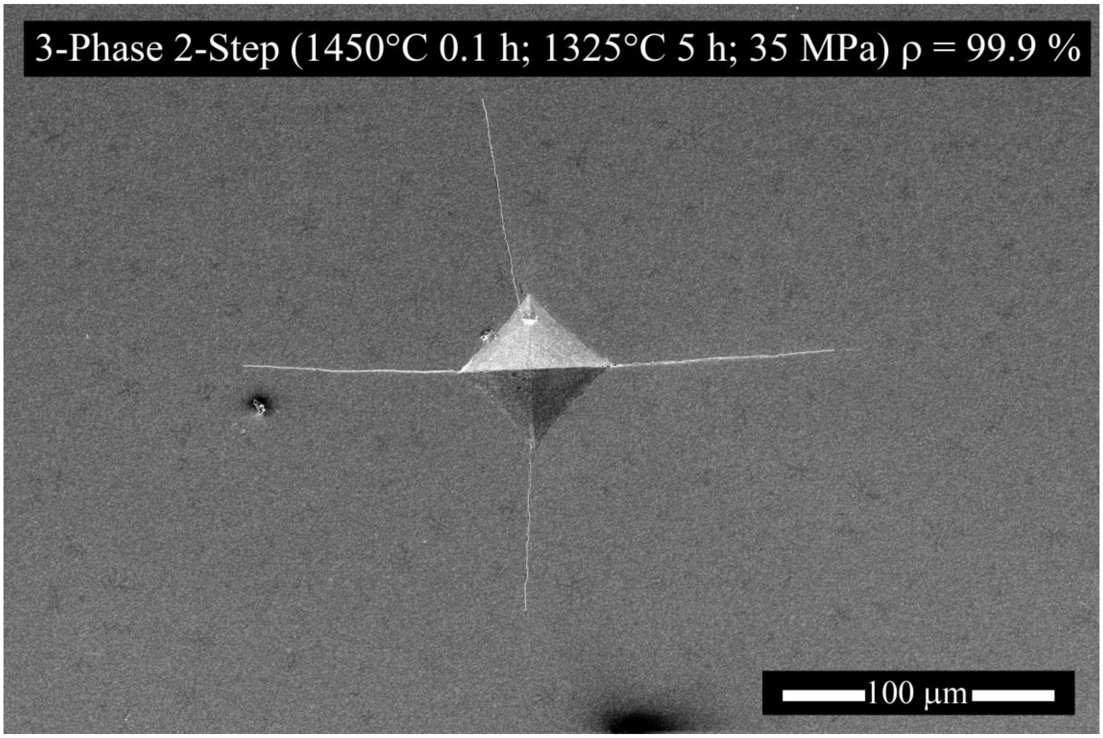

Figure 6.24: Vickers indentation on the three-phase, two-step sintered sample

Although an increase in elastic modulus has been reported in graphene and in certain types of antisite defects for SiC, a definitive explaining on the increased of the elastic modulus with flash sintering cannot currently be presented.[93, 94] Due to the increased hardness attributed to large defect generation with flash sintering, it is hypothesize that the increase in elastic moduli and fracture toughness in this three-phase system is also related to high defect concentrations after flash sintering. This can explain why an increase in mechanical properties is not seen with single phase 8YSZ, due to 8YSZ being saturated in oxygen vacancies to begin with.[95] Nevertheless, the results in this study shows that an increase in hardness and fracture toughness in a three-phase composite can be achieved with flash sintering (Figure 6.25).

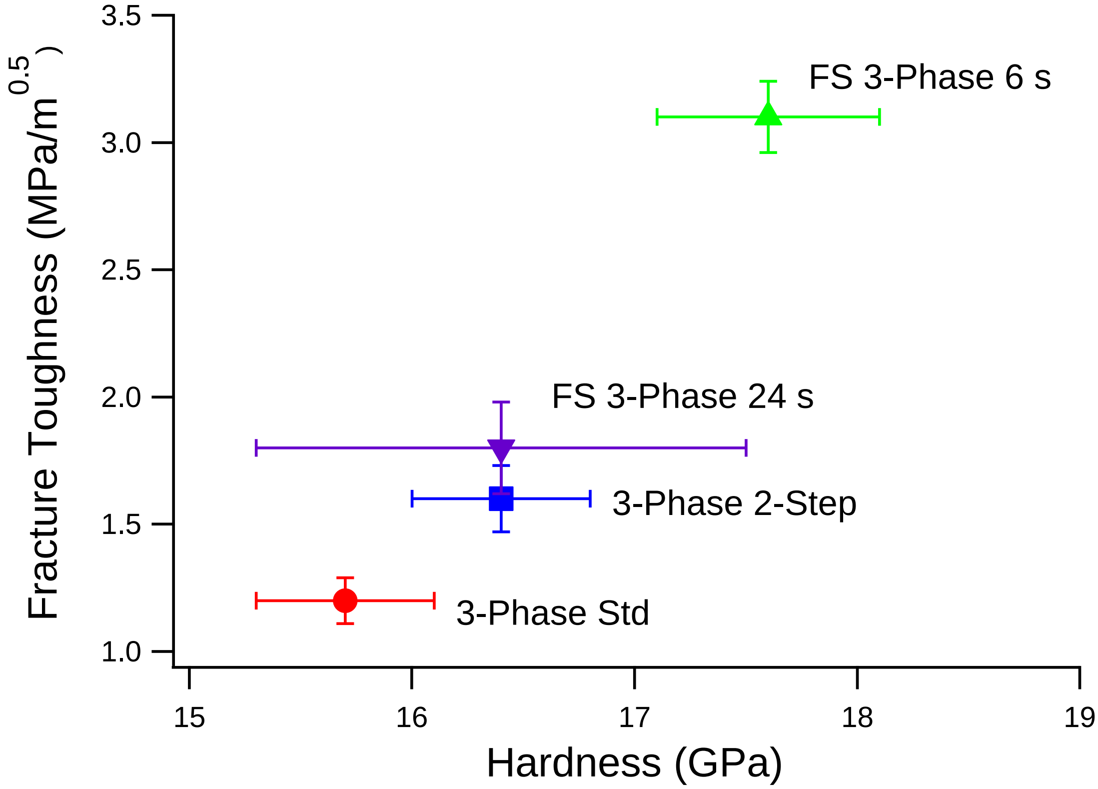

Figure 6.25: Fracture toughness vs hardness plot of the three-phase samples

6.4 Conclusions

Mechanical indentation testing on flash sintered single phase 8YSZ and three-phase (alumina, spinel, 8YSZ) composites were done. For single phase 8YSZ, a current control of 1 hour was required at a flash condition of 680 V/cm; 50 mA/mm^2 to achieve high density and reduction of large pores. In comparison to a conventionally sintered 8YSZ sample, no significant change in hardness, elastic moduli, or fracture toughness is seen with flash sintered 8YSZ samples. In the case for the three-phase composites, an increase in mechanical properties are seen with the flash sintered samples; most notably with flash sintering at 650 V/cm; 50 mA/mm^2 for only 6 seconds. Increase in hardness is attributed to point defects generated from the flash sintering process blocking dislocation movements. This is especially true with a current control hold for only 6 seconds due to the limited formation of softer high alumina spinel preventing and annealing out of the point defects generated during flash sintering, which can occur during longer hold times. A definitive explanation for the increase in elastic moduli and fracture toughness in the three-phase composition is still lacking, and more work needs to be done in this area. Addition mechanical testing such as with ultrasonic indentation needs to be done to confirm the elastic modulus.

CHAPTER 7: SUMMARY AND FUTURE WORK

Flash sintering of multiphase composite ceramic systems were carried out with successful results. With the inherent complex nature of flash sintering, careful selection of the applied field and current hold times need to be done to achieve proper sintering. With ideal electric fields and current control holds, fine grained composites with improved mechanical properties was achieved.

The use of zirconia as a catalysis for flash sintering was demonstrated with successful results. Flash sintering of two-phase composites without zirconia showed extensive channeling of the current though the center of the sample. With the addition of just a trace amount of zirconia, channeling of the current was prevented. This allowed for a uniformly dense and fine grained microstructure.

In-situ data provided insight on the ultra-rapid heating and solid solutioning that can occur with flash sintering of composites. With most of the published research on flash sintering being on single phase systems, this work provides a starting point for the application of flash sintering on other composite systems. Although diffusion models and in-situ data can possibly explain the enhanced kinetics with flash sintering of multiphase composites, they cannot explain the enhanced mechanical properties seen in this study.

Additional work needs to be done to study the effects of flash sintering on properly densified composites. The reported increase in hardness, elastic moduli, and fracture toughness are especially interesting and requires a further systematic study. A simple experiment to verify these results would be to collect indentation data after various stages of heat treatment are done to anneal out any point defects. Ultrasonic indentation and notched three-point bend test can also be done to verify the enhanced mechanical properties reported in Chapter 6.

From this work it can be determined that flash sintering of composites uniquely has its own sets of challenges. This study showed that two separate compositions that are difficult to flash sinter on their own can be easily flashed in a two-phase composite. This seems to indicate that the interface between dissimilar phases can be an important factor in flash sintering. For a better understanding how flash sintering effects a composite system, a more detailed analysis of the interface between this interface needs to be done. In-situ TEM will be invaluable in this regard due to transient nature of flash sintering.

REFERENCES

[1] M. Cologna, B. Rashkova, and R. Raj, "Flash Sintering of Nanograin Zirconia in <5 s at 850°C," *J. Am. Ceram. Soc.*, **93** [11] 3556–3559 (2010).

[2] M. Cologna, A.L.G. Prette, and R. Raj, "Flash-Sintering of Cubic Yttria-Stabilized Zirconia at 750°C for Possible Use in SOFC Manufacturing," *J. Am. Ceram. Soc.*, **94** [2] 316–319 (2011).

[3] M. Cologna, J.S.C. Francis, and R. Raj, "Field assisted and flash sintering of alumina and its relationship to conductivity and MgO-doping," *J. Eur. Ceram. Soc.*, **31** [15] 2827–2837 (2011).

[4] J.A. Downs and V.M. Sglavo, "Electric Field Assisted Sintering of Cubic Zirconia at 390°C," *J. Am. Ceram. Soc.*, **96** [5] 1342–1344 (2013).

[5] H. Yoshida, Y. Sakka, T. Yamamoto, J.-M. Lebrun, and R. Raj, "Densification behaviour and microstructural development in undoped yttria prepared by flash-sintering," *J. Eur. Ceram. Soc.*, **34** [4] 991–1000 (2014).

[6] K.S. Naik, V.M. Sglavo, and R. Raj, "Flash sintering as a nucleation phenomenon and a model thereof," *J. Eur. Ceram. Soc.*, **34** [15] 4063–4067 (2014).

[7] P. Dahl, I. Kaus, Z. Zhao, M. Johnsson, M. Nygren, K. Wiik, T. Grande, and M.-A. Einarsrud, "Densification and properties of zirconia prepared by three different sintering techniques," *Ceram. Int.*, **33** [8] 1603–1610 (2007).

[8] T.G. Nieh and J. Wadsworth, "Hall-petch relation in nanocrystalline solids," *Scr. Metall. Mater.*, **25** [4] 955–958 (1991).

[9] T. Chen and M.L. Mecartney, “Superplastic compression, microstructural analysis and mechanical properties of a fine grain three-phase alumina–zirconia–mullite ceramic composite,” *Mater. Sci. Eng. A*, **410–411** 134–139 (2005).

[10] J.P. Angle, J.J. Steppan, P.M. Thompson, and M.L. Mecartney, “Parameters influencing thermal shock resistance and ionic conductivity of 8 mol% yttria-stabilized zirconia (8YSZ) with dispersed second phases of alumina or mullite,” *J. Eur. Ceram. Soc.*, **34** [16] 4327–4336 (2014).

[11] S. Dey, J.W. Drazin, Y. Wang, J.A. Valdez, T.G. Holesinger, B.P. Uberuaga, and R.H.R. Castro, “Radiation Tolerance of Nanocrystalline Ceramics: Insights from Yttria Stabilized Zirconia,” *Sci. Rep.*, **5** 7746 (2015).

[12] T.D. Shen, S. Feng, M. Tang, J.A. Valdez, Y. Wang, and K.E. Sickafus, “Enhanced radiation tolerance in nanocrystalline MgGa2O4,” *Appl. Phys. Lett.*, **90** [26] 263115 (2007).

[13] C.M. Hoo, D. Men, L. Taherabadi, and M.L. Mecartney, “Grain-Boundary Sliding in a Superplastic Three-Phase Alumina–Zirconia–Mullite Ceramic Composite,” *J. Am. Ceram. Soc.*, **94** [7] 2171–2180 (2011).

[14] D. Men and M.L. Mecartney, “Superplasticity and machinability in a four-phase ceramic,” *Mater. Res. Bull.*, **47** [8] 1925–1931 (2012).

[15] S.K. Jha, J.M. Lebrun, and R. Raj, “Phase transformation in the alumina–titania system during flash sintering experiments,” *J. Eur. Ceram. Soc.*, **36** [3] 733–739 (2016).

[16] C.E.J. Dancer, “Flash sintering of ceramic materials,” *Mater. Res. Express*, **3** [10] 102001 (2016).

[17] M. Yu, S. Grasso, R. Mckinnon, T. Saunders, and M.J. Reece, “Review of flash sintering: materials, mechanisms and modelling,” *Adv. Appl. Ceram.*, **116** [1] 24–60 (2017).

[18] M. Biesuz and V.M. Sglavo, “Flash sintering of alumina: Effect of different operating conditions on densification,” *J. Eur. Ceram. Soc.*, **36** [10] 2535–2542 (2016).

[19] T. Saunders, S. Grasso, and M.J. Reece, “Ultrafast-Contactless Flash Sintering using Plasma Electrodes,” *Sci. Rep.*, **6** srep27222 (2016).

[20] K.S. Naik, V.M. Sglavo, and R. Raj, “Field assisted sintering of ceramic constituted by alumina and yttria stabilized zirconia,” *J. Eur. Ceram. Soc.*, **34** [10] 2435–2442 (2014).

[21] R. Raj, “Joule heating during flash-sintering,” *J. Eur. Ceram. Soc.*, **32** [10] 2293–2301 (2012).

[22] J.S.C. Francis and R. Raj, “Influence of the Field and the Current Limit on Flash Sintering at Isothermal Furnace Temperatures,” *J. Am. Ceram. Soc.*, **96** [9] 2754–2758 (2013).

[23] R.I. Todd, E. Zapata-Solvas, R.S. Bonilla, T. Sneddon, and P.R. Wilshaw, “Electrical characteristics of flash sintering: thermal runaway of Joule heating,” *J. Eur. Ceram. Soc.*, **35** [6] 1865–1877 (2015).

[24] Y. Dong and I.-W. Chen, “Onset Criterion for Flash Sintering,” *J. Am. Ceram. Soc.*, **98** [12] 3624–3627 (2015).

[25] R. Chaim, “Liquid Film Capillary Mechanism for Densification of Ceramic Powders during Flash Sintering,” *Materials*, **9** [4] 280 (2016).

[26] R. Chaim, “Numerical model for particle size effects on flash sintering temperature of ionic nanoparticles,” *J. Mater. Sci.*, **53** [19] 13853-13864 (2018).

[27] K. Terauds, J.-M. Lebrun, H.-H. Lee, T.-Y. Jeon, S.-H. Lee, J.H. Je, and R. Raj, “Electroluminescence and the measurement of temperature during Stage III of flash sintering experiments,” *J. Eur. Ceram. Soc.*, **35** [11] 3195–3199 (2015).

[28] J.-M. Lebrun, C.S. Hellberg, S.K. Jha, W.M. Kriven, A. Steveson, K.C. Seymour, N. Bernstein, S.C. Erwin, *et al.*, "In-situ measurements of lattice expansion related to defect generation during flash sintering," *J. Am. Ceram. Soc.*, **100** [11] 4965–4970 (2017).

[29] M. Biesuz and V.M. Sglavo, "Current-induced abnormal and oriented grain growth in corundum upon flash sintering," *Scr. Mater.*, **150** 82–86 (2018).

[30] M. Biesuz and V.M. Sglavo, "Flash sintering of ceramics," *J. Eur. Ceram. Soc.*, **39** [2-3] 115-143 (2018).

[31] S.K. Jha, H. Charalambous, H. Wang, X.L. Phuah, C. Mead, J. Okasinski, H. Wang, and T. Tsakalakos, "In-situ observation of oxygen mobility and abnormal lattice expansion in ceria during flash sintering," *Ceram. Int.*, **44** [13] 15362–15369 (2018).

[32] Z.A. Munir, D.V. Quach, and M. Ohyanagi, "Electric Current Activation of Sintering: A Review of the Pulsed Electric Current Sintering Process: Electric Current Activation of Sintering," *J. Am. Ceram. Soc.*, **94** [1] 1–19 (2011).

[33] R. Orrù, R. Licheri, A.M. Locci, A. Cincotti, and G. Cao, "Consolidation/synthesis of materials by electric current activated/assisted sintering," *Mater. Sci. Eng. R Rep.*, **63** [4–6] 127–287 (2009).

[34] O. Guillon, J. Gonzalez-Julian, B. Dargatz, T. Kessel, G. Schierning, J. Räthel, and M. Herrmann, "Field-Assisted Sintering Technology/Spark Plasma Sintering: Mechanisms, Materials, and Technology Developments," *Adv. Eng. Mater.*, **16** [7] 830–849 (2014).

[35] U. Anselmi-Tamburini, S. Gennari, J.E. Garay, and Z.A. Munir, "Fundamental investigations on the spark plasma sintering/synthesis process: II. Modeling of current and temperature distributions," *Mater. Sci. Eng. A*, **394** [1–2] 139–148 (2005).

[36] P.K.M. K, D. Yadav, J.-M. Lebrun, and R. Raj, "Flash sintering with current rate: A different approach," *J. Am. Ceram. Soc.*, **102** [2] 823–835 (2019).

[37] H. Charalambous, S.K. Jha, K.H. Christian, R.T. Lay, and T. Tsakalakos, "Flash Sintering using Controlled Current Ramp," *J. Eur. Ceram. Soc.*, **38** [10] 3689–3693 (2018).

[38] X.L. Phuah, H. Wang, H. Charalambous, S.K. Jha, T. Tsakalakos, X. Zhang, and H. Wang, "Comparison of the grain growth behavior and defect structures of flash sintered ZnO with and without controlled current ramp," *Scr. Mater.*, **162** 251–255 (2019).

[39] E. Gil-González, A. Perejón, P. E. Sánchez-Jiménez, M. J. Sayagués, R. Raj, and L. A. Pérez-Maqueda, "Phase-pure $BiFeO_3$ produced by reaction flash-sintering of Bi_2O_3 and Fe_2O_3," *J. Mater. Chem. A*, **6** [13] 5356–5366 (2018).

[40] B. Yoon, D. Yadav, S. Ghose, and R. Raj, "Reactive flash sintering: MgO and α-Al_2O_3 transform and sinter into single-phase polycrystals of $MgAl_2O_4$," *J. Am. Ceram. Soc.*, **102** [5] 2294-2303 (2019).

[41] B. Yoon, D. Yadav, S. Ghose, P. Sarin, and R. Raj, "On the synchronicity of flash sintering and phase transformation," *J. Am. Ceram. Soc.*, **102** [6] 3110-3116 (2019).

[42] H. Zhang, Y. Wang, J. Liu, X. Xu, L. Chen, and D. Liu, "Reaction assisted flash sintering of Al_2O_3-YAG ceramic composites with eutectic composition," *Ceram. Int.*, (2019).

[43] R. Ma, D. Erb, and K. Lu, "Flash pyrolysis of polymer-derived SiOC ceramics," *J. Eur. Ceram. Soc.*, **38** [15] 4906–4914 (2018).

[44] J. Xia, K. Ren, and Y. Wang, "One-second flash joining of zirconia ceramic by an electric field at low temperatures," *Scr. Mater.*, **165** 34–38 (2019).

[45] B. McWilliams, J. Yu, and F. Kellogg, "Sintering aluminum alloy powder using direct current electric fields at room temperature in seconds," *J. Mater. Sci.*, **53** [12] 9297-9304 (2018).

[46] V.L. Blair, S.V. Raju, A. Fry, M. Kornecki, J. Wolfenstine, and R.E. Brennan, "Flash Sintering of Li-Ion Conducting Lithium Lanthanum Titanate for Li–Air Batteries," ARL-TR-8417 (2018).

[47] D.J. Sprouster, E. Kardoulaki, R. Weidner, A.M. Raftery, M. Elbakhshwan, R. Pokharel, H.M. Reiche, D.D. Byler, *et al.*, "In situ X-ray characterization of uranium dioxide during flash sintering," *Materialia*, **2** 176–182 (2018).

[48] P. Sarin, W. Yoon, K. Jurkschat, P. Zschack, and W.M. Kriven, "Quadrupole lamp furnace for high temperature (up to 2050K) synchrotron powder x-ray diffraction studies in air in reflection geometry," *Rev. Sci. Instrum.*, **77** [9] 093906 (2006).

[49] R. Raj, "Analysis of the Power Density at the Onset of Flash Sintering," *J. Am. Ceram. Soc.*, **99** [10] 3226-3232 (2016).

[50] D. Yang, R. Raj, and H. Conrad, "Enhanced Sintering Rate of Zirconia (3Y-TZP) Through the Effect of a Weak dc Electric Field on Grain Growth," *J. Am. Ceram. Soc.*, **93** [10] 2935–2937 (2010).

[51] S. Ghosh, A.H. Chokshi, P. Lee, and R. Raj, "A Huge Effect of Weak dc Electrical Fields on Grain Growth in Zirconia," *J. Am. Ceram. Soc.*, **92** [8] 1856–1859 (2009).

[52] H.Y. Akinori Uehashi, "Enhancement of sintering rates in $BaTiO_3$ by controlling of DC electric current," *J. Ceram. Soc. Jpn.*, **123** [1438] 465–468 (2015).

[53] A.C. Sutorik, C. Cooper, and G. Gilde, “Visible Light Transparency for Polycrystalline Ceramics of MgO·2Al2O3 and MgO·2.5Al2O3 Spinel Solid Solutions,” *J. Am. Ceram. Soc.*, **96** [12] 3704–3707 (2013).

[54] B. Hallstedt, “Thermodynamic Assessment of the System MgO–Al_2O_3,” *J. Am. Ceram. Soc.*, **75** [6] 1497–1507 (1992).

[55] E. Bichaud, J.M. Chaix, C. Carry, M. Kleitz, and M.C. Steil, “Flash sintering incubation in Al2O3/TZP composites,” *J. Eur. Ceram. Soc.*, **35** [9] 2587–2592 (2015).

[56] S.M. Lakiza and L.M. Lopato, “Stable and Metastable Phase Relations in the System Alumina–Zirconia–Yttria,” *J. Am. Ceram. Soc.*, **80** [4] 893–902 (1997).

[57] D. Pavlyuchkov, G. Savinykh, and O. Fabrichnaya, “Experimental investigation and thermodynamic modeling of the ZrO2–MgO–Al_2O_3 system,” *J. Eur. Ceram. Soc.*, **34** [5] 1397–1408 (2014).

[58] T. Sasamoto, H. Hara, and T. Sata, “Mass-spectrometric Study of the Vaporization of Magnesium Oxide from Magnesium Aluminate Spinel,” *Bull. Chem. Soc. Jpn.*, **54** [11] 3327–3333 (1981).

[59] R.K. Kirby, “Platinum—A thermal expansion reference material,” *Int. J. Thermophys.*, **12** [4] 679–685 (1991).

[60] H. Yoshida, P. Biswas, R. Johnson, and M.K. Mohan, “Flash-sintering of magnesium aluminate spinel (MgAl2O4) ceramics,” *J. Am. Ceram. Soc.*, **100** [2] 554–562 (2017).

[61] J. Kondoh, T. Kawashima, S. Kikuchi, Y. Tomii, and Y. Ito, “Effect of Aging on Yttria-Stabilized Zirconia I. A Study of Its Electrochemical Properties,” *J. Electrochem. Soc.*, **145** [5] 1527–1536 (1998).

[62] R.H.J. Hannink, P.M. Kelly, and B.C. Muddle, "Transformation Toughening in Zirconia-Containing Ceramics," *J. Am. Ceram. Soc.*, **83** [3] 461–487 (2000).

[63] D. Kok, S.K. Jha, R. Raj, and M.L. Mecartney, "Flash sintering of a three-phase alumina, spinel, and yttria-stabilized zirconia composite," *J. Am. Ceram. Soc.*, **100** [7] 3262–3268 (2017).

[64] D. Kok, D. Yadav, E. Sortino, S.J. McCormack, K.-P. Tseng, W.M. Kriven, R. Raj, and M.L. Mecartney, "α-Alumina and spinel react into single-phase high-alumina spinel in <3 seconds during flash sintering," *J. Am. Ceram. Soc.*, **102** [2] 644–653 (2019).

[65] G.R. Blair, "Determination of Spectral Emissivity of Ceramic Bodies at Elevated Temperatures," *J. Am. Ceram. Soc.*, **43** [4] 197–203 (1960).

[66] E.D. Palik, *Handbook of Optical Constants of Solids*. Academic Press, 2012.

[67] S. Alaruri, L. Bianchini, and A. Brewington, "Effective spectral emissivity measurements of superalloys and YSZ thermal barrier coating at high temperatures using a 1.6μm single wavelength pyrometer," *Opt. Lasers Eng.*, **30** [1] 77–91 (1998).

[68] E. Yalamaç, O. Culha, and A. Karataş, "Mechanical properties of interface layers between cosintered alumina and spinel compacts," *Adv. Appl. Ceram.*, **114** [1] 18–27 (2015).

[69] J. Narayan, "A new mechanism for field-assisted processing and flash sintering of materials," *Scr. Mater.*, **69** [2] 107–111 (2013).

[70] X. Su, G. Bai, Y. Jia, Z. Wang, W. Wu, X. Yan, T. Ai, P. Zhao, *et al.*, "Flash sintering of lead zirconate titanate (PZT) ceramics: Influence of electrical field and current limit on densification and grain growth," *J. Eur. Ceram. Soc.*, **38** [10] 3489–3497 (2018).

[71] S.-W. Kim, S.G. Kim, J.-I. Jung, S.-J.L. Kang, and I.-W. Chen, "Enhanced Grain Boundary Mobility in Yttria-Stabilized Cubic Zirconia under an Electric Current," *J. Am. Ceram. Soc.*, **94** [12] 4231–4238 (2011).

[72] K.E. Sickafus, J.M. Wills, and N.W. Grimes, "Structure of Spinel," *J. Am. Ceram. Soc.*, **82** [12] 3279–3292 (1999).

[73] S.T. Murphy, C.A. Gilbert, R. Smith, T.E. Mitchell, and R.W. Grimes, "Non-stoichiometry in MgAl2O4 spinel," *Philos. Mag.*, **90** [10] 1297–1305 (2010).

[74] H. Jagodzinski and H. Saalfeld, "Kationenverteilung und Strukturbeziehungen in Mg-Al-Spinellen," *Z. Für Krist. - Cryst. Mater.*, **110** [1–6] 197–218 (1958).

[75] Y. Okuyama, N. Kurita, and N. Fukatsu, "Defect structure of alumina-rich nonstoichiometric magnesium aluminate spinel," *Solid State Ion.*, **177** [1–2] 59–64 (2006).

[76] A. Karakuscu, M. Cologna, D. Yarotski, J. Won, J.S.C. Francis, R. Raj, and B.P. Uberuaga, "Defect Structure of Flash-Sintered Strontium Titanate," *J. Am. Ceram. Soc.*, **95** [8] 2531–2536 (2012).

[77] H. Charalambous, S.K. Jha, H. Wang, X.L. Phuah, H. Wang, and T. Tsakalakos, "Inhomogeneous reduction and its relation to grain growth of titania during flash sintering," *Scr. Mater.*, **155** 37–40 (2018).

[78] W. Qin, H. Majidi, J. Yun, and K. van Benthem, "Electrode Effects on Microstructure Formation During FLASH Sintering of Yttrium-Stabilized Zirconia," *J. Am. Ceram. Soc.*, **99** [7] 2253–2259 (2016).

[79] Y. Zhang, J.-I. Jung, and J. Luo, “Thermal runaway, flash sintering and asymmetrical microstructural development of ZnO and ZnO–Bi_2O_3 under direct currents,” *Acta Mater.*, **94** 87–100 (2015).

[80] J. Pappis and W.D. Kingery, “Electrical Properties of Single-Crystal and Polycrystalline Alumina at High Temperatures,” *J. Am. Ceram. Soc.*, **44** [9] 459–464 (1961).

[81] D.B. Marshall, T. Noma, and A.G. Evans, “A Simple Method for Determining Elastic-Modulus-to-Hardness Ratios using Knoop Indentation Measurements,” *J. Am. Ceram. Soc.*, **65** [10] c175–c176 (1982).

[82] G.R. Anstis, P. Chantikul, B.R. Lawn, and D.B. Marshall, “A Critical Evaluation of Indentation Techniques for Measuring Fracture Toughness: I, Direct Crack Measurements,” *J. Am. Ceram. Soc.*, **64** [9] 533–538 (1981).

[83] J.G. Pereira da Silva, A.N. Yamchelou, A. Debris, C. Wieck, H. Jelitto, H.A. Al-Qureshi, and R. Janssen, “Mechanical strength and defect distributions in flash sintered 3YSZ,” *J. Eur. Ceram. Soc.*, **37** [8] 2901–2905 (2017).

[84] J. Gong, “Indentation toughness of ceramics: a statistical analysis,” *Ceram. Int.*, **28** [7] 767–772 (2002).

[85] W. Yao, J. Liu, T.B. Holland, L. Huang, Y. Xiong, J.M. Schoenung, and A.K. Mukherjee, “Grain size dependence of fracture toughness for fine grained alumina,” *Scr. Mater.*, **65** [2] 143–146 (2011).

[86] R.L. Stewart and R.C. Bradt, “Fracture of Polycrystalline MgAl2O4,” *J. Am. Ceram. Soc.*, **63** [11–12] 619–623 (1980).

[87] K. Waetzig and A. Krell, "The Effect of Composition on the Optical Properties and Hardness of Transparent Al-rich MgO· $\mathrm{N}Al_2O_3$ Spinel Ceramics," *J. Am. Ceram. Soc.*, **99** [3] 946–953 (2016).

[88] H. Suematsu, K. Yatsui, and T. Yano, "The Relationship between the Hardness and the Point-Defect-Concentration in Neutron-Irradiated $MgO{\cdot}3.0Al_2O_3$ Single Crystals," *Jpn. J. Appl. Phys.*, **40** [2S] 1097 (2001).

[89] T. Iseki, M. Tezuka, C.-S. Kim, T. Suzuki, H. Suematsu, and T. Yano, "Hardening by Point Defects in Neutron Irradiated A1N and SiC," *J. Nucl. Sci. Technol.*, **30** [1] 68–77 (1993).

[90] H. Suematsu, T. Iseki, T. Yano, Y. Saito, T. Suzuki, and T. Mori, "Point Defect Hardening in MgO·3Al2O3," *J. Am. Ceram. Soc.*, **75** [7] 1742–1747 (1992).

[91] T. Suzuki and T. Tonokawa, "Contribution of Point Defects to Elastic Modulus," *Jpn. J. Appl. Phys.*, **35** [5S] 3240 (1996).

[92] J.R. Townsend, J.A. DiCarlo, R.L. Nielsen, and D. Stabell, "The elastic bulk effect of point defects in metals," *Acta Metall.*, **17** [4] 425–436 (1969).

[93] J. Xi, P. Zhang, C. He, H. Zang, D. Guo, and T. Li, "The role of point defects in the swelling and elastic modulus of irradiated cubic silicon carbide," *Nucl. Instrum. Methods Phys. Res. Sect. B Beam Interact. Mater. At.*, **356–357** 62–68 (2015).

[94] G. López-Polín, C. Gómez-Navarro, V. Parente, F. Guinea, M.I. Katsnelson, F. Pérez-Murano, and J. Gómez-Herrero, "Increasing the elastic modulus of graphene by controlled defect creation," *Nat. Phys.*, **11** [1] 26–31 (2015).

[95] Y. Dong, L. Qi, J. Li, and I.-W. Chen, "A computational study of yttria-stabilized zirconia: I. Using crystal chemistry to search for the ground state on a glassy energy landscape," *Acta Mater.*, **127** 73-84 (2017).

APPENDIX

Flash Sintering Set-Up at UC Irvine

Main components of flash sintering apparatus

A. Computer with MatLab Installed
B. ATS Series 3420 Split Tube Furnace
C. Glassman High Voltage EV 1.5F2.0 Power Supply
D. Keithley Series 2000 High Performance Digital Multimeter
E. The Imaging Source USB 2.0 Monochrome Camera, DMK 41BU02.H
F. 1/2" 25-135mm F1.8 Manual Iris, Vario-focal, C-mount, H5Z2518C-MP
G. Tektronix IEEE-488.2 USB to GPIB Interface Adapter, KUSB-488B

Minor components

H. Edmund Heat Absorbent Glass, KG-3 50mm
I. Surepure Chemetals 99.95 Pure Platinum Wire
J. SPI Supplies Platinum Paint, 04990-AB
K. Kanthal KAPM-1.0mm Resistance Wire
L. Nanoporus Alumina Ceramic Tube, 0.187" OD, 0.094" ID, 12" Long
    McMaster-Carr #8746K13
M. High-Voltage Wire 18 Gauge, 0.14" OD, 25ft
    McMaster-Carr #8296K17
N. Touch-Safe DIN-Rail Mount Block w/ Screw Terminals, 4 Circuits
    McMaster-Carr #8839T11
O. Steel DIN 3 Rail, 7.5mm Deep, 1m Long
    McMaster-Carr #8961K15
P. Stackable Pin-to-Pin Push-In Connectors, Male/Female Plug, 15 Amps,
    McMaster-Carr #802K76
Q. Electrical-Insulating Sleeving, High-Temperature Expandable Rubber, 0.17" ID
    McMaster-Carr #2573K13
R. Electrical-Insulating Sleeving, High-Temperature Expandable Rubber, 0.23" ID
    McMaster-Carr #2573K14

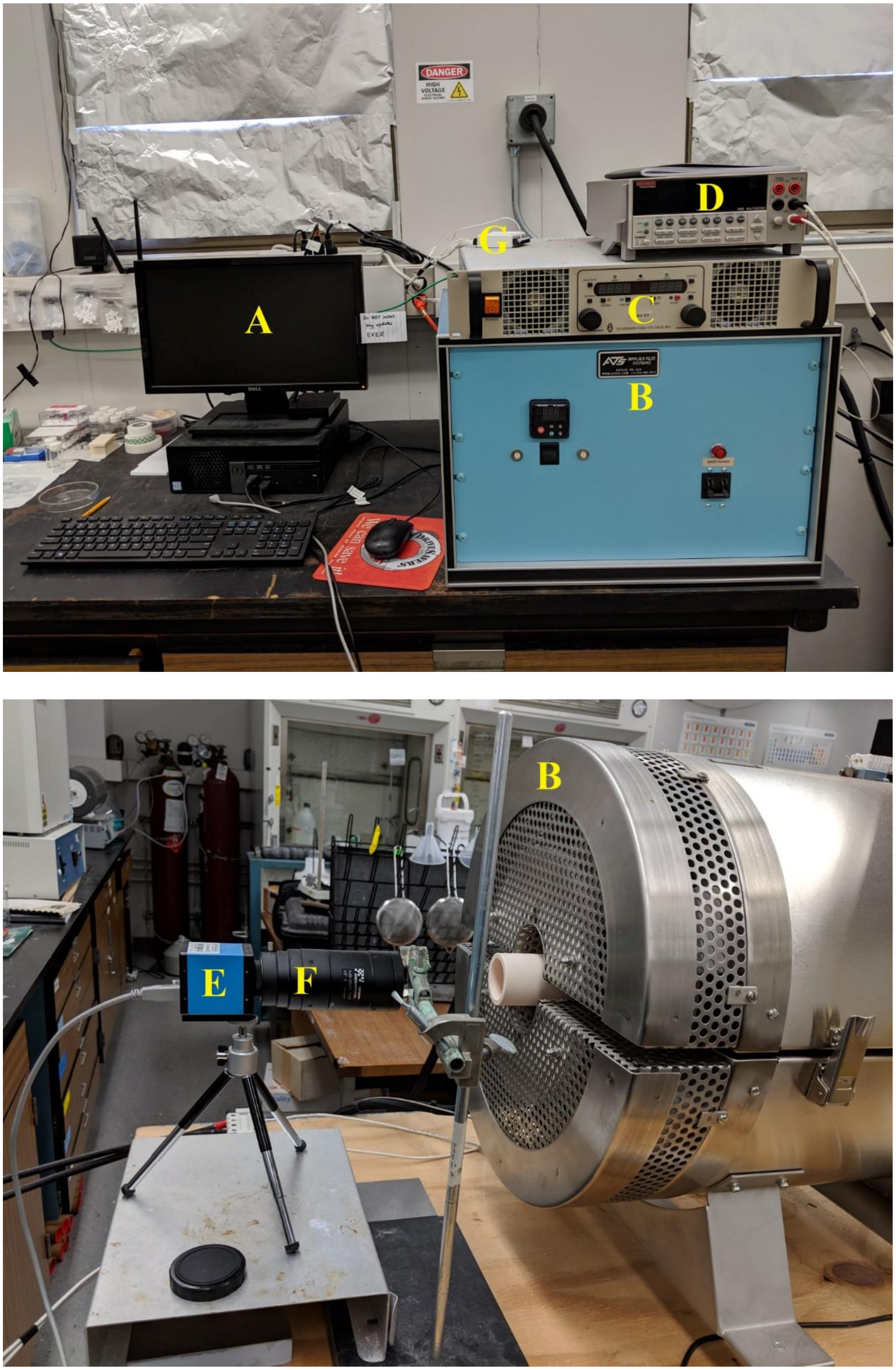

Figure A1: Images of Flash Sintering Set-Up at UCI with Major Components Labeled

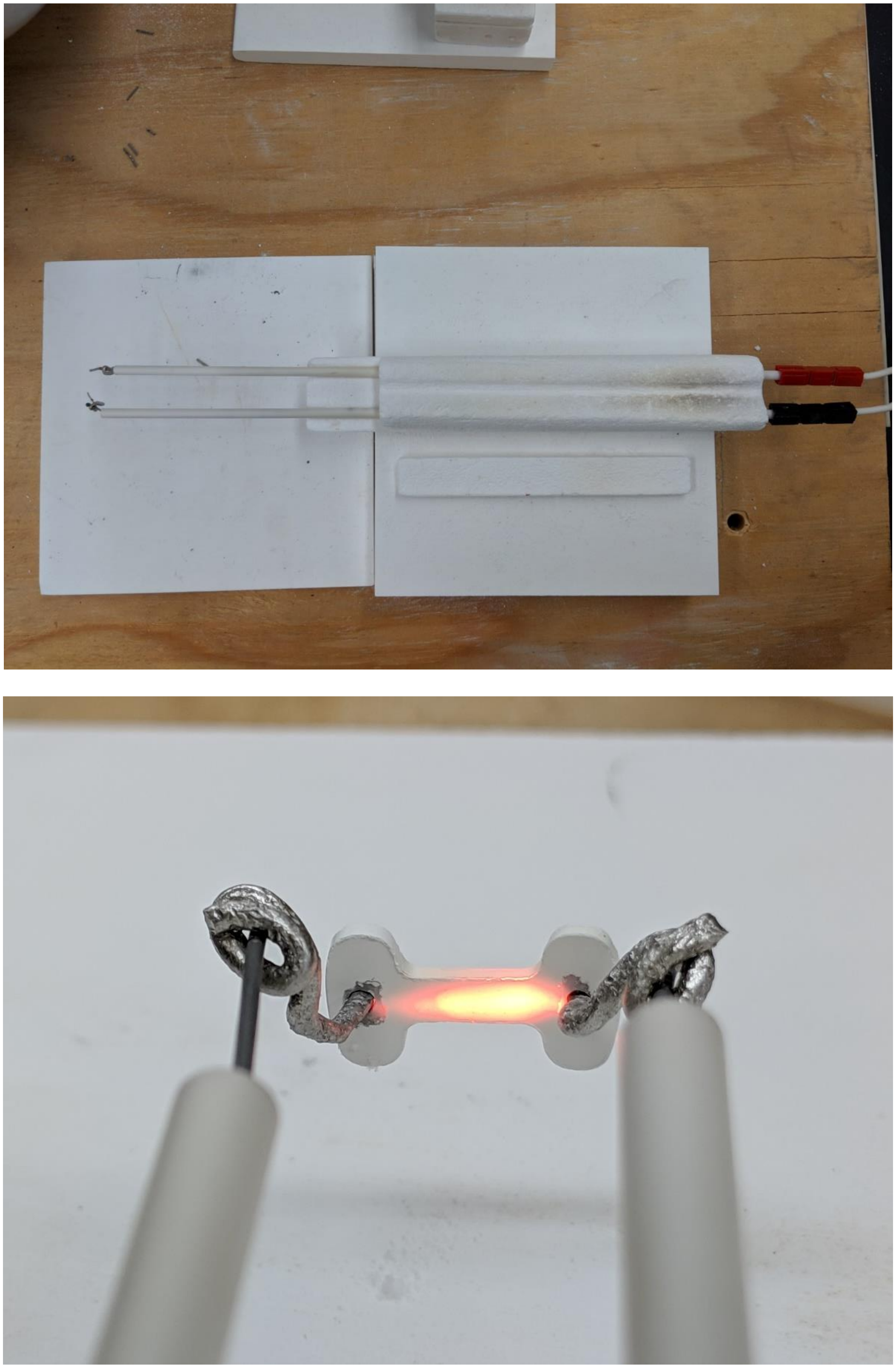

Figure A2: Images of electrodes for the flash sintering set up, sample undergoing flash in second image